Vacuum Ultraviolet Optical Properties of Micro-Pulling Down Method-Grown, Nd^{3+}-Doped Fluoride Crystals

Marilou Macasieb Cadatal

DOCTOR OF PHILOSOPHY

Department of Functional Molecular Science

School of Physical Sciences

The Graduate University for Advanced Studies

2008

Vacuum ultraviolet optical properties of micro-pulling down method-grown, Nd^{3+}-doped fluoride crystals

In 1977, Yang and De Luca proposed the feasibility of generating tunable laser sources spanning the wavelength range from 165 to 260 nm by using rare-earth doped wide band gap dielectric hosts. Their proposal that was purely based on spectroscopic data resulted to the first rare-earth doped fluoride laser in the ultraviolet region (250-400nm) using Ce^{3+}:$YLiF_4$ in 1979. Succeeding research have resulted to tunable ultraviolet rare-earth doped fluoride lasers such as Ce^{3+}:LiSAF and Ce^{3+}:LiCAF. The feasibility of having a tunable vacuum ultraviolet (100-190nm) laser from rare-earth doped fluorides have been confirmed by the first demonstration of 172-nm emission from Nd^{3+}:LaF_3 in 1985 and a second report in 1992 after improvement of the pumping scheme. Over twenty years after the first report, research is still geared towards finding a suitable host for the development of the shortest wavelength solid-state laser. This work aims to identify Nd^{3+}-doped fluoride hosts that could serve as the shortest wavelength solid-state laser material. Among the fluoride hosts that this work considers are $YLiF_4$, LaF_3, and $(La_{1-x},Ba_x)F_{3-x}$. Their optical properties in the vacuum ultraviolet region are characterized in terms of transparency, fluorescence spectra, and lifetime. Although, Nd^{3+}:$YLiF_4$ is found to be sufficiently transparent in the vacuum ultraviolet region with a long lifetime (21.7ns), it has a longer wavelength absorption edge and its fluorescence emission at around 181 nm is longer than the reported emission from Nd^{3+}:LaF_3. Based on this preliminary study, a new material is developed, which is Nd^{3+}:$(La_{1-x},Ba_x)F_{3-x}$ (x=0.1) or Nd^{3+}:$(La_{0.9},Ba_{0.1})F_{2.9}$. LaF_3 is mixed with BaF_2 in order to shift the absorption edge to a shorter wavelength. For the growth of this new material, the micro-pulling down method was utilized because it is capable of fast and economical crystal growth. Characterization of the vacuum ultraviolet optical properties of Nd^{3+}:$(La_{0.9},Ba_{0.1})F_{2.9}$ reveals that it has a shorter wavelength absorption edge at 180 nm with better transparency in the vacuum ultraviolet region, a more intense and broader vacuum ultraviolet fluorescence with a bandwidth of 12 nm, thereby enabling better tunability and amplification of as short as 4.3 fs pulses. Its emission wavelength at 178 nm is, however, longer and its fluorescence decay time at 6.1 ns is faster. In this regard, Nd^{3+}:$(La_{0.9},Ba_{0.1})F_{2.9}$ would be more suitable as a vacuum ultraviolet scintillator because of its high light yield and fast decay time. To investigate the feasibility of a solid-state pump source, a CZ method-grown Nd^{3+}:LaF_3 cut into a cuboid was excited by the third harmonics of a (290 nm) Ti:sapphire regenerative amplifier. Fluorescence characteristics are similar for the femtosecond and nanosecond pumping schemes. However, for the femtosecond case, fluorescence could have been through frequency up-conversion by energy transfer. The effect of doping concentration was also investigated both in the infrared and vacuum ultraviolet regions. The effect of Nd^{3+} concentration needs further study in order to identify whether concentration quenching would play an important role in improving light yield in the vacuum ultraviolet region. By carrying out further work in this direction, the optimum concentration level would be determined. With the improvement of the quality and size of Nd^{3+}-doped fluorides, an efficient and reliable vacuum ultraviolet laser will be realizable.

ABSTRACT

In 1977, Yang and De Luca proposed the feasibility of generating tunable laser sources spanning the wavelength range from 165 to 260 nm by using rare-earth doped wide band gap dielectric hosts. Their proposal that was purely based on spectroscopic data resulted to the first rare-earth doped fluoride laser in the ultraviolet region (wavelength from 250-400nm) using Ce^{3+}:$YLiF_4$ in 1979. Succeeding research have given birth to tunable ultraviolet rare-earth doped fluoride lasers such as Ce^{3+}:LiSAF and Ce^{3+}:LiCAF. The feasibility of having a tunable vacuum ultraviolet (wavelength from 100-190nm) laser from rare-earth doped fluorides have been confirmed by the first demonstration of 172-nm emission from Nd^{3+}:LaF_3 in 1985 and a second report in 1992 after improvement of the pumping scheme. Over twenty years after the first report, research is still continuously geared towards finding a suitable host for the development of the shortest wavelength solid-state laser. This work aims to identify Nd^{3+}-doped fluoride hosts for the possible shortest wavelength vacuum ultraviolet laser. Among the fluoride hosts that this work considers are $YLiF_4$, LaF_3, and $(La_{1-x},Ba_x)F_{3-x}$. Their optical properties in the vacuum ultraviolet region are characterized in terms of transparency, fluorescence spectra, and lifetime. Although, Nd^{3+}:$YLiF_4$ is found to be sufficiently transparent in the vacuum ultraviolet region with a long lifetime (21.7ns), it has a longer wavelength absorption edge and its fluorescence emission at around 181 nm is longer than the reported emission from Nd^{3+}:LaF_3. Based on this preliminary study, a new material is developed, which is Nd^{3+}:$(La_{1-x},Ba_x)F_{3-x}$ (x=0.1) or Nd^{3+}:$(La_{0.9},Ba_{0.1})F_{2.9}$. LaF_3 is mixed with BaF_2 in order to shift the absorption edge to a shorter wavelength. For the growth of this new material, the micro-pulling down method was utilized because it is capable of fast and economical crystal growth. Characterization of the

vacuum ultraviolet optical properties of Nd^{3+}:$(La_{0.9},Ba_{0.1})F_{2.9}$ reveals that it has a shorter wavelength absorption edge at 180 nm with better transparency in the vacuum ultraviolet region, a more intense and broader vacuum ultraviolet fluorescence with a bandwidth of 12 nm, thereby enabling better tunability and amplification of as short as 4.3 fs pulses. Its emission wavelength at 178 nm is, however, longer and its fluorescence decay time at 6.1 ns is faster. In this regard, Nd^{3+}:$(La_{0.9},Ba_{0.1})F_{2.9}$ would be more suitable as a vacuum ultraviolet scintillator because of its high light yield and fast decay time. To investigate the feasibility of a solid-state pump source, a CZ method-grown Nd^{3+}:LaF_3 cut into a cuboid was excited by the third harmonics of a (290 nm) Ti:sapphire regenerative amplifier. Fluorescence characteristics are similar for the femtosecond and nanosecond pumping schemes. However, for the femtosecond case, fluorescence was due to a multi-photon process. The effect of doping concentration was also investigated both in the infrared and vacuum ultraviolet regions. The effect of Nd^{3+} concentration needs further study in order to identify whether concentration quenching would play an important role in improving light yield in the vacuum ultraviolet region. By carrying out further work in this direction, the optimum concentration level would be determined. With the improvement of the quality and size of Nd^{3+}-doped fluorides, an efficient and reliable vacuum ultraviolet laser will be realizable in the near future.

TABLE OF CONTENTS

LIST OF FIGURES

LIST OF TABLES

LIST OF ABBREVIATIONS

α	absorption coefficient	MgF_2	magnesium fluoride
BaF_2	barium fluoride	μ-PD	micro-pulling down
BS	Bridgman-Stockbarger	min	minute
c	speed of light	mJ	millijoule
^oC	Celcius	μm	micrometer
CaF_2	calcium fluoride	n	number density
CCD	charge coupled device	N_2	nitrogen
Ce^{3+}	trivalent cerium	Nd^{3+}	trivalent neodymium
cm	centimeter	nm	nanometer
CZ	Czochralski	nm	nanometer
$\Delta\nu$	frequency bandwith	Pa	Pascal
DUV	deep ultraviolet	Pr^{3+}	trivalent praseodymium
e-beam	electron beam	ps	picosecond
Er^{3+}	trivalent erbium	RE	rare earth
eV	electron volt	RF	radio frequency
F_2	fluoride	σ_A	absorption cross section
fs	femtosecond	σ_F	fluorescence cross section
g	gram	τ	lifetime
Ho^{3+}	trivalent holmium	THz	terahertz
hr	hour	Tm^{3+}	trivalent thulium
Hz	hertz	TMP	turbomolecular pump
Ir	iridium	t_p	pulse duration
IR	infrared	UV	ultraviolet
λ	wavelength	VUV	vacuum ultraviolet
$(La_{1-x}Ba_x)F_{3-x}$	lanthanum barium fluoride	YAG	yttrium aluminum garnet
LaF_3	lanthanum fluoride	Yb	ytterbium
LuF_3	lutetium fluoride	YF_3	yttrium fluoride
m	meter	$YLiF_4$	yttrium lithium fluoride

Chapter 1. Introduction

Research efforts have continuously been geared towards the generation of deep ultraviolet (DUV) and vacuum ultraviolet (VUV) radiation from laser materials for scientific and industrial applications such as photolithography [1,2] and spectroscopy [3,4] and from scintillators for gamma ray detection [5]. The DUV region spans the wavelength range from 250 nm down to 190 nm while the VUV region includes wavelengths from 190 nm to 100 nm. While there are available VUV laser sources such as frequency conversion in nonlinear crystals [6], these have limited tunability and low conversion efficiency. In 1976 Yang and DeLuca proposed the generation of VUV radiation from dipole allowed interconfigurational d-f transitions in rare earth doped wide bandgap fluorides [7]. This is an attractive scheme due to its simplicity, reliability, and efficiency. It is also possible to obtain good-quality laser beams, controlled adjustment of the spectral width, and multi-wavelength operation from only one laser oscillator [8]. Since the first experimental verification of their proposal [9], several woks have reported luminescence from several trivalent rare earth-doped fluorides [10-12]. Among these, Ce^{3+}-activated fluorides, particularly Ce^{3+}:$LiCaAlF_6$ [13-15] and Ce^{3+}:$LiSrAlF_6$ [16,17] have been proven to be efficient ultraviolet (UV) active media. In spite of the encouraging results delivered by these materials, transition energies are not large enough for VUV emission. For the case of VUV emission, only Nd^{3+}:LaF_3 has been reported to lase [18, 19]. Work on this material, however, did not progress due to rapid saturation of the laser output brought about by loss mechanisms such as color center formation resulting from excited state absorption. Moreover, it had limited tunability and it required electron beam pumping. Because of this, there is a continuing

search for appropriate activator-matrix complexes and active medium-pump source combinations suitable for generating efficient VUV tunable lasers.

On the other hand, even though the number of known scintillators comes up to several hundreds, new and better materials are still needed in order to satisfy many requirements dependent on particular applications. For example, hydrothermal method grown large-sized ZnO crystal has recently been shown to be a fast scintillator for extreme ultraviolet photolithography [20]. High-performance scintillators should both be fast and efficient [21]. Nd^{3+}-doped fluorides are viable scintillator candidates because of their characteristic decay times of the order of 10 ns arising from the parity-allowed d-f transition [22]. Crystals having high light yields can also be engineered by choosing the right activator-host material combination. Their ability to emit in the VUV region is also advantageous for specific applications. For instance, gamma ray scintillators that emit VUV fluorescence are strongly required for a gas scintillation microwire stripped detector for high-resolution positron emission tomography (PET) application [23]. Material research for VUV scintillators is also ongoing.

Innovation of crystal growth methods plays an important role in developing VUV laser materials and scintillators. Classical methods for mass production of single crystals for industrial applications, for example Czochralski and Bridgman have already been well established [24]. However, these techniques are time and raw materials consuming especially for single crystal material screening. It is also difficult to combine screening with the establishment of appropriate growth conditions required for high quality crystal production [24]. The micro-pulling down (μ-PD) method is a relatively new crystal growth technique mainly developed at Tohoku University, Japan to meet the challenges in materials research. Recent improvements of this method made the quality

of μ-PD grown crystals comparable with those prepared by Czochralski, Bridgman-Stockbarger, or other classical growth techniques [25]. Owing to a fast growth speed, a high quality crystal can be grown using less than 1 g of raw material in 5 – 12 h, thereby allowing growth of large crystals at a shorter time and at a lower cost compared with the other melt growth methods mentioned earlier [25]. Moreover, this method has the capability of controlling the shape of the grown crystal to produce fibers, rods, and tubes [25]. This method was initially designed for the growth of oxide crystals and several works have demonstrated the advantages of this method [26-28]. However, because fluoride materials have found considerable attention, innovation of the μ-PD apparatus to accommodate fluoride crystal growth was carried out. Moreover, extensive research is put into the improvement of this method to facilitate the screening of fluoride host lattices, dopant concentration and optimization of the growth parameters. The demonstration of radio luminescence from a μ-PD grown Ce:PrF_3 shows that this method is capable of efficiently growing fluoride crystals [29].

1.1 Motivation and purpose

Over twenty years after the successful demonstration of the Nd^{3+}:LaF_3 laser have passed but no successful material research for VUV laser media has been reported. It is thus apparent that the development of new and efficient solid-state emitters in the VUV spectral region is an important and promising field of research. An integral step towards this goal is the characterization of spectroscopic properties of various combinations of wide band gap hosts and doping ions displaying optical activity in the VUV region.

The primary aim of this work is to develop and characterize fluoride materials

for their suitability as short wavelength laser media. For this purpose, Nd^{3+}-doped fluorides are considered.

Firstly, the optical properties of CZ method-grown Nd^{3+}-doped LaF_3 and $YLiF_4$ are characterized in terms of transmission and fluorescence.

However, a fast and economical yet efficient crystal growth method is necessary for materials screening of new crystals. Because of this, the μ-PD method modified for fluoride crystal growth is used to grow crystals for characterization purposes. In this regard, Nd^{3+}-doped LaF_3 and $(La_{(1-x)},Ba_x)F_{(3-x)}$ (x=0.1) or $(La_{0.9},Ba_{0.1})F_{2.9}$ crystals are grown and characterized.

During characterization, it is, however, inevitable that a material could display scintillator properties. In this case, the suitability of the material as a scintillator is also explored.

1.2 Outline

In chapter 1, the background of this work is presented and the purpose of this work is laid out.

Chapter 2 presents the current status of rare earth-doped fluorides as short wavelength light sources. The properties that make fluorides prominent short wavelength laser media are also presented.

Chapter 3 gives a background on scintillators. A scintillator is defined and its ideal properties are discussed. Examples of scintillators are also presented.

In chapter 4, crystal growth techniques are also discussed. Emphasis is given to the Czochralski (CZ) and the micro-pulling down (μ-PD) methods.

Chapter 5 summarizes the experimental set-ups used for the characterization of

the fluorides. The process of growing the Nd^{3+}:$(La_{0.9},Ba_{0.1})F_{2.9}$ crystal by the μ-PD method is also discussed.

In chapter 6, results of the characterization of CZ method-grown Nd^{3+}:LaF_3 and Nd^{3+}:$YLiF_4$ are discussed. This chapter also discusses the results of the characterization of μ-PD method-grown Nd^{3+}:LaF_3 and Nd^{3+}:$(La_{0.9},Ba_{0.1})F_{2.9}$.

This work is summarized and recommendations for further study are presented in chapter 7.

References

[1] T. Suganuma, H. Kubo, O. Wakabayashi, H. Mizoguchi, K. Nakao, Y. Nabekawa, T. Togashi, and S. Watanabe, "157-nm coherent light source as an inspection tool for F2 laser lithography," Opt. Lett. **27**, 46-48 (2002).

[2] R. H. French, R. C. Wheland, D. J. Jones, J. N. Hilfiker, R. A. Synowicki, F. C. Zumsteg, J. Feldman, A. E. Feiring, "Fluoropolymers for 157nm Lithography: Optical Properties from VUV Absorbance and Ellipsometry Measurements", in Optical Microlithography XIII, C. J. Progler,ed. (SPIE 4000, 2000) pp. 1491-1502.

[3] L. Skuja, K. Kajihara, M. Hirano, and H. Hosono, "Fluorine laser-induced silicon hydride Si–H groups in silica," J. Non-Cryst. Solids **353**, 526-529 (2007).

[4] R. H. French, D. J. Jones, H. Müllejans, S. Loughin, A. D. Dorneich, P. F. Carcia, "Optical Properties of Aluminum Nitride: Determined from Vacuum Ultraviolet Spectroscopy and Spectroscopic Ellipsometry," J. Mat. Res. **14**, 4337-4344 (1999).

[5] V.N. Makhov, N. Yu. Kirikova, M. Kirm, J. C. Krupa, P. Liblik, A. Lushchik, Ch. Lushchik, E. Negodin and G. Zimmerer, "Luminescence properties of $YPO_4:Nd^{3+}$: a promising VUV scintillator material," Nucl. Instrum. Methods Phys. Res. A **486**, 437-442 (2002).

[6] C.T. Chen, Junhua Lu, T. Togashi, T. Suganuma, T. Sekikawa, S. Watanabe, Zuyan Xu, and Jiyang Wang, "Second-harmonic generation from a $KBe_2BO_3F_2$ crystal in the deep ultraviolet," Opt. Lett. **27**, 637-639 (2002).

[7] K.H. Yang and J.A. DeLuca, "VUV fluorescence of Nd^{3+}-, Er^{3+}-, and Tm^{3+}-doped trifluorides and tunable coherent sources from 1650 to 2600 Å," Appl. Phys. Lett. **29**, 499-501 (1976).

[8] R. Moncorge, "Spectroscopy of broad-band UV-emitting materials based on

trivalent rare-earth ions," in Ultraviolet Spectroscopy and UV Lasers, M.A. Dubinskii and P. Misra, eds. (Marcel and Drekker New York, 2002), pp. 337-395.

[9] D.J. Ehrlich, P.F. Moulton, and R.M. Osgood, Jr., "Ultraviolet solid-state Ce:YLF laser at 325 nm," Opt. Lett. **4**, 184-186 (1979).

[10] V.N. Makhov, M.N. Khaidukov, N. Yu Kirikova, M. Kirm, J.C. Krupa, T. V. Ouvarova, and G. Zimmerer, "VUV spectroscopy of wide band-gap crystals doped with rare earth ions," Nucl. Instr. Meth. Phys. Res. A **470**, 290-294 (2001).

[11] V.N. Makhov, N.M. Khaidukov, N.Yu.Kirikova, M.Kirm, J.C. Krupa, T.V. Ouvarova, G. Zimmerer, "VUV emission of rare-earth ions doped into fluoride crystals," J. Lumin. **87-89**, 1005-1007 (2000).

[12] J.C. Krupa and M. Queffelec, "UV and VUV optical excitations in wide band gap materials doped with rare earth ions: 4f–5d transitions," J. Alloys Comp. **250**, 287-292 (1997).

[13] M.A. Dubinskii, V.V. Semashko, A.K. Naumov, R.Y. Abdulsabirov, and S.L. Korableva, "Spectroscopy of a new active medium of a solid-state UV laser with broadband single-pass gain," Laser Phys. **3**, 216-217 (1993).

[14] N. Sarukura, M.A. Dubinskii, Z. Liu, V.V. Semashko, A.K. Naumov, S.L. Koraleva, R. Yu Abdulsabirov, K. Edamatsu, Y. Suzuki, T. Itoh, and Y. Segawa, "Ce^{3+} activated fluoride crystals as prospective media for widely tunable ultraviolet ultrafast lasers with direct 10-ns pumping," IEEE J. Selected Topics in Q. Electron. **1**, 792-804 (1995).

[15] Z. Liu, T. Kozeki, Y. Suzuki, N. Sarukura, K. Shimamura, T. Fukuda, M. Hirano, and H. Hosono, "Chirped-pulse amplification of ultraviolet femtosecond pulses by use of Ce^{3+}:$LiCaAlF_6$ as a broadband, solid-state gain medium,"Opt. Lett. **26**, 301-303 (2001).

[16] J.F. Pinto, G.H. Rosenblatt, L. Esterowitz, and G.J. Quarles, "Tunable solid-state laser action in Ce^{3+}:$LiSrAlF_6$," Elect. Lett. **30**, 240-241 (1994).

[17] C.D. Marshall, S.A. Payne, J.A. Speth, W.F. Krupke, G.J. Quarles, V. Castillo, and B.H. T. Chai, "Ultraviolet laser emission properties of Ce^{3+}-doped $LiSrAlF_6$ and LiCaAlF6," J. Opt. Soc. Am. B **11**, 2054-2065 (1994).

[18] R.W. Waynant and P.H. Klein, "Vacuum ultraviolet laser emission from Nd^{+3}:LaF_3," Appl. Phys. Lett. **46**, 14-16 (1985).

[19] M.A. Dubinskii, A.C. Cefalas, E. Sarantopoulou, S.M. Spyrou, C.A. Nicolaides, R.Y. Abdulsabirov, S.L. Korableva, and V.V. Semashko, "Efficient LaF_3:Nd^{3+}-based vacuum-ultraviolet laser at 172 nm," J. Opt. Soc. Am. B **9**, 1148-1150 (1992).

[20] M. Tanaka, M. Nishikino, H. Yamatani, K. Nagashima, T. Kimura, Y. Furukawa, H. Murakami, S. Saito, N. Sarukura, H. Nishimura, K. Mima, Y. Kagamitani, D. Ehrentraut, T. Fukuda, "Hydrothermal method grown large-sized zinc oxide single crystal as fast scintillator for future extreme ultraviolet lithography", Appl. Phys. Lett. **91**, 231117-1-231117-2 (2007).

[21] W. Drozdowski, A. Wojtowicz, D. Wisniewski, T. Lukasiewics, and J. Kisielewski, "Scintillation properties of Pr-activated $LuAlO_3$," Opt. Materials **28**, 102-105 (2006).

[22] J. Becker, J.Y. Gesland, N.Yu. Kirikova, J.C. Krupa, V.N. Makhov, M. Runne, M. Queffelec, T.V. Uvarova, and G. Zimmerer, "Fast VUV emission of rare earth ions (Nd^{3+}, Er^{3+}, Tm^{3+}) in wide bandgap crystals," J. Alloys Comp. **275-277**, 205-208 (1998).

[23] H. Takahashi, University of Tokyo, Tokyo, Japan (private communication, 2006).

[24] A. Novoselov, A. Yoshikawa, and T. Fukuda, "The micro-pulling down method: fast and economic solution for materials screening," Current Topics in Cryst. Growth Res. **7**, 87-111 (2004).

[25] A. Yoshikawa, M. Nikl, G. Boulon, and T. Fukuda, "Challenge and study for developing of novel single crystalline optical materials using micro-pulling-down method," Opt. Mater. **30**, 6-10 (2007).

[26] B.M. Epelbaum, K. Inaba, S. Uda, and T. Fukuda, "Micro-pulling down growth studies of lead tungstate crystals: aspects of incongruent melt vaporization," J. Crystal Growth **178**, 426-429 (2007).

[27] A. Yoshikawa, T. Akagi, M. Nikl, N. Solovieva, K. Lebbou, C. Dujardin, C. Pédrini and T. Fukuda , "$\{Y_{3-x},Yb_x\}[Ga]_2(Ga)_3O_{12}$ and $\{Lu_2Yb_1\}[Al]_2(Al)_3O_{12}$ single crystals for scintillator application grown by the modified micro-pulling-down method," Nucl. Instrum. Methods Phys. Res. A **486**, 79-82 (2002).

[28] A. Yoshikawa, H. Itagaki, T. Fukuda, K. Lebbou, A. El Hassouni, A. Brenier, C. Goutaudier, O. Tillement and G. Boulon, "Synthesis, crystal growth and second harmonic generation properties of trivalent rare-earth-doped non-linear tungsten–bronze-type structure $Ba_2Na_{1-3x}RE_xNb_5O_{15}$ (RE=Sc,Y,La,Gd,Yb and Lu)," J. Crystal Growth **247**, 148-156 (2003).

[29] A. Yoshikawa, T. Satonaga, K. Kamada, H. Sato, M. Nikl, N. Solovieva, and T. Fukuda, "Crystal growth of Ce: PrF_3 by micro-pulling-down method," J. Cryst. Growth **270**, 427-432 (2004).

Chapter 2. Fluorides as Solid-State Laser Media

In 1976 Yang and DeLuca proposed a scheme of generating DUV and VUV radiation from rare earth (RE)-doped wide bandgap dielectric crystals. They reported broadband VUV fluorescence from Nd^{3+}, Er^{3+}, and Tm^{3+}-doped LaF_3, YF_3, $LiYF_4$, and LuF_3 by e-beam as well as by VUV excitation. With VUV excitation, they observed large Stokes shifts (>5000 cm^{-1}) and high fluorescence quantum yield of 0.8. They also estimated the threshold power for lasing in these crystals and proposed the molecular H_2 laser as a possible pumping source. With this scheme, a tunable laser system from 165 to 260 nm was projected [1]. Although their proposal was based from purely spectroscopic considerations, it presented an attractive means of generating tunable short wavelength radiation..

Yang and DeLuca's proposal was confirmed experimentally in 1979 when D.J. Ehrlich *et al.* reported the first stimulated emission from the 5d-4f transition in Ce^{3+}:$YLiF_4$ (Ce:YLF). It emitted at 325.5 nm when it was optically pumped at 249 nm [2]. However, Ce:YLF laser operation is limited by poor performance characteristics brought about by an early onset of saturation and roll off in the above-threshold gain and power output as well as a drop in the output for pulse repetition rates above 0.5 Hz. Although lasing from Ce:YLF is ground breaking, the existence of solarization leading to color center formation prevents this material to be of practical use, thereby hindering its further development. In 1980, the same group reported the operation of an optically pumped Ce^{3+}:LaF_3 laser [3]. Limitations of this laser medium include low output power and high lasing threshold. Moreover, successive researches have not been able to reproduce the lasing results. Subsequent experiments on other Ce^{3+}-doped fluorides have not been very successful due to the formation of transitory or permanent color

centers. Such color centers were essentially due to absorption of the pump and/or the laser radiation from emitting 5d states leading to the promotion of an electron into the conduction band followed by trapping by impurities or defects [4-8]. Recent investigations, however, showed that by an appropriate choice of activator-matrix complexes and active medium-pump source combinations, efficient tunable lasers using d-f transitions can be created [9-12]. In 1992, M.A. Dubinskii *et al.* reported emission from Ce^{3+}:$LuLiF_4$ (Ce:LLF) pumped by a KrF excimer laser. This material has almost the same optical properties as Ce:YLF but with smaller solarization effect [9]. Slope efficiencies of more than 50% were obtained with this material when pumped with either a Ce^{3+}:$LiSrAlF_6$ (Ce:LiSAF) laser at 290 nm [13] or the frequency doubled yellow output (289 nm) of a copper vapour laser [14]. Moreover, continuous tunability was achieved from 305-333 nm [14]. In 1993, the same group reported Ce^{3+}:$LiCaAlF_6$ (Ce:LiCAF) which can be pumped by the fourth harmonic of a Nd:YAG laser. Remarkably, no solarizaion effect was observed in this crystal [10, 11]. In 1994, Ce:LiSAF was reported. It can also be pumped with the fourth harmonic of a Nd:YAG laser and it has similar laser properties as the Ce:LiCAF crystal [15, 16]. Succeeding works on Ce:LiCAF revealed the usability of this crystal as a UV laser material. For instance, Liu *et al.* used a CZ method-grown Ce:LiCAF as a gain medium for UV chirped pulse amplification. They reported 6-mJ, 115 fs, 290 nm pulses [17]. In spite of the encouraging results delivered by Ce^{3+}-doped fluorides, emission wavelength is not short enough for DUV and VUV applications. This is because emission from Ce^{3+} activators typically arise from the $5d \rightarrow {}^2F_{5/2}$ transitions whose maximum energy lies at about 265 nm.

Ho^{3+}, Pr^{3+}, and Tm^{3+} are among the other RE dopants that have been studied

for applications in the DUV and VUV regions. However, no lasing action has been demonstrated from them [18-20]. Only in the case of Nd^{3+} doping was lasing in the VUV region achieved. For the case of Nd^{3+}-doping, typical transitions from the $4f^25d$ to the different levels of the 4I manifold in the $4f^3$ configuration enable emission in the VUV (<200nm). Despite research efforts, laser emission based on this transition was only demonstrated in LaF_3 host. In 1982, R.W. Waynant reported the first lasing in the VUV region from a rare earth-doped fluoride crystal [21]. Exciting a 0.1% Nd^{3+}-doped LaF_3 crystal with an electron beam/dimer molecule (Kr_2) optical pump, a 172-nm pulse was generated with an estimated energy of 32 μJ. Lasing was only observed from a lightly doped sample (0.1% Nd) due to strong absorption at higher doping concentrations [21, 22]. Then in 1992, Dubinskii *et al.* reported lasing at 172 nm from a Nd^{3+}:LaF_3 crystal grown using the Bridgman-Stockbarger method [12]. They used the 157-nm emission from a pulsed-discharge molecular F_2 laser. A maximum slope efficiency of 21% and a conversion efficiency of 14% were obtained. Moreover, they were able to achieve maximum output energy of 0.4 mJ at 172 nm. Despite the impressive slope efficiency obtained with Nd^{3+}-doped fluorides, there was rapid saturation of the laser output due to loss mechanisms probably similar to that in Ce^{3+}-doped crystals, such as color center formation resulting from excited state absorption. Because of this, there is still a need to look for better host materials.

2.1 Attributes of rare-earth-doped fluorides

The optical properties of undoped wide band gap dielectric crystals in the VUV region are mainly due to transitions from electronic states between the valence and conduction band. The high value of the absorption coefficient, for photon energies

higher than the crystal's band gap, is due to transitions involving delocalized electronic states in the conduction band. This arises from the crystal symmetry. The crystal's energy bands are formed from the energy levels of atoms when they are brought close together. On the other hand, local lattice imperfections, vacancies and other point defects, and dislocations bring about the formation of allowed states connected with the perturbation area. The electron is localized in the perturbation area and the smaller the perturbation energy, the greater the localization area. In this case, transitions are taking place between the valence band and the localized states in the conduction band. The width of the band gap is proportional to the value of the electron exchange energy between any two neighboring atoms because electrons may, with some probability, be located near any atom. Therefore, electrons are not localized near individual atoms but move freely through the crystal jumping from one atom to another by the exchange process. The energy gap (band gap) therefore depends on the exchange energy. But the exchange energy itself is dependent on the area of the overlapping of the atomic wave functions. The more the atomic wave functions overlap; the greater will be the exchange energy. It follows that energy levels corresponding to inner shell electrons do not split as intensely as those of the outer shells, since the inner shell electrons are localized in smaller areas of space. As the exchange energy increases, bands become wider and as a consequence band gaps become narrower. Therefore, the band gap width depends on the atomic number of the elements belonging to the same group. In other words, the higher the atomic number of an element is, the smaller is its band gap [23]. When a trivalent rare earth ion is embedded into a crystalline lattice, some of its well-localized energy states belonging to the $4f^n$ ground electronic configuration or the $4f^{n-1}$-5d first excited configurations are located between the valence band and the conduction band of the

host. The location of the $4f^n$ ground state is very close to the top of the valence band as estimated by UV or X-ray photoelectron spectroscopy [24]. When the interaction of the electrons with the ions and with other electrons is taken into account, the energy levels are lowered and split into a band of definite width due to Stark splitting arising from the crystal field effect. Since fluorides have a broad bandgap of around 10 eV [20], the optical window where it is transparent is wide enough to record the absorption peaks attributed to trivalent RE electronic transitions in the UV and VUV spectral domain as well as emission from high lying localized trivalent RE states.

The operating wavelength of light emitting devices is basically limited by the band gap of the material. Materials with larger band gaps would be capable of generating light with shorter wavelengths. Another factor in choosing the proper material is the tunability of the laser emission, thus materials with broad gain bandwidths are preferable. Fluorides have very good potential as laser gain media because they satisfy these criteria as indicated below:

(1) They have low phonon energy about 300-500 cm^{-1}.

(2) They have good transparency down to nearly 100 nm

(3) They have small nonlinearity

(4) Thermal lensing is weak

(5) High emission cross-sections

(6) Long metastable decay time

(7) Refractive index is about 1.5

Fluorides can have a band gap greater than 6.2 eV and hence they are capable of emitting light with wavelengths shorter than 200 nm [20]. Moreover, fluorides generally have broad fluorescence bandwidths. This is because of the nature of the

interconfigurational transitions from $4f^{n-1}5d \rightarrow 4f^n$. If a $4f^n$ electron is excited into the 5d level, the crystal field perturbation introduced by the fluoride host lattice becomes much stronger than the spin-orbit interaction because of the large radius of a 5d electron. The strong crystal field interaction results in broad bandwidth emission for interconfigurational transitions. In the absence of induced absorption effects, broad fluorescence bandwidths could be a precursor for broad gain bandwidths therefore enabling the emission to be tuned over a range of wavelengths. Aside from these, there are non-toxic and robust hosts that can be chosen from a wide selection of complex fluorides. Another noteworthy feature of fluorides is their transparency down to the VUV region [24]. Fluorides are highly transparent from the VUV to IR due to low energy phonons and high ionicity that lead to less absolute fundamental absorption with respect to other oxide or sulphide materials [24].

References

[1] K.H. Yang and J.A. DeLuca, "VUV fluorescence of Nd^{3+}, Er^{3+}, and Tm^{3+}-doped trifluorides and tunable coherent sources from 1650 to 2600 Å", Appl. Phys. Lett., **29** (1976) 499.

[2] D.J. Ehrlich, P.F. Moulton, and R.M. Osgood, Jr., "Ultraviolet solid-state Ce:YLF laser at 325 nm", Opt. Lett., **4** (1979) 184-186.

[3] D.J. Ehrlich, P.F. Moulton, and R.M. Osgood, Jr., "Optically pumped Ce:LaF_3 laser at 286 nm", Opt. Lett., **5** (1980) 339-341.

[4] D.S. Hamilton, *Tunable Solid State Lasers*, Berlin: Springer, 1985, pp. 80-90.

[5] Ki-Soo Lim and D.S. Hamilton, "Optical gain and loss studies in Ce^{3+}:$YLiF_4$", J. Opt. Soc. Am. B, **6** (1989) 1401.

[6] J.F Owen, P.B. Dorain, and T. Kobayasi, "Excited-state absorption in Eu^{+2}:CaF_2 and Ce^{+3}:YAG single crystals at 298 and 77 K", J. Appl. Phys. **52**, (1981) 1216-1223.

[7] D.S. Hamilton, S.K. Gayen, G.J. Pogatshnik, and R.D. Ghen, "Optical-absorption and photoionization measurements from the excited states of Ce^{3+}:$Y_3Al_5O_{12}$", Phys. Rev. B, **39**, (1989) 8807-8815.

[8] G.J. Pogatshnik and D.S. Hamilton, "Excited-state photoionization of Ce^{3+} ions in Ce^{3+}:CaF_2", Phys. Rev. B, **36** (1987) 8251-8257.

[9] M.A. Dubinskii, R.Y. Abdulsabirov, S.L. Korableva, A.K. Naumov, and V.V. Semashko, "A New Active Medium for a Tunable Solid-state UV Laser with an Excimer Pump", Laser Phys. **4** (1994) 480-484.

[10] M.A. Dubinskii, V.V. Semashko, A.K. Naumov, R.Y. Abdulsabirov, and S.L. Korableva, "Spectroscopy of a New Active Medium of a Solid State UV Laser with Broadband Single-Pass Gain", Laser Phys., **3** (1993) 216-217.

[11] M.A. Dubinskii, V.V. Semashko, A.K. Naumov, R.Y. Abdulsabirov, and S.L. Korableva, "Ce^{3+}-doped Colquiriite", J. Mod. Opt., **40** (1993) 1-5.

[12] M.A. Dubinskii, A.C. Cefalas, E. Sarantopoulou, S.M. Spyrou, C.A. Nicolaides, R.Y. Abdulsabirov, S.L. Korableva, and V.V. Semashko, "Efficient LaF_3:Nd^{3+}-based vacuum-ultraviolet laser at 172 nm", J. Opt. Soc. Am. B, **9** (1992) 1148-1150.

[13] P. Rambaldi, R. Moncorge, J.P. Wolf, C. Pedrini, J.Y. Gesland, "Efficient and stable pulsed laser operation of Ce:$LiLuF_4$ around 308 nm", Opt. Commun., **146** (1998) 163.

[14] A.J.S. McGonigle, S. Girard, D.W. Coutts, R. Moncorge, "10 kHz continuously tunable Ce:LiLuF laser", Elect. Lett. **35** (1999) 1640-1641.

[15] J.F. Pinto, G.H. Rosenblatt, L. Esterowitz, and G.J. Quarles, "Tunable solid-state laser action in Ce^{3+}:doped. LiSrAlF", Elect. Lett. **30** (1994) 240-241.

[16] C.D. Marshall, S.A. Payne, J.A. Speth, W.F. Krupke, G.J. Quarles, V. Castillo, and B.H. T. Chai, "Ultraviolet laser emission properties of Ce^{3+}-doped $LiSrAlF_6$ and $LiCaAlF_6$", J. Opt. Soc. Am. B, **11** (1994) 2054-2065.

[17] Z. Liu, T. Kozeki, Y. Suzuki, N. Sarukura, K. Shimamura, T. Fukuda, M. Hirano, and H. Hosono, "Chirped-pulse amplification of ultraviolet femtosecond pulses by use of Ce^{3+}:$LiCaAlF_6$ as a broadband, solid-state gain medium", Opt. Lett., **26** (2001) 301.

[18] V.N. Makhov, M.N. Khaidukov, N. Yu Kirikova, M. Kirm, J.C. Krupa, T. V. Ouvarova, and G. Zimmerer, "VUV spectroscopy of wide band-gap crystals doped with rare earth ions", Nucl. Instr. Meth. Phys. Res. A, **470** (2001) 290-294.

[19] V.N. Makhov, N.M. Khaidukov, N.Yu.Kirikova, M.Kirm, J.C. Krupa, T.V. Ouvarova, G. Zimmerer, "VUV emission of rare-earth ions doped into fluoride crystals", J. Lumin., **87-89** (2000) 1005-1007.

[20] J.C. Krupa and M. Queffelec, "UV and VUV optical excitations in wide band gap

materials doped with rare earth ions: 4f–5d transitions", J. Alloys Comp., **250** (1997) 287-292.

[21] T. Srinivasan, H. Egger, K. Boyer, H. Pummer, C. K. Rhodes, T. S. Luk, D. F. Muller, M. Rothschild, J. Bokor, R. R. Freeman, W. E. Cooke, H. Schomburg, H. F. Döbele, B. Rückle, L. A. Bloomfield, B. Couillaud, Ph. Dabkiewicz, H. Gerhardt, T. W. Hansch, R. Hilblg, R. Wallenstein, R. M. Jopson, C. B. Collins, F. W. Lee, D. M. Shemwell, B. D. DePaola, S. Olariu, I. Iovitzu Popescu, R. W. Waynant, M. D. Levenson, K. Jain, C. G. Willson and B. J. Lin, "Vacuum Ultraviolet Laser Emission from Nd^{3+}:LaF_3", Appl. Phys. B, 12^{th} International Quantum Electronics Conference, **28** (1982) 198-207.

[22] R.W. Waynant and P.H. Klein, "Vacuum ultraviolet laser emission from Nd^{+3}:LaF_3", Appl. Phys. Lett., **46** (1985) 14.

[23] M.A. Dubinski and P. Misra, *Ultraviolet Spectroscopy and UV Lasers*, Marcel Dekker, Inc., 2002

[24] M.F. Joubert, Y. Guyot, B. Jacquier, J. P. Chaminade and A. Garcia, "Fluoride crystals and high lying excited states of rare earth ions", J. Fluor. Chem. **107**, (2001) 235.

Chapter 3. Scintillators

Scintillators are fluorescent materials that mediate the detection of high energy (ionizing) electromagnetic or charged particle radiation. A scintillator absorbing high-energy radiation fluoresces at a characteristic Stokes-shifted (longer) wavelength that can be detected by conventional detectors like photodiodes or photomultiplier tubes. A schematic diagram of how a scintillator typically works is shown in Fig. 3.1. If the properties of the scintillator are known, the high-energy radiation that it absorbed can in turn be characterized. Radiation detectors are typically useful for imaging by utilizing high-penetration power radiation and for spectroscopy by utilizing characteristic radiation from each atom. As part of a detection unit, the broad application of scintillators comprises various scientific disciplines such as high-energy physics, nuclear physics, astronomy, and mineral exploration. It has also found applications in product quality control, airport security, nuclear safeguards verification, cargo container inspection, toxic dumpsite monitor, and environmental monitoring [1, 2]. Moreover, Positron Emission Tomography (PET) for medical imaging has gained popularity as a common clinical tool for detection of tumors. Extensive efforts have been put forth towards the development of more efficient scintillators for detecting gamma rays of around 511 keV that have been emitted by positron tracers in the body (arising from electron-positron annihilation). Single crystal scintillators with high density (greater than 7 g/cm^3), short decay time (less than 100 ns), and high output efficiency (8500 photons/MeV) is favorable for this application. [3-6].

Although the number of known scintillators amounts to several hundreds, new and better ones are still being developed in order to satisfy requirements for particular applications. High-performance scintillators should both be fast and efficient [1].

3.1 The scintillation decay time

An important requirement imposed on present day scintillators pertains to the scintillation decay time, i.e. the faster the better. Generally, the decay rate of an excited state is given by

$$\Gamma = \frac{1}{\tau} \propto \frac{n}{\lambda_{em}^3} \left(\frac{n^2+2}{3} \right)^2 \sum_f |\langle f|\mu|i\rangle|^2 , \tag{3.1}$$

where Γ is the scintillation decay time, τ is the fluorescence decay time, λ_{em} is the emission wavelength, n is the refractive index, and μ is the dipole operator connecting the initial state $|i\rangle$ with the final state $\langle f|$. The matrix element connecting an initial state with a final state via the dipole operator will only be of appreciable size for transitions between states of different parity. Therefore transitions between 5d and 4f as in the trivalent lanthanides like Ce^{3+}, Pr^{3+}, and Nd^{3+} and in the divalent lanthanides like Eu^{2+} are of interest. Also, transitions between levels of the p- and s- configurations as in Tl^{+}, Pb^{2+}, and Bi^{3+}, are parity allowed. These are precisely the activator ions encountered in scintillators [14].

Transitions starting from a less than half-filled configuration and terminating in a more than half-filled ground-state configuration are usually spin forbidden, and therefore slow. This is the situation in Tl^{+}:NaI, $Bi_4Ge_3O_{12}$ and Tl^{+}:CsI where τ>200ns. The same applies for self trapped exciton emission where τ>1000 ns, and when Tm^{3+} ($4f^{12}$) and Er^{3+} ($4f^{12}$) are the activator ions. For Eu^{2+}, decay times are usually around 1 μs [14].

Excluding those lanthanides where non-radiative relaxation to high-lying 4f-levels takes place leaves Ce^{3+}, Pr^{3+}, and Nd^{3+} as the remaining options for fast decay

scintillators. A survey of the literature data reveals that the lifetime of the lowest 5d-state of Ce^{3+} in inorganic compounds ranges from 17 to 60 ns, that of Pr^{3+} is about two times shorter and that of Nd^{3+} again two times shorter [14].

Knowing that one is restricted to Ce^{3+}, Pr^{3+}, or Nd^{3+}, the fundamental limits on the wavelength of emission obtainable with these activators is explored. For example, for the case of Ce^{3+} activator, Fig. 3.2 compiles the data available on the emission wavelength of the 5d $\rightarrow$ $^2F_{5/2}$ transition in Ce^{3+} [14]. It ranges from the deep ultraviolet at 265 nm for Ce^{3+} in $KMgF_3$ to the red part at 700 nm in $MgSc_2S_4$. At the same site in the same host, the luminescence to the ground state in Pr^{3+} appears always 1.50 eV higher in energy than in the case of Ce^{3+}. For Nd^{3+} the difference is 2.82 eV. It implies that emission to the ground state in Pr^{3+} will be restricted to the 210-400 nm region, and for Nd^{3+} emission will be restricted to the VUV region. The shortening of the emission wavelength in going from Ce^{3+} to Pr^{3+} to Nd^{3+} is for a large part responsible for the two and four times shortening of decay time of Pr^{3+} and Nd^{3+} luminescence as dictated by equation 3.1.

3.2 The scintillation light output

If it is assumed that all charge carriers will be transferred to activator ions and that the intrinsic luminescence quantum efficiency of the activator ion is unity, then the light output of the scintillation crystal will fully be determined by the number of electron-hole pairs created in the ionization track. Therefore, the scintillation light output can be expressed as

$$n_{e-h} = \frac{E_\gamma}{\beta E_g} \quad , \tag{3.2}$$

where $n_{e\text{-}h}$ is the number of electron-hole pairs created during illumination, E_g is the band gap of the material, E_γ is the emission output, and β is a weight factor, which is reported to be close to 2.5 as determined experimentally and theoretically. Fig. 3.3. shows the curve describing the fundamental limit on light output assuming β=2.5. The hatched bars indicate the range of band gap values typical for the type of compounds indicated in the figure [14].

In the last decade, the promising Ce-activated crystals such as perovskites: $LuAlO_3$ (LuAP) [12, 43-44] and $YAlO_3$ (YAP) [5, 15-17] and orthosilicates: Lu_2SiO_5 (LSO) and Y_2SiO_5 (YSO) [5, 18,19], have been investigated thoroughly. Following these studies, the same host materials activated with other ions, like praseodymium (Pr) or ytterbium (Yb), have also received some attention [1, 15, 20,21]. For the case of Ce- and Pr-doped scintillators, the presence of traps and parasitic absorption lowers the light yield. Further investigation on the hole localization as well as the electronic structure of the traps are necessary to improve performance [5,15]. Another way of addressing the need for efficient scintillators is the development of new materials. Recently, scintillation properties of fluorides have been investigated [22,23] and the advantages of VUV scintillator materials have been demonstrated. For instance, V.N. Makhov has shown that there are Nd-doped crystals possessing simultaneously both high light output and relatively good timing properties of the VUV luminescence. Such crystals can be considered as promising materials for fast VUV scintillators [24,25]. BaF_2 is also a common, very fast scintillator for the detection of X-rays, gamma rays or other high-energy particles. One of its applications is the detection of 511 keV gamma photons in positron emission tomography. Because of these, RE-doped fluorides as VUV scintilators are gaining attention.

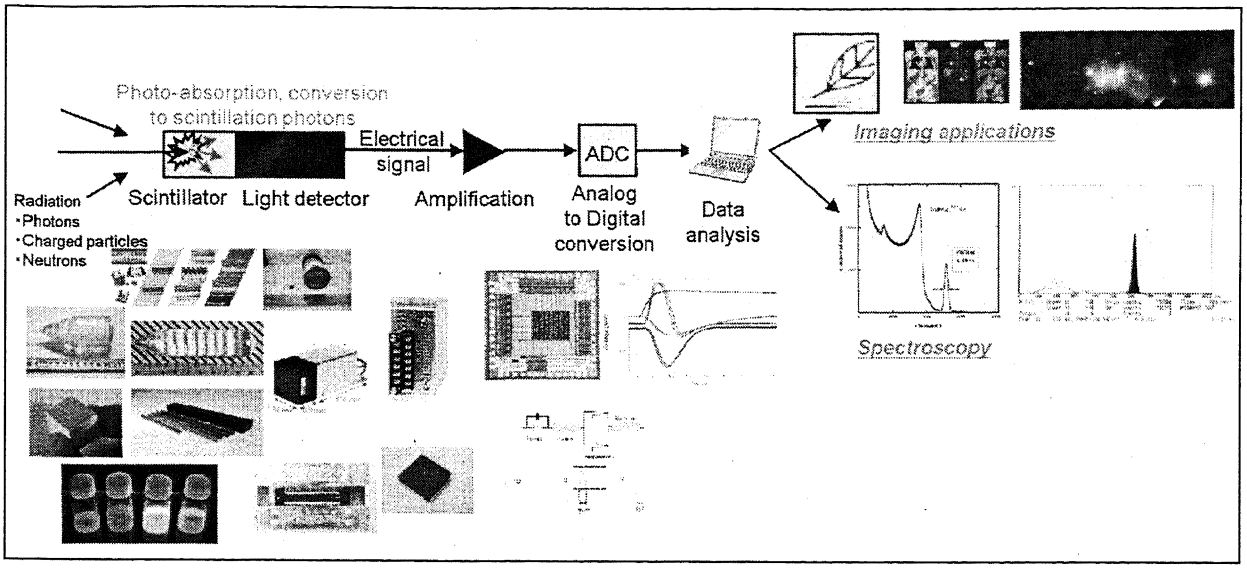

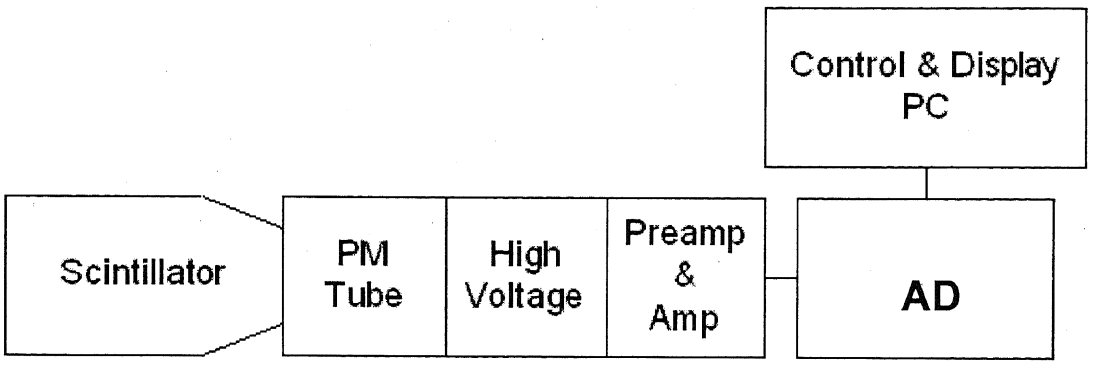

Fig. 3.1. Schematic diagram for the detection of radiation by a scintillator. The scintillator absorbs high-energy radiation and fluoresces at a characteristic Stokes-shifted wavelength, which is readily detectable by conventional detectors such as an avalanche photodiode or a photomultiplier (PMT) tube. The signal is then digitized by an analog-digital converter (AD).

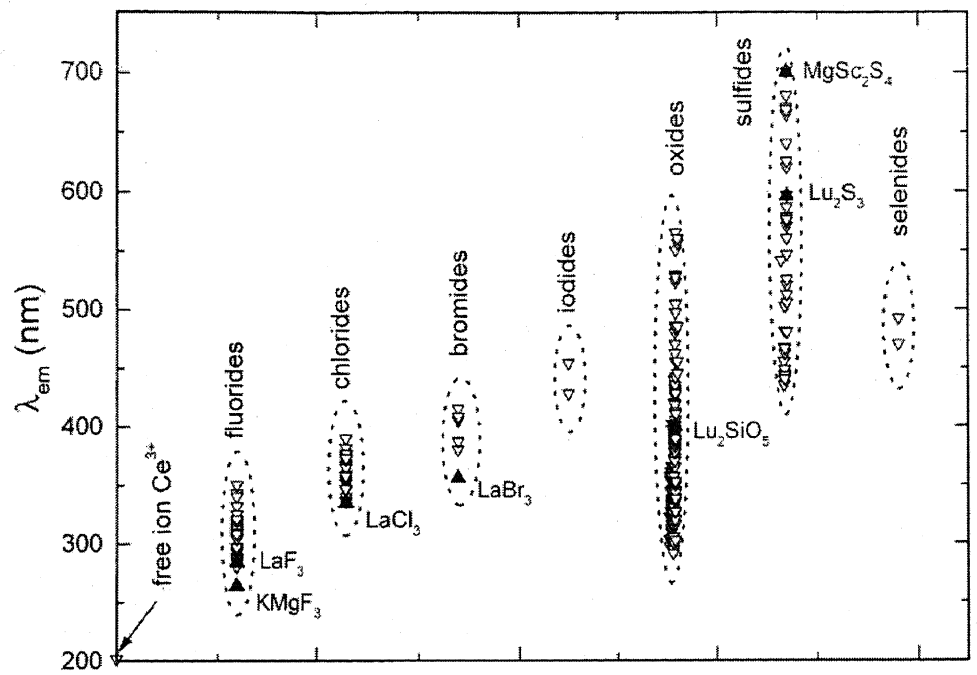

Fig. 3.2. The emission wavelength for the transition between 5d and the ground state of Ce^{3+} in different compounds. Fluorides are among the hosts that have the shortest emission wavelengths and hence, are among the fastest scintillators.

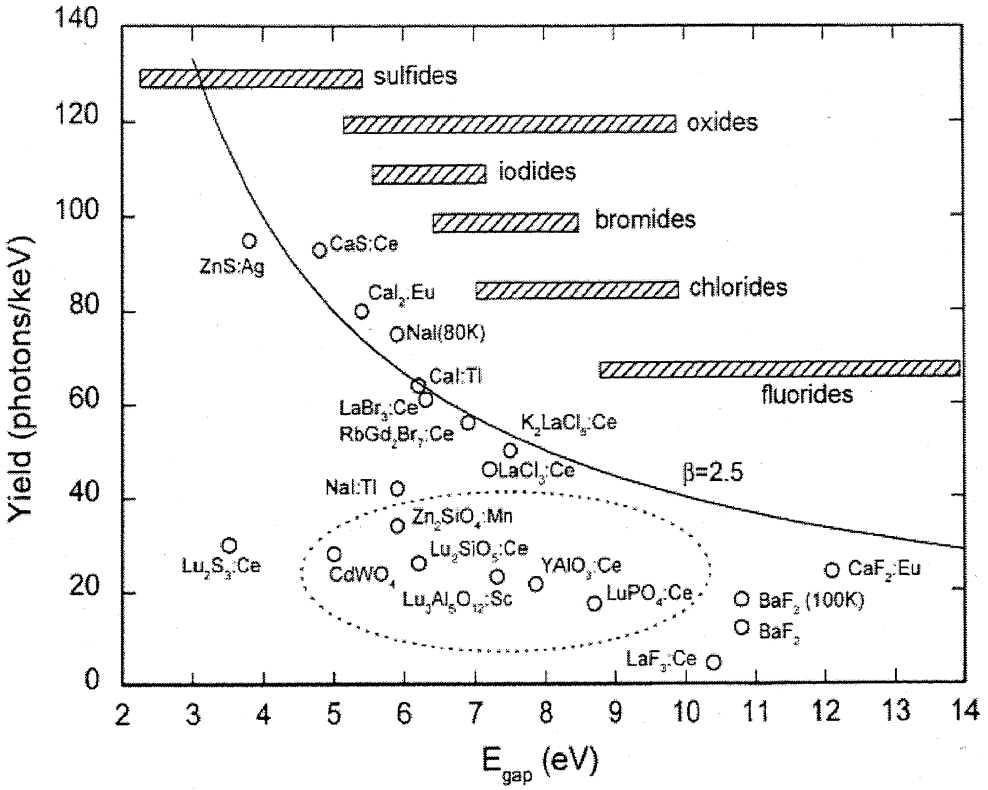

Fig. 3.3. Light yield of different scintillators and cathode ray tube phosphors. The dashed circle indicates some of the most commonly used scintillators.

References

[8] W. Drozdowski, A. Wojtowicz, D. Wisniewski, T. Lukasiewics, and J. Kisielewski, "Scintillation properties of Pr-activated $LuAlO_3$", Opt. Materials, **28** (2006) 102-105.

[9] C.L. Melcher and J.S. Schweitzer, "A promising new scintillator: cerium-doped lutetium oxyorthosilicate", Nucl. Instr. Meth. Phys. Res. A, **314** (1992) 212.

[10] H. Ishibashi, Oyo Buturi, "Single crystals in PET for medical innovations", **75** (2006) 0560-0564

[11] A. Novoselov, A. Yoshikawa, and T. Fukuda, "The Micro-Pulling Down Method: Fast and Economic Solution for Materials Screening", Current Topics in Cryst. Growth Res. **7** (2004) 87-111.

[12] A. Lempicki and J. Glodo, "Ce-doped scintillators: LSO and LuAP", Nucl. Instr. Meth. Phys. Res. A, **416** (1998) 333-344.

[13] V.N. Makhov, N.Yu. Kirikova, M. Kirm, J.C. Krupa, P. Liblik, A. Lushchik, Ch. Lushchik, E. Negodin and G. Zimmerer, "Luminescence properties of $YPO_4:Nd^{3+}$:a promising VUV scintillator material",Nucl.Instr.Meth.Phys.Res.A,**486** (2002) 437.

[43] C. Dujardin, C. Pedrini, J.C. Gacon, A.G. Petrosyan, A.N. Belsky and A.N. Vasil'ev, "Luminescence properties and scintillation mechanisms of cerium- and praseodymium-doped lutetium orthoaluminate", J. Phys.: Condens. Matter., **9** (1997) 5229.

[44] A.J. Wojtowicz, P. Szupryczynski, D. Wisniewski, J. Glodo and W. Drozdowski, "Electron traps and scintillation mechanism in LuAlO3:Ce", J. Phys.: Condens. Matter., **13** (2001) 9599.

[45] A.J. Wojtowicz, J. Glodo, A. Lempicki and C. Brecher, "Recombination and

scintillation processes in $YalO_3$:Ce", J. Phys. Condens. Matter., **10** (1998) 8401.

[46] W. Drozdowski, A.J. Wojtowicz, D. Wiśniewski, P. Szupryczyński, S. Janus, J.L. Lefaucheur and Z. Gou, "VUV spectroscopy and low temperature thermoluminescence of LSO:Ce and YSO:Ce", J. Alloys Comp. **380** (2004) 146.

[47] C.L. Melcher and J.S. Schweitzer, "A promising new scintillator: cerium-doped lutetium oxyorthosilicate", Nucl. Instr. Meth. A **314** (1992) 212.

[48] S. Nicolas, E. Descroix, Y. Guyot, M.F. Joubert, C. Pedrini, Z.K.L. Ovanesyan, G.O. Shirinyan and A. Petrosyan, "Spectroscopic and colour centre studies of Pr-doped $LuAlO_3$", Opt. Mater. **19** (2002) 129.

[49] W. Drozdowski, T. Łukasiewicz, A.J. Wojtowicz, D. Wiśniewski and J. Kisielewski, "Thermoluminescence and scintillation of praseodymium-activated $Y_3Al_5O_{12}$ and $LuAlO_3$ crystals ", J. Cryst. Growth **275** (2005) e709-e714.

[50] M. Nikl, N. Solovieva, E. Mihokova, M. Dusek, A. Vedda, M. Martini, K. Shimamura and T. Fukuda, "Scintillation Decay of $LiCaAlF_6:Ce^{3+}$ Single Crystals", Phys. Status Solidi (a) **187** (2001) R1-R3.

[51] M. Nikl, E. Mihokova, Z. Malkova, A. Vedda, M. Martini, K. Shimamura and T. Fukuda, "Ce^{3+} luminescence in a $LiBaF_3$ single crystal at low temperatures", Phys. Rev. B **66** (2002) 184101.

[40] V.N. Makhov, M.N. Khaidukov, N. Yu Kirikova, M. Kirm, J.C. Krupa, T. V. Ouvarova, and G. Zimmerer, "VUV spectroscopy of wide band-gap crystals doped with rare earth ions", Nucl. Instr. Meth. Phys. Res. A, **470** (2001) 290-294.

[52] P. Dorenbos, C.W.E. van Eijk. R.W. Hollander, P. Schotanus, "Scintillation properties of Nd^{3+} doped LaF_3 crystals", Nucl. Sci. IEEE Transactions, **37** (1990) 119-123.

Chapter 4. Crystal Growth Techniques

An essential aspect of materials science is the crystal growth process. It determines progress, industrial development, and transfer of various fundamental ideas from sophisticated mathematical equations and original hypotheses to daily life. A number of crystal growth techniques were developed during the last century. This work will focus on two particular crystal growth techniques. The first one is the Czochralski (CZ) process, which is a classical melt growth technique that is widely practiced in research and industry. The second one is the Micro-pulling down (μ-PD) method, which is a relatively new technique considered to be a logical continuation of the CZ process of growing a crystal from the melt

4.1 The Czochralski method

The Czochralski (CZ) method was discovered in 1916 by Jan Czochralski and the first paper citing its results was published in 1918. Professor Czochralski started the crystal growth of metals by immersion of a narrow capillary in the crucible with melt. The first CZ apparatus used by J. Czochralski is shown in Fig. 4.1. A small nucleus of crystal is then formed in the capillary. Slowly pulling up the melt allowed growing metallic monocrystalline wires with diameters of about 1 mm and lengths up to 150 mm [1,2]. Since its invention, the CZ method is continuously improved and developed and several modifications have been carried out to suit the growth of a particular type of crystal. The most important application may be the growth of large cylindrical ingots, or boules, of single crystal silicon for semiconductor applications. A schematic diagram of the CZ growth process is shown in Fig. 4.2. The crystal growth starts from a mixture of powder raw materials. The raw materials are usually high purity elements. They are

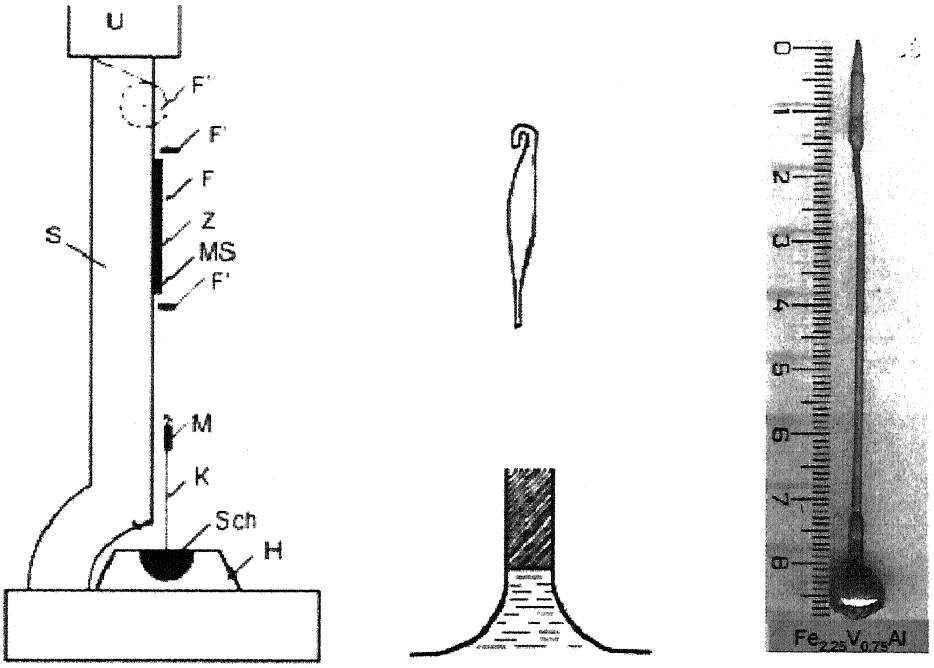

Fig. 4.1. The first CZ apparatus utilized by J. Czochralski. It was used for the growth of metals by immersion of a narrow capillary in the crucible containing the melt.

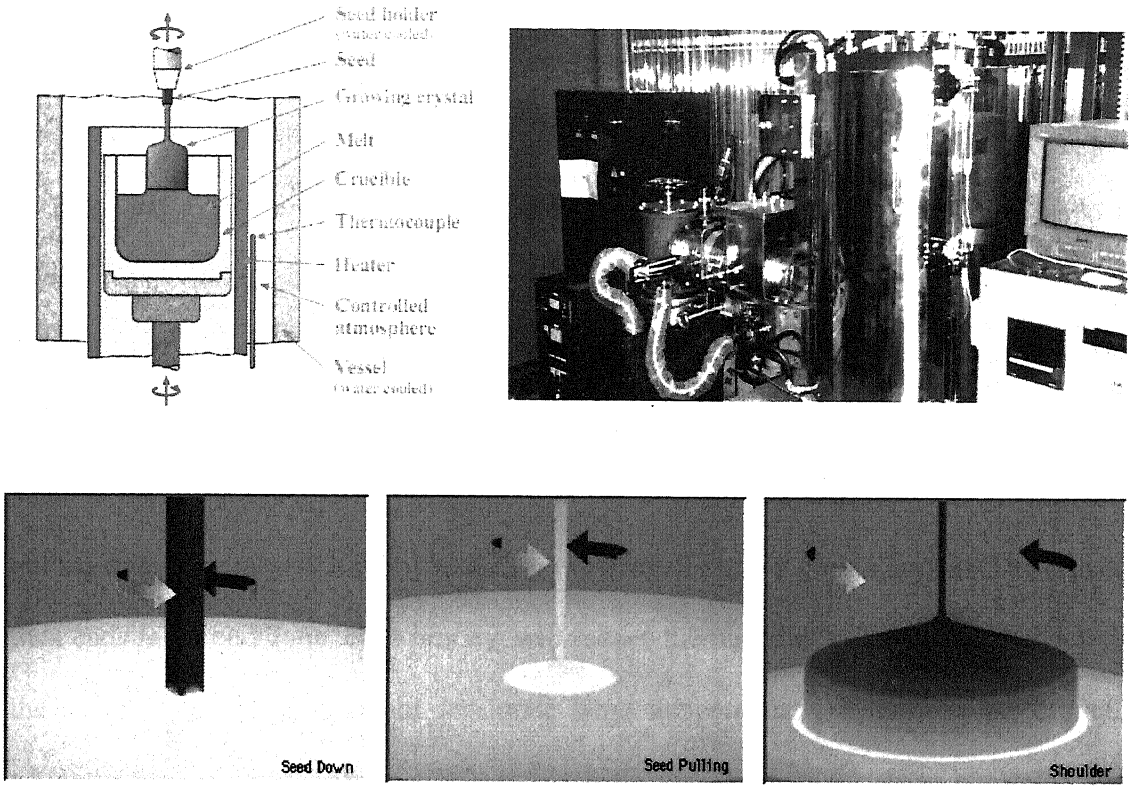

Fig. 4.2. Schematic diagram of the CZ process of pulling a crystal from the melt. Large single crystals are grown by inserting a small seed crystal into a crucible filled with molten raw material. The seed is rotated while slowly pulled up from the melt.

melted together in stoichiometric amounts under very pure argon atmosphere in the CZ apparatus. The crystal growth process is initiated by immersion of a seed crystal in the melt. The beginning of crystallization process occurs on the seed crystal. The seed crystal is then withdrawn from the melt. For homogeneity, the seed crystal and the crucible are rotated during this process. Initially, the seed crystal is pulled fast. This will cause the diameter of the growing crystal to be a few mm. This process is called necking and it ensures that the crystal will be dislocation free even though the seed crystal may contain dislocations. After necking, the growth speed is decreased to allow the crystal diameter to increase. The growing crystal is pulled out with a constant velocity of around 0.5-1 mm/hr. The obtained crystals are cylindrical with a diameter of about 2 mm and a length of about 80 mm. In order to terminate crystal growth, the pulling rate is increased, thereby reducing the diameter of the grown crystal. The crystal then ends in an end cone. This process will reduce thermal shock. The thermal shock of the rapidly cooling end would introduce large temperature gradients in the crystal, which in turn produce a stress gradient that will cause dislocations to be nucleated and driven into the crystal resulting to cracks. The growth process can be performed with different growth rates and different temperatures of the melt in order to change the diameter of the growing crystal. However, pulling at a rate of about 0.05 mm/hr could allow the growth of better quality crystals without growth patterns [1,2]. A sample of a crystal grown by the CZ process is shown in Fig. 4.3.

The CZ process is already well established for industrial applications especially in the growth of Silicon wafers for semiconductor and electronic device applications. However this technique is time and raw materials consuming especially for single crystal material screening. It is also difficult to combine screening with the

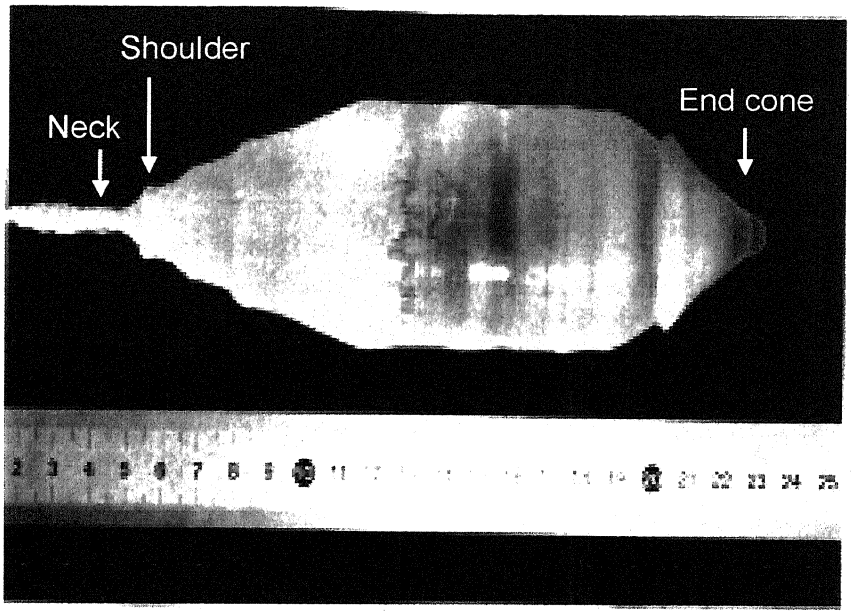

Fig. 4.3. Ce:LiCAF crystal grown by the CZ process. The neck and the conical end are clearly seen.

establishment of appropriate growth conditions required for high quality crystal production. These result to delay in the production and development of applications requiring newly developed crystals [3]. Therefore, for the systematic study of the growth and optimization of new materials, a faster and more economical yet efficient means of crystal growth method is required.

4.2 The micro-pulling down method

The micro-pulling down (μ-PD) method was proposed by Dr. Ohnishi at the Electrotechnical Laboratory in Tsukuba Japan. It was later established at the Fukuda Laboratory at the Institute of Material Research (IMRAM) Tohoku University in Sendai, Japan. Development of this method started in 1994.

This new method is relatively simple and it could be considered as a logical continuation of the classical methods of crystal pulling from the melt [4]. The first apparatus was resistively heated and was used to grow oxides. The schematic diagram for the initial resistively heated μ-PD apparatus is shown in Fig. 4.4 [3]. Powder raw material is placed in a crucible made of metal, for instance Pt or Pt/Rh, that is stable at high temperature corresponding to the melting point of the crystalline material to be grown. Moreover, the crucible material should be non-reactive with the raw materials that it contains. The crucible has a micro nozzle with a capillary at the bottom. The temperature of the nozzle can be controlled to a high degree of accuracy by the power load to the Pt-wire after heater. The weight of a crucible charge is less than 1 gram and additional feeding can be provided during the growth process. The crucible is resistively heated directly. After it has reached the material's melting point, a thin seed crystal is touched to the hanging melt droplet at the nozzle. The fiber is then pulled down with a

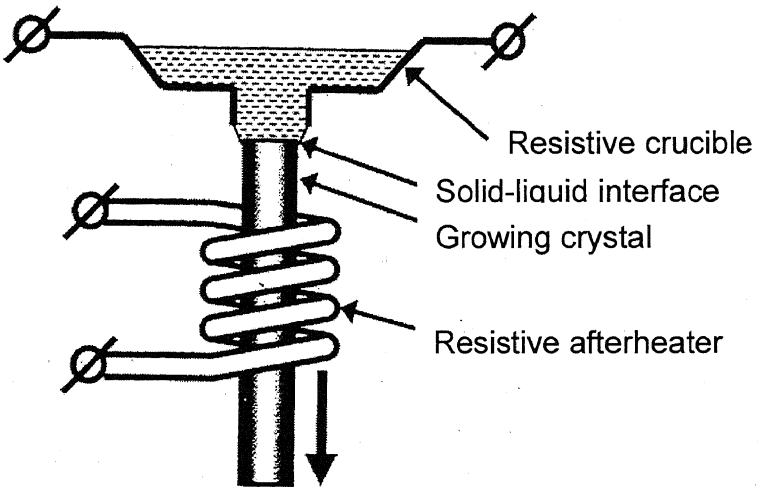

Fig. 4.4. The original resisitively-heated μ-PD apparatus [3].

velocity of 0.01-20 mm/min. Optimum speed depends on the size of the nozzle used. Pulling a crystal too fast would lead to a diameter smaller than the nozzle diameter and therefore to surface irregularities. Alignment of the seed and the nozzle is controlled by a micro X-Y stage. Growth is usually conducted in air atmosphere. The crystal diameter can be controlled from 0.15-2.0 mm by using an after-heater. An optical microscope can visually monitor the growth process. This provides excellent conditions for *in situ* observation of the growth interface through a fully transparent meniscus. This was demonstrated for the case of $PbWO_4$ growth experiments [5].

Later, a double-die modification for *in situ* clad/core doping was proposed [6]. Radio frequency (RF) heating of the carbon crucible was suggested [7]. Finally, growth of high melting (above 1700 °C) materials was performed using an Ir crucible. To prevent oxidation of the crucible, growth atmosphere should also be controlled precisely. An improved set up shown in Fig. 4.5 was implemented. An Ir crucible is placed on an aluminum pedestal with Ir after-heater and proper thermal insulation in a vertical quartz tube. A RF generator then heats it. The conical bottom of the crucible has a central capillary opening of about 0.3-0.5 mm in diameter and 1 mm in length. The end face of the crucible bottom is slightly depressed and varied from 0.5-1.0 mm in different growth experiments. The edge definition is maintained by precise sharpening of the crucible tip. This is necessary for stable growth. The crucible temperature is controlled by the power applied to the movable RF coil. Moreover, high density and high purity (99.7%) alumina ceramic is used to surround the crucible thereby providing thermal insulation. The crystal growth is performed in neutral Ar/N_2 or slightly oxidizing/reducing atmosphere by adding an appropriate amount of O_2/H_2. The seed is attached to a high purity aluminum seed holder coupled to the micro X-Y stage for

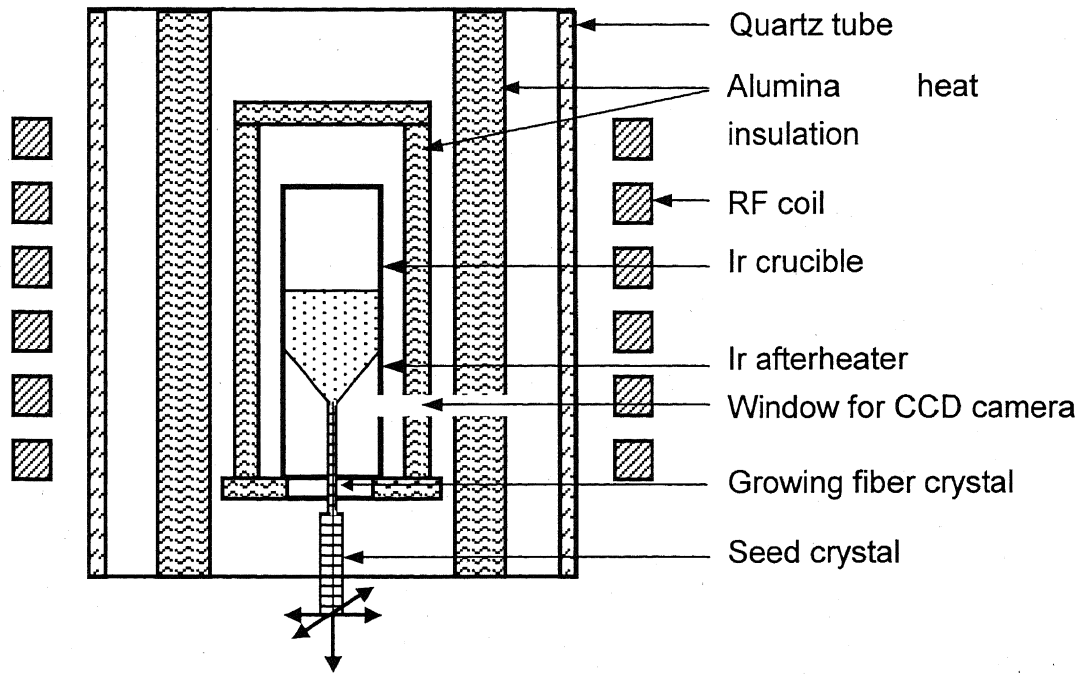

Fig. 4.5. Schematic diagram of the RF heated μ-PD apparatus with an Ir crucible. A window for CCD camera allows *in situ* observation of the crystal growth process [3].

precise alignment to the crucible bottom. The seed is brought into contact with the melt, which comes to the crucible tip through the orifice hole by capillary action. A small window for a CCD camera is made in the after-heater and the alumina ceramic shield. This enables observation of the hanging meniscus, the solid-liquid interface, and the growing crystal. Recent improvements of this method have made the quality of μ-PD crystals comparable with those prepared by CZ, Bridgman, or other classical growth techniques [4]. Several works on the successful growth of oxide crystals have demonstrated the advantages of this method. [5, 8-12]. From these, the following features were established:

(a) Owing to a fast growth speed, a high quality single crystal can be grown using less than 1 g of raw material in 5 – 12 hours, thereby allowing growth of large crystals at a shorter time and at a lower cost compared with other melt growth methods like CZ or BS. This very high growth speed makes this method a unique tool for single crystalline material screening.

(b) Moreover, this method has the capability to control the shape of the grown crystal to produce a fiber, rod, tube, and so on since the crucible not only serves as a container for the melt but also as a shaper (die) for shaped crystal growth [4]. Examples of crucibles and shaped crystals grown by this technique are shown in Fig. 4.6a and Fig. 4.6b, respectively.

(c) Repeated seeding can be utilized to produce a few crystals of similar length without cooling the hot zone to room temperature [13]. The design of the μ-PD machine allows sealing failure for 5-10 min without oxidation of the Ir crucible. The just-grown crystal is cut and removed, then the system is sealed again and the seeding procedure is repeated. The number of crystals grown is limited by the

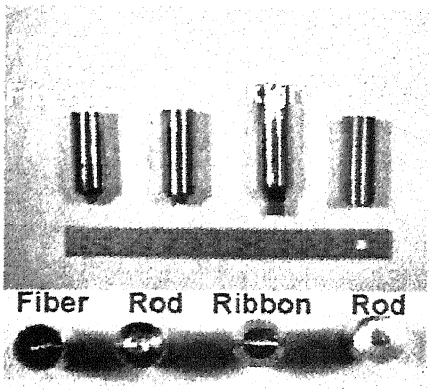

Fig. 4.6a. Crucibles used for shaped crystal growth

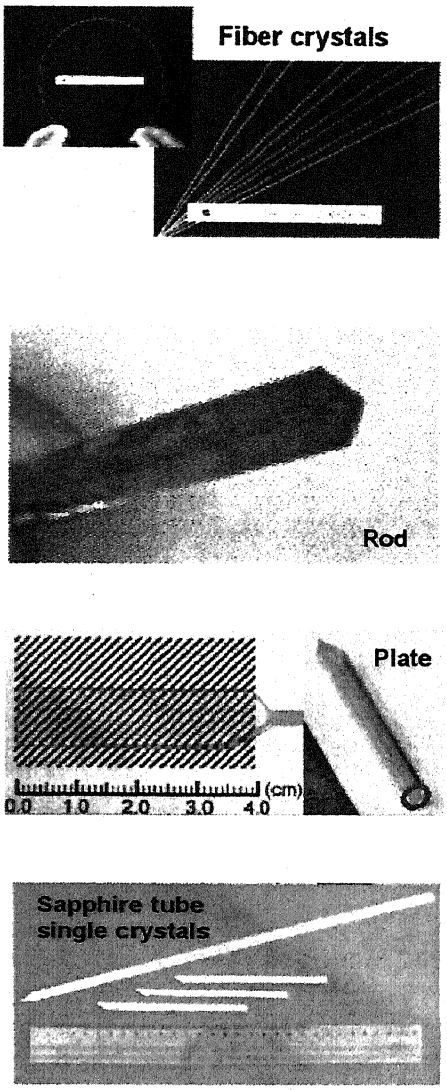

Fig. 4.6b. Shaped crystals grown by the μ-PD method

crucible charge.

(d) Lower thermal distortion decreases the density of cracks.

(e) The use of a narrow nozzle suppresses melt convection. For fast pulling rates, this leads to the effective segregation coefficient near unity and allows growth even from an incongruent melt composition.

(f) Crystal growth in the downward direction decreases the probability of bubble inclusion in the grown crystal because the lighter density of air bubbles compared to the melt causes them to rise to the top of the crucible.

(g) It is easy to add charge from the top of the crucible without disturbing the growing crystal. This would allow the growth of long fibers or crystals.

(h) By changing the nozzle, multiple crystals can be grown at the same time. Multi-crystal growth is demonstrated in Fig. 4.7.

A comparison between the CZ and the μ-PD methods are summarized in Table 4.1.

On the other hand, fluorides have found considerable attention because of their applications in various fields such as laser materials, optical materials for VUV, and just recently, as scintillators. Considering these applications, innovation of the μ-PD apparatus to accommodate fluoride crystal growth was carried out. Moreover, extensive research is put into the improvement of this method to facilitate the screening of fluoride host lattices, dopant concentration and optimization of the growth parameters. The concept is similar with the previously discussed growth scheme of oxide compounds. However, for fluoride crystal growth, the growth chamber has to be kept in vacuum. The growth chamber can be evacuated to 10^{-5} Torr by rotary and diffusion pumps in order to remove oxygen traces [5]. It is also equipped with a CaF_2 window to enable visual observation of the meniscus region, solid-liquid interface, and the growing

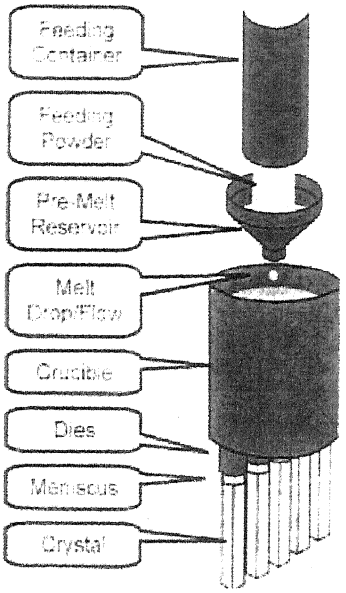

Schematic diagram for multiple crystal growth.

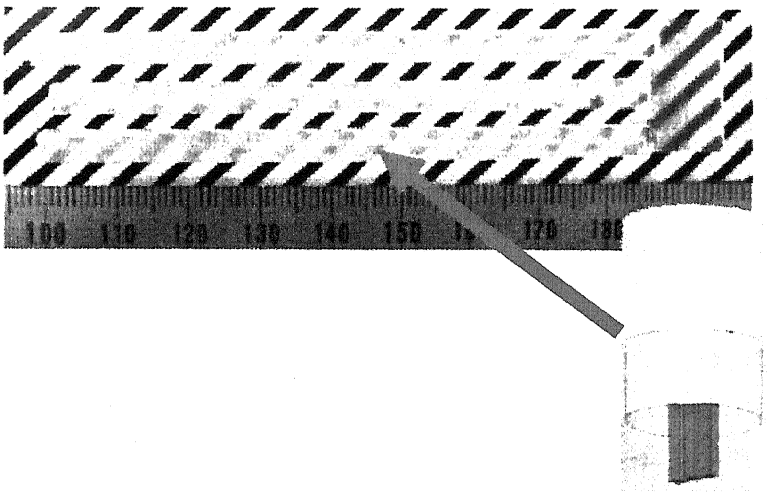

Fig. 4.7. Multiple crystals grown at the same time by the μ-PD method.

Table 4.1 Comparison between the CZ and the μ-PD methods

	CZ	μ-PD
Growth direction	Upward	Downward
Typical Growth rate	0.05 – 2 mm/hr	0.05-10 mm/min
Amount of raw material	plenty	< 1 g
Maximum crystal diameter	400 mm	0.05 - 10 mm
Maximum crystal length	1-2 m	1 m
Stage of development	Grow crystals for actual devices	Research stage for materials screening
Other characteristics	Large crystals	Shaped crystal growth, multi-crystal growth
	Less inclusion of heavy solid particles	Less inclusion of air bubbles
	batch charge of raw material	Continuous charging of raw material
	Large material loss (up to 40%) due to post-processing (cutting, polishing)	Low material loss, "ready to use" fibers

crystal by a CCD camera. Moreover, carbon or platinum was used as crucible material and the crucible is surrounded by refractory carbon and heated using a RF generator. A schematic diagram of the μ-PD apparatus modified for fluoride crystal growth is shown in Fig. 4.8. Although the μ-PD method is not as well developed and established as the CZ method, it has been proven useful for the growth of high-quality crystals particularly for materials screening. The demonstration of radio luminescence (RL) from a μ-PD grown Ce:PrF_3 shows that this method is capable of efficiently growing fluoride crystals for applications mentioned earlier [14].

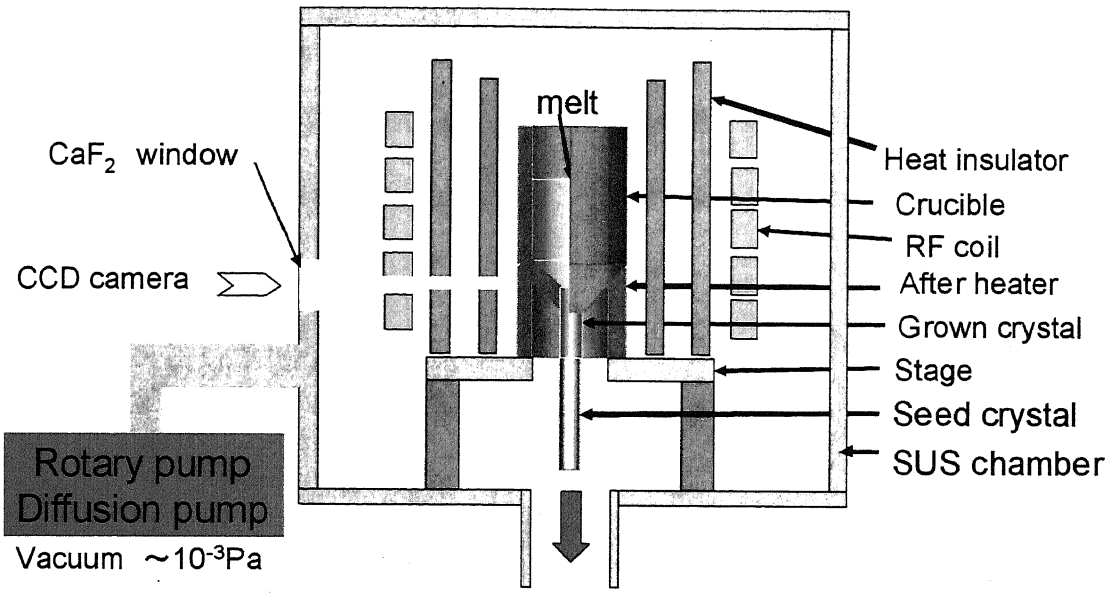

Fig. 4.8. The μ-PD apparatus modified for fluoride crystal growth.

References

[1] E. Talik, "Ninetieth anniversary of Czochralski method", J. Alloys Compd. **442** (2007) 70-73.

[2] T. Fukuda and V. Chani, *Advances in Materials Research, Shaped Crystals Growth by Micro-Pulling-Down Technique*, (Springer, Germany, 2007).

[3] A. Novoselov, A. Yoshikawa, and T. Fukuda, "The Micro-Pulling Down Method: Fast and Economic Solution for Materials Screening", Current Topics in Cryst. Growth Res. **7** (2004) 87-111.

[4] A. Yoshikawa, M. Nikl, G. Boulon, and T. Fukuda, "Challenge and study for developing of novel single crystalline optical materials using micro-pulling-down method", Opt. Mater. **30**, (2007) 6.

[5] B.M. Epelbaum, K. Inaba, S. Uda, and T. Fukuda, "Micro-pulling down growth studies of lead tungstate crystals: aspects of incongruent melt vaporization", J. Cryst. Growth, **178** (1997) 426.

[6] B.M. Epelbaum, K. Inaba, S. Uda, K. Shimamura, M. Imaeda, V.V. Kochurikhin, and T. Fukuda, "A double-die modification of micro-pulling-down method for in situ clad/core doping of fiber crystal", J. Cryst. Growth, **179** (1997) 559.

[7] N. Schafer, T. Yamada, K. Shimamura, H.J. Koh, and T. Fukuda, "Growth of Si_xGe_{1-x} crystals by the micro-pulling-down method", J. Cryst. Growth, **166** (1996) 675.

[8] D.H. Yoon, M. Hashimoto, T. Fukuda, "Growth and Characterization of $K_3Li_{2-x}Nb_{5+x}O_{15+2x}$ Micro Single Crystals Formed by the μ-Pulling Down Method for Blue SHG Applications", Jpn. J. Appl. Phys, **33** (1994) 3510.

[9] B. M. Epelbaum and D. Hofmann, "Facet formation during fiber pulling from the melt", J. Crystal Growth **237-239** (2002) 2098.

[10] A. Yoshikawa, T. Akagi, M. Nikl, N. Solovieva, K. Lebbou, C. Dujardin, C. Pédrini and T. Fukuda, "$\{Y_{3-x},Yb_x\}[Ga]_2(Ga)_3O_{12}$ and $\{Lu_2Yb_1\}[Al]_2(Al)_3O_{12}$ single crystals for scintillator application grown by the modified micro-pulling-down method", Nucl. Instrum. Methods Phys. Res. A **486** (2002) 79.

[11] J. W. Shur, T. I. Shin, S. M. Lee, S. W. Baek and D. H. Yoon, "Photoluminescence properties of Nd: $LiNbO_3$ co-doped with ZnO fiber single crystals grown by micro-pulling-down method", Mater. Sci. Eng. B **105** (2003)16.

[12] A. Yoshikawa, H. Itagaki, T. Fukuda, K. Lebbou, A. El Hassouni, A. Brenier, C. Goutaudier, O. Tillement and G. Boulon, "Synthesis, crystal growth and second harmonic generation properties of trivalent rare-earth-doped non-linear tungsten–bronze-type structure $Ba_2Na_{1-3x}RE_xNb_5O_{15}$ (RE=Sc, Y, La, Gd, Yb and Lu)", J. Crystal Growth **247** (2003)148.

[13] V. I. Chani, A. Yoshikawa, Y. Kuwano, K. Hasegawa, and T. Fukuda, "Growth of $Y_3Al_5O_{12}$:Nd fiber crystals by micro-pulling-down technique", J. Crystal Growth **204** (1999)155.

[14] A. Yoshikawa, T. Satonaga, K. Kamada, H. Sato, M. Nikl, N. Solovieva, and T. Fukuda, "Crystal growth of Ce:PrF_3 by micro-pulling-down method", J. Cryst. Growth **270** (2004) 427.

Chapter 5. Methodology

In this chapter, the procedure, apparatus, and experimental set-up for the growth and characterization of Nd^{3+}-doped crystals are presented.

5.1. Transmission measurements

Transmission measurements were performed at the BL7B beam line of the ultraviolet synchrotron orbital radiation facility (UVSOR) at the Institute for Molecular Science. A 1-m focal length Seya-Namioka monochromator operating at room temperature was used. The beam flux at the sample position was about 10^{10} photons/s around 200nm with a 0.1 mm slit. To obtain the transmission spectra, the Seya-Namioka monochromator was used to select the excitation wavelength and the transmitted signal was detected by a photomultiplier. These apparatus were aligned collinearly and were placed in a chamber that is evacuated to better than $1x10^{-9}$ Torr by an ion pump. The absorption edge was defined as the onset of transmission drop from the level of the longest wavelength. It is estimated from the intersection of a linear fit to the flat transmission at long wavelength and a linear fit to the steepest observed transmission drop.

5.2 Fluorescence spectral measurements

The schematic diagram for fluorescence measurement is shown in Fig. 5.1. A F_2 laser (PSX-100) operating at 157 nm, a repetition rate of 100 Hz, a pulse energy of 1 mJ, and a pulse duration of 5-ns excites the sample placed inside a vacuum chamber. The temporal characteristics of the F_2 laser used is shown in Fig. 5.2. Furthermore, the optical path from the laser to the vacuum chamber is purged with N_2 gas to prevent the

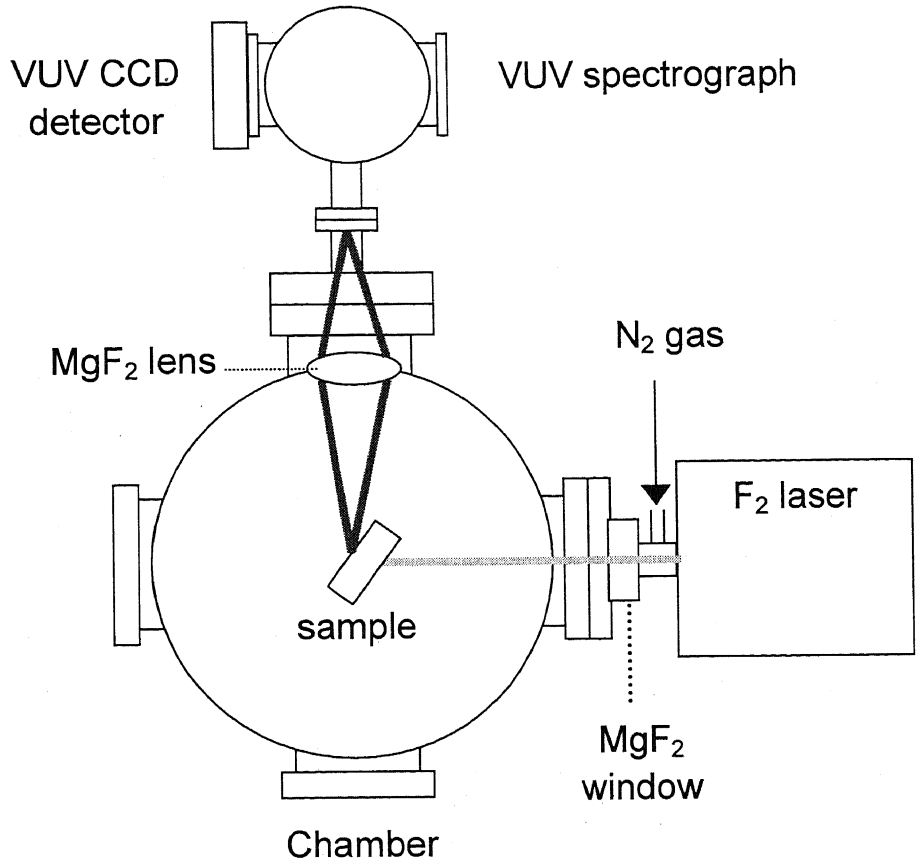

Fig. 5.1. Schematic diagram for measuring the fluorescence spectrum using an F_2 laser excitation.

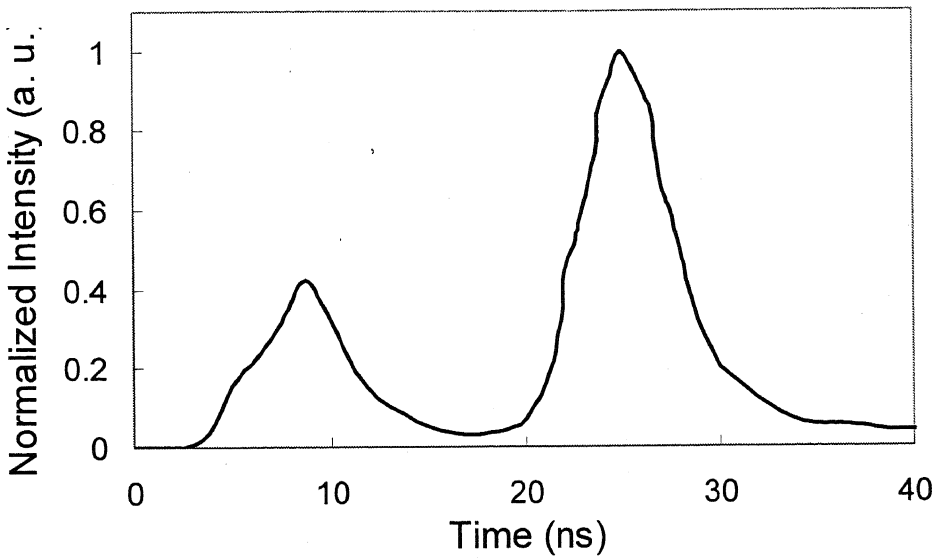

Fig. 5.2. Temporal profile of the F_2 excitation laser. The stronger peak is the 157-nm excitation pulse with a pulse width of 5 ns. The weaker peak comes from the inherent red light (700 nm) emission from fluorine ions.

absorption of the 157-nm excitation by oxygen. A MgF_2 lens then collects and focuses the fluorescence onto the entrance slit of a spectrograph with 1 nm resolution. A VUV charge-coupled device (CCD) array detects the fluorescence spectrum. In all measurements, the spectrum is corrected for the spectrograph and CCD detector spectral responses.

For further investigation of the feasibility of an all-solid-state VUV laser, Nd^{3+}:LaF_3 is excited by a Ti:sapphire regenerative amplifier. For the case of femtosecond excitation, the 290-nm pulses (third harmonic) operating at 1 KHz, 30 mW (30 μJ), 100 fs pulses were used to excite a 3mmx3mmx3cm cuboid Nd^{3+}:LaF_3. A 20 cm focusing lens was used to focus the pulses from the top view port onto the top of the crystal. The schematic diagram is also shown in Fig. 5.3

5.3 Fluorescence temporal measurements

Temporal measurements to determine the fluorescence lifetimes are performed using a specially designed VUV Seya-Namioka spectrometer and streak camera combination. Optical materials typically used in streak camera units are UV-grade and are thus highly absorbent at wavelengths below 200 nm. To address this issue, reflection type input optics and MgF_2 windows were used. Moreover, since VUV radiation is strongly absorbed by oxygen, a vacuum chamber from the input slit to the streak tube was designed. The VUV spectrometer has a Seya-Namioka type holographic grating with a groove density of 600 gr/mm and a linear dispersion of 8 nm/mm. It covers the spectral range from 100 to 600 nm wavelength region with a spectral resolution of 1 nm. The imaging unit consists of Al and MgF_2-coated mirrors with greater than 80% single reflection from 125 to 850 nm. The effective F number is 4. The streak camera system

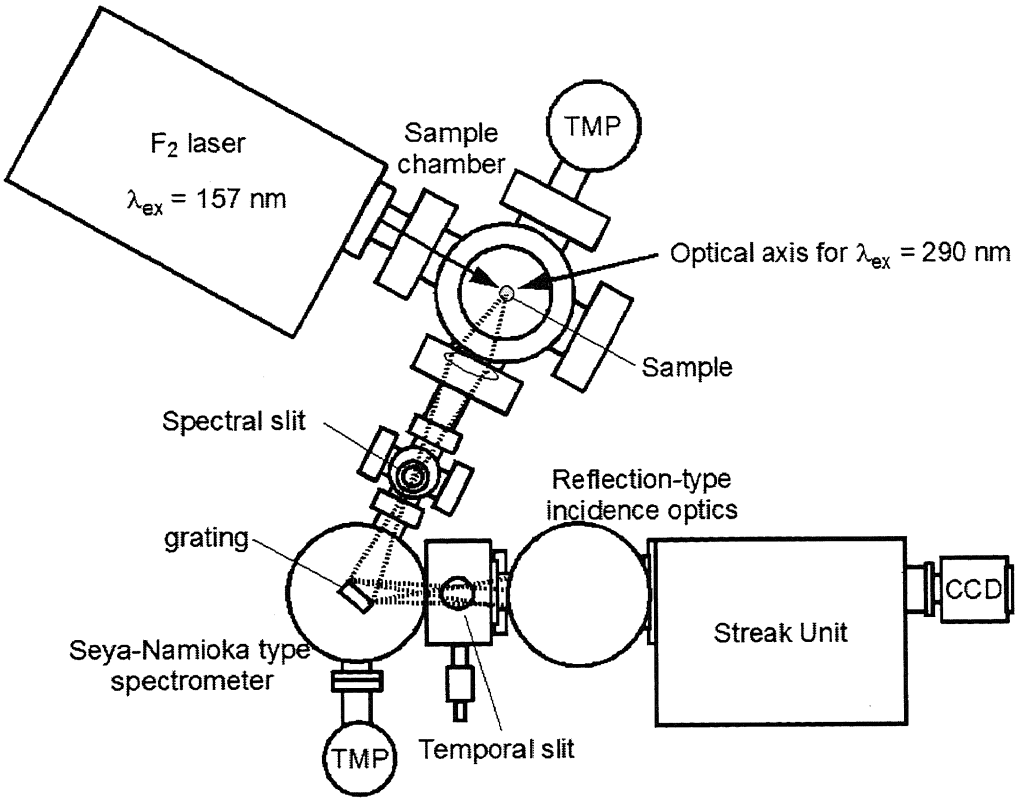

Fig. 5.3. Schematic diagram of the Seya-Namioka spectrometer and streak camera combination used to capture the streak camera image as well as to measure the temporal profile of the fluorescence. The crystal is pumped with the F_2 laser and the third harmonics of a Ti:sapphire regenerative amplifier during independent experiments.

has two kinds of scan units. One scan unit is for synchronized scanning. It can measure high repetition rate events synchronously between 75 MHz to 165 MHz. According to specifications, the rated temporal resolution is 2 ps at 800 nm. The other scan unit is the slow scan speed unit, which can measure an event or a single shot up to 2MHz. According to specifications, the rated temporal resolution is 50 ps or less. The spectrometer is connected to the vacuum chamber where the fluoride sample is placed. The schematic diagram of the streak camera system is shown in Fig. 5.3. The entire system is maintained at a vacuum level of 10^{-6} Torr. Since the streak camera displays the streak image in pixels, the captured image must be calibrated spectrally and temporally in order to display the axes in wavelength (nm) and time (ns). Spectral calibration is achieved by measuring the streak image of a source with known wavelength. On the other hand, temporal calibration is achieved by recording streak images at two consecutively known time intervals.

5.4 Fluoride crystal growth by the micro-pulling down method

The μ-PD apparatus modified for fluoride crystal growth that was shown in Fig. 4.8. High purity LaF_3, BaF_2, and NdF_3 at a molar ratio of 90:10:1 are prepared as starting materials for obtaining Nd^{3+}:$(La_{1-x},Ba_x)F_{3-x}$ (x=0.1) or Nd^{3+}:$(La_{0.9},Ba_{0.1})F_{2.9}$. They are thoroughly mixed and placed inside a graphite crucible. The growth chamber is then evacuated to 10^{-4} Torr using rotary and diffusion pumps. By radio frequency (RF) heating, the crucible is baked at 600 °C for 1 hour in order to remove oxygen traces from the moisture of raw materials and adsorbates on the chamber surface. Simultaneously, the chamber is further evacuated to 10^{-5} Torr. After baking, the recipient is filled with a mixture of non-reactive gases Ar and CF_4, until ambient pressure. The crucible is heated

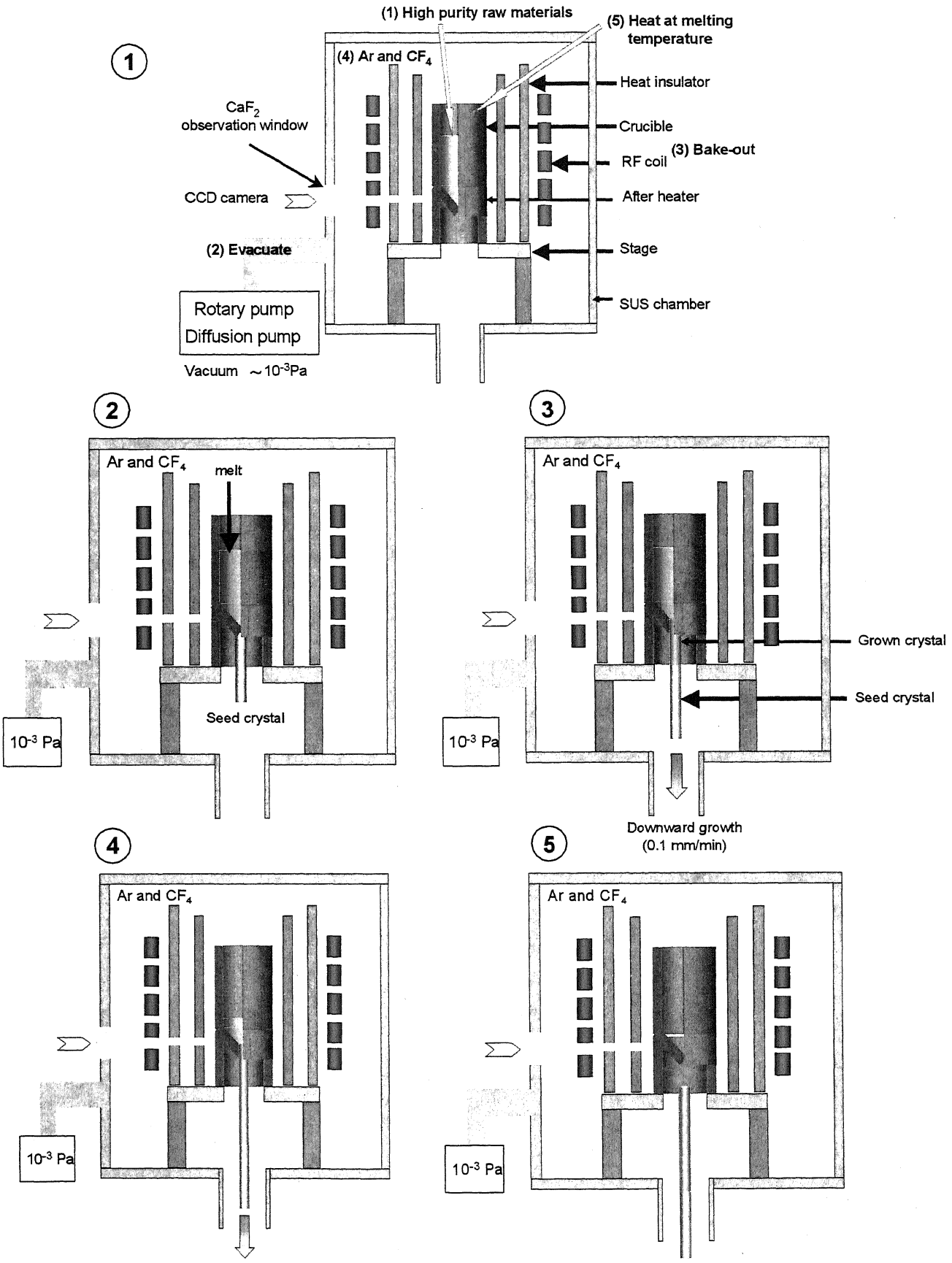

Fig. 5.4. Growth of fluoride crystals by the μ-PD method.

to a melting temperature of about 1450 °C. The crystal is grown with a pulling rate of 0.1 mm/min and with complete solidification of the melt charged in the crucible. A summary of the growth process is shown in Fig. 5.4

The phase diagram for the LaF_3-BaF_2 system, shown in Fig. 5.5, indicates that $La_{(1-x)}Ba_xF_{3-x}$ with $0.2< x <0.5$ is eutectic [1]. This automatically discriminates against barium ratios from 20% to 50% since at these ratios, the constituents exist as a liquid for temperatures greater than 1390 °C. However, as the temperature is decreased during the growth process, the melt then start to solidify into its different constituents, thereby producing an incongruent crystal. An option is to use barium ratios from 50% to 100%. However, spectroscopic results for crystals with these ratios, as shown in Fig. 5.6, indicate that the transmission property of the crystal in the VUV region is not improved. Less than 20% Barium ratios seem to be the best. During the actual growth process, the crystal is already cloudy when $x = 0.15$; thus $x = 0.1$ was chosen.

For comparison, a Nd^{3+}:LaF_3 crystal is also grown from a stoichiometric mixture of high-purity LaF_3 and NdF_3.

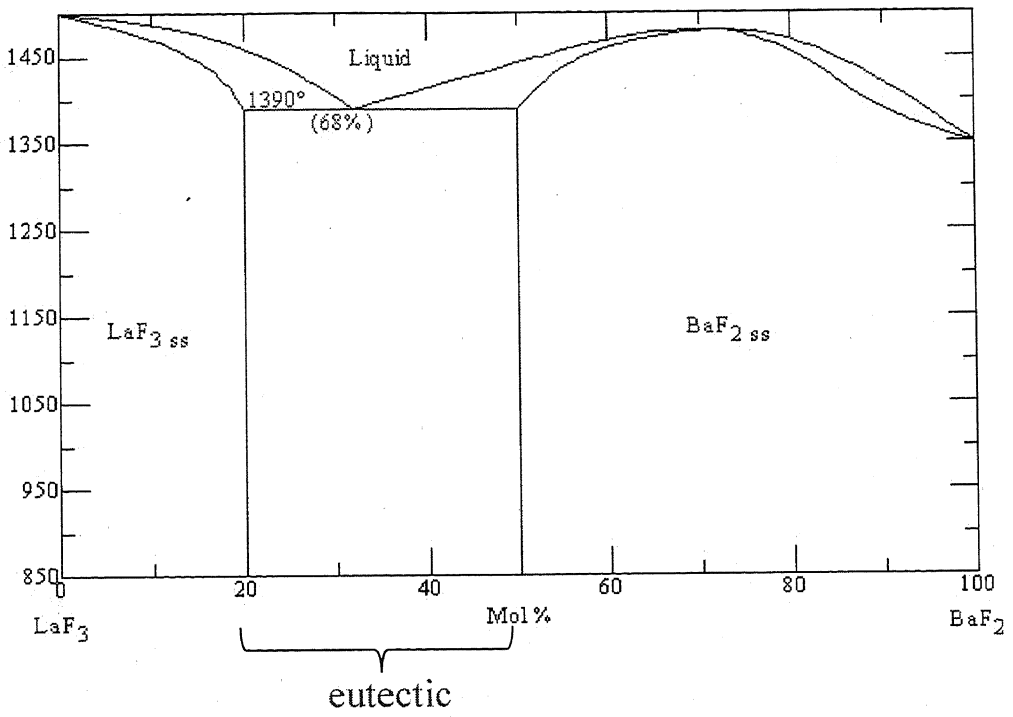

Fig. 5.5. Phase diagram of a LaF_3-BaF_2 system. It is eutectic at Barium ratios from 20%<x<50% [1].

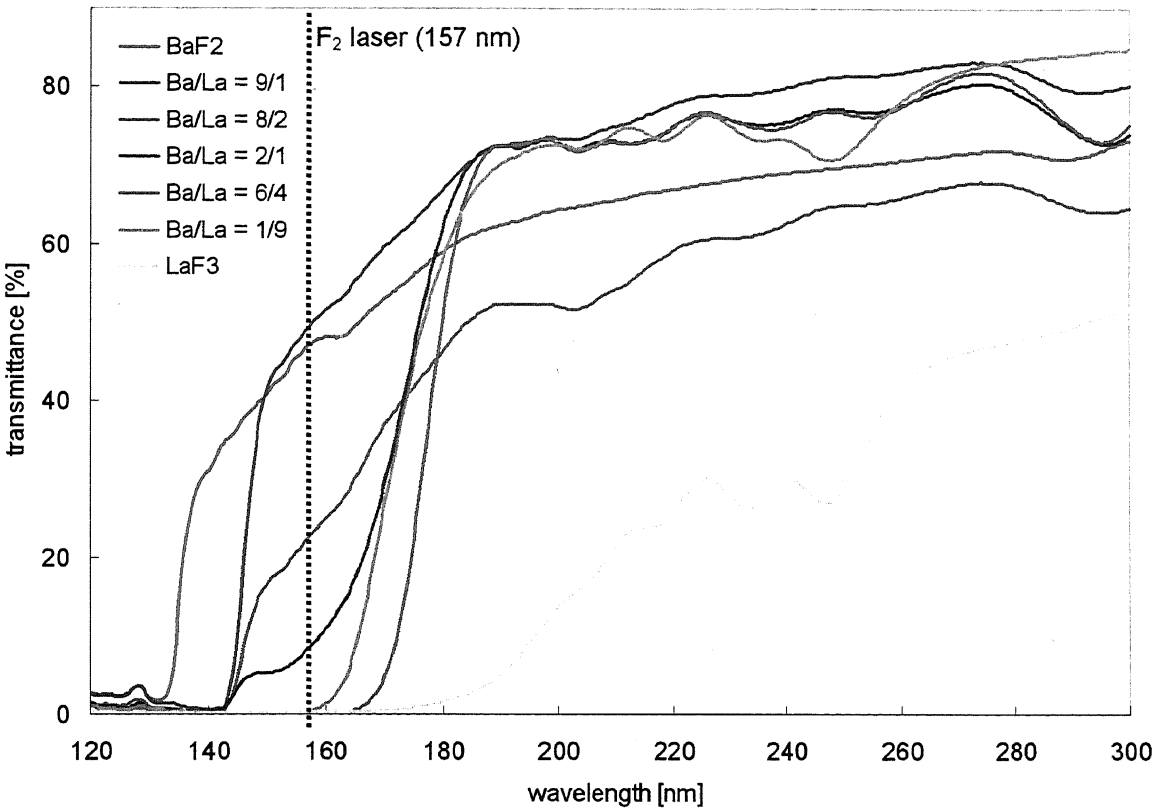

Fig. 5.6. Effect of different Barium/Lanthanum ratios on the transmission characteristics of $La_{(1-x)}Ba_xF_{3-x}$. The LaF_3 curve is included to provide a measure on its transmission range that starts from 170nm.

References

[1] B. P. Sobolev and N. L. Tkachenko, "Phase diagrams of BaF_2-(Y, Ln)F_3 systems," J. Less-Common Met. **85**, 155-170 (1982).

Chapter 6. Characterization of Nd^{3+}-doped Fluorides

The first step in the development of a new laser material is the characterization of its optical properties. Two CZ method-grown fluoride crystals namely, Lanthanum Fluoride (LaF_3) and Yttrium Lithium Fluoride ($YLiF_4$) and two μ-PD method-grown fluorides namely Lanthanum Barium Fluoride ($(La_{1-x},Ba_x)F_{3-x}$) and LaF_3, all doped with Neodymium (Nd^{3+}) ions are investigated and characterized in terms of absorption, VUV fluorescence, and fluorescence lifetime.

6.1. Optical properties of CZ method-grown Nd^{3+}:LaF_3

Figure 6.1 shows the absorption spectrum for a 1 mm thick Nd^{3+}:LaF_3. It has an absorption edge at 168 nm. This was estimated using the technique described in Section 5.1. Its ability to absorb strongly around 157 nm makes the F_2 laser a good pumping source for observing fluorescence from Nd^{3+}:LaF_3. The absorption cross section, σ_A, at the proposed 157-nm excitation wavelength is 3.2×10^{-19} cm^2. It was calculated using

$$\sigma_A = \alpha/n \ , \qquad (6.1)$$

where α is the absorption coefficient and n is the number of absorbers or number density, which is related to the doping concentration.

The fluorescence spectrum of Nd^{3+}: LaF_3 is shown in Fig. 6.2. Fluorescence peak in the VUV region is observed at 172 nm, which is in good agreement with previous reports [1-3]. This observed fluorescence peak originates from the $4f^25d \rightarrow 4f^3$ electric dipole-allowed transitions of the Nd^{3+} ions. 172 nm (58×10^3 cm^{-1}) corresponds to the dipole allowed transition from the $4f^25d$ configuration to the $^4I_{11/2}$ manifold of the $4f^3$ configuration. The simplified energy-level diagram of Nd^{3+} ions in LaF_3 indicating

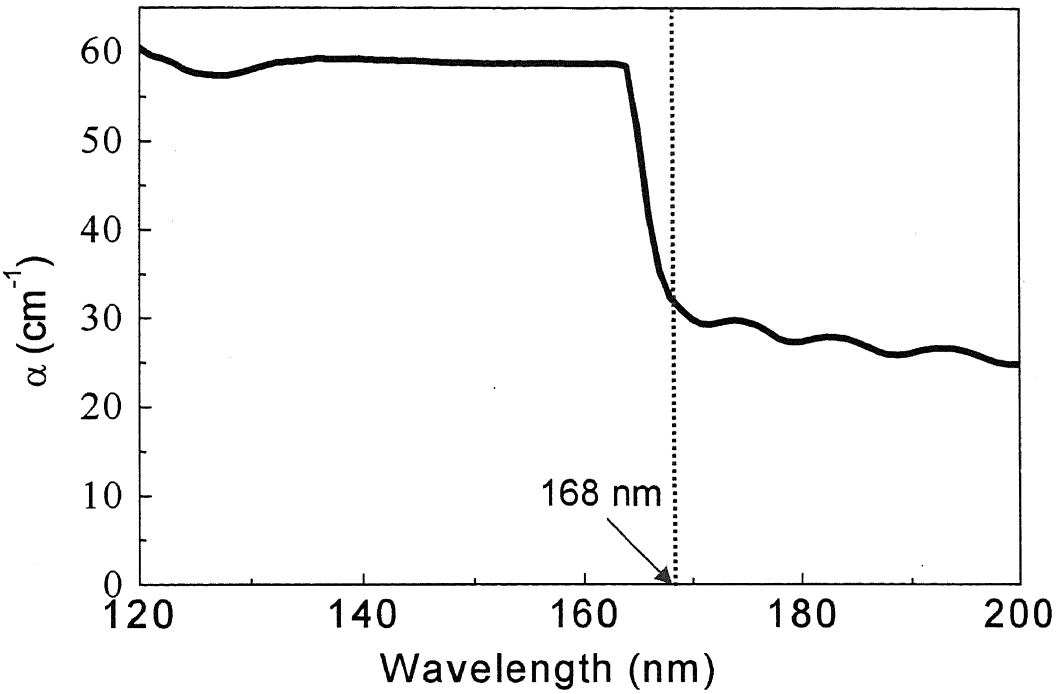

Fig. 6.1. Absorption spectra of a 1 mm thick, CZ method-grown Nd^{3+}:LaF_3.

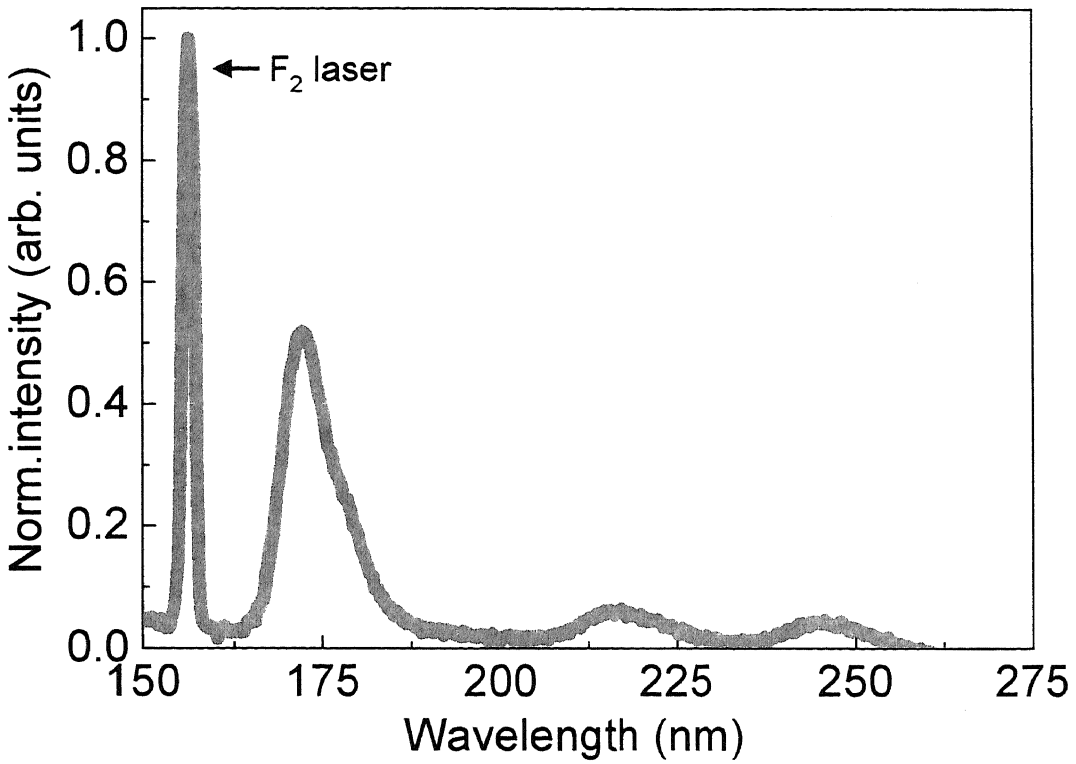

Fig. 6.2. Fluorescence spectra of Nd^{3+}: LaF_3. Strongest fluorescence peak is located at 172 nm.

the absorption at 157 nm and the emission transition at 172 nm is shown in Fig. 6.3.

The fluorescence temporal profile is shown in Fig. 6.4 and the fluorescence lifetime is determined to be 9.85 ns. This corresponds to when the fluorescence signal decays to 1/e.

6.2. Optical properties of CZ method-grown Nd^{3+}:$YLiF_4$

The absorption spectrum of the 13 mm thick Nd^{3+}:$YLiF_4$ sample is shown in Fig. 6.5. The absorption edge is at 181 nm. This absorption edge was also estimated using the technique described in Section 5.1. Also, the 157 nm emission from the F_2 laser is a suitable pump for observing fluorescence. The absorption cross section at 157 nm is 1.67×10^{-20} in accordance with Eqn. 6.1.

Figure 6.6 shows the fluorescence from Nd^{3+}:$YLiF_4$. In contrast to Nd:LaF_3, two fluorescence peaks are observed in the DUV region. The dominant peak is at 181 nm while the weaker peak is at 185 nm. The peak at 181 nm (55×10^3 cm^{-1}) comes from the transition from the lowest level of $4f^2 5d$ configuration to the $^4I_{9/2}$ manifold of the $4f^3$ configuration. On the other hand, the peak at 185 nm (54×10^3 cm^{-1}) arises from the transition between the $4f^2 5d$ configuration to the $^4I_{11/2}$ manifold of the $4f^3$ configuration. These transitions are indicated on the simplified energy-level diagram of Nd^{3+} ions in $YLiF_4$ shown in Fig. 6.7.

The temporal profile is shown in Fig. 6.8. Fluorescence lifetime is determined to be 21.79 ns.

Table 6.1 shows a summary of the optical properties of these two materials. Although Nd^{3+}:$YLiF_4$ has a lower absorption cross section at its emission wavelength (181 nm) and a longer lifetime compared with Nd^{3+}:LaF_3, it has a longer absorption

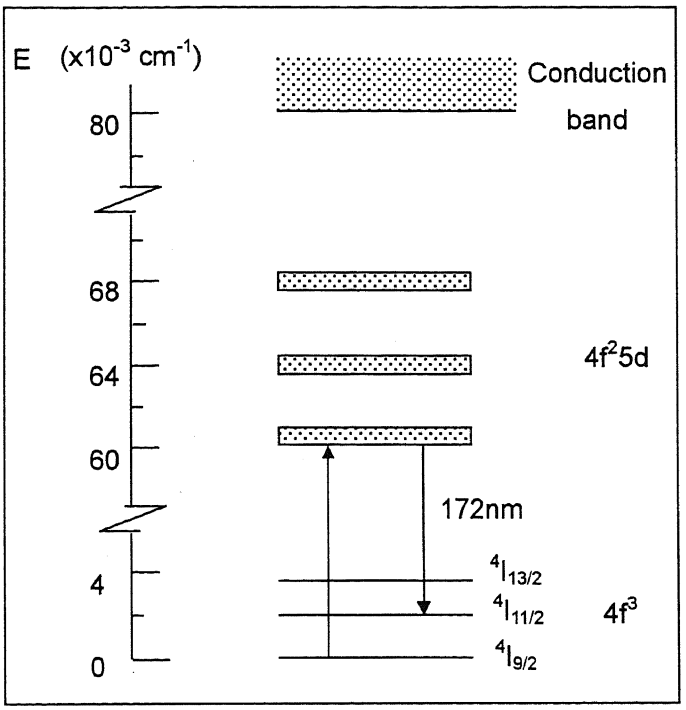

Fig. 6.3. Energy level diagram of Nd^{3+}: LaF_3 showing the allowed transition resulting to fluorescence at 172 nm.

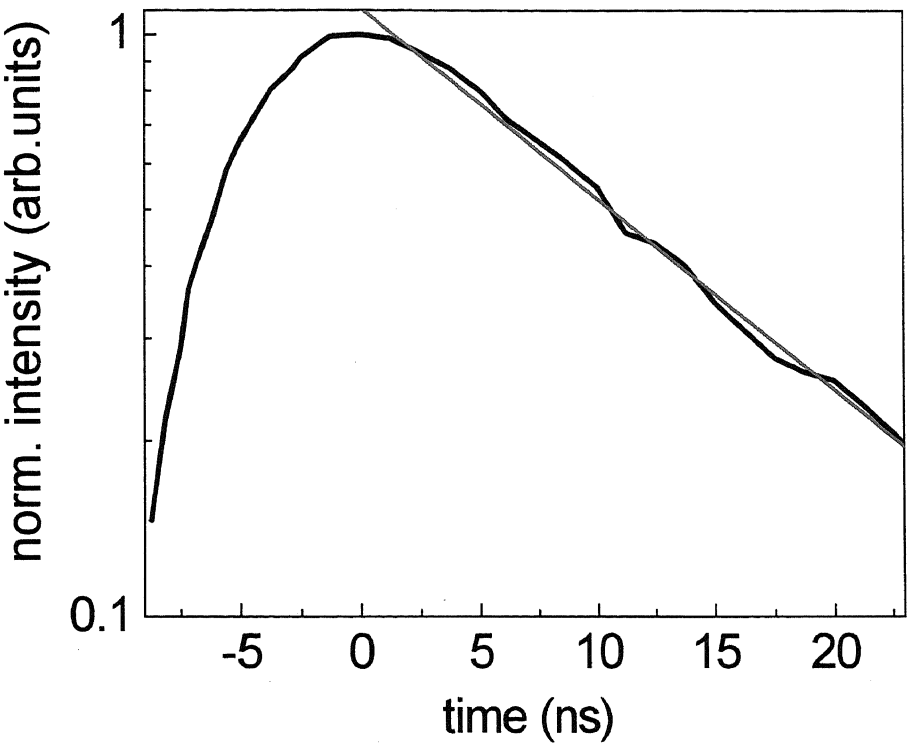

Fig. 6.4. Temporal profile for the decay of Nd^{3+}: LaF_3 fluorescence. Lifetime is 9.85 ns.

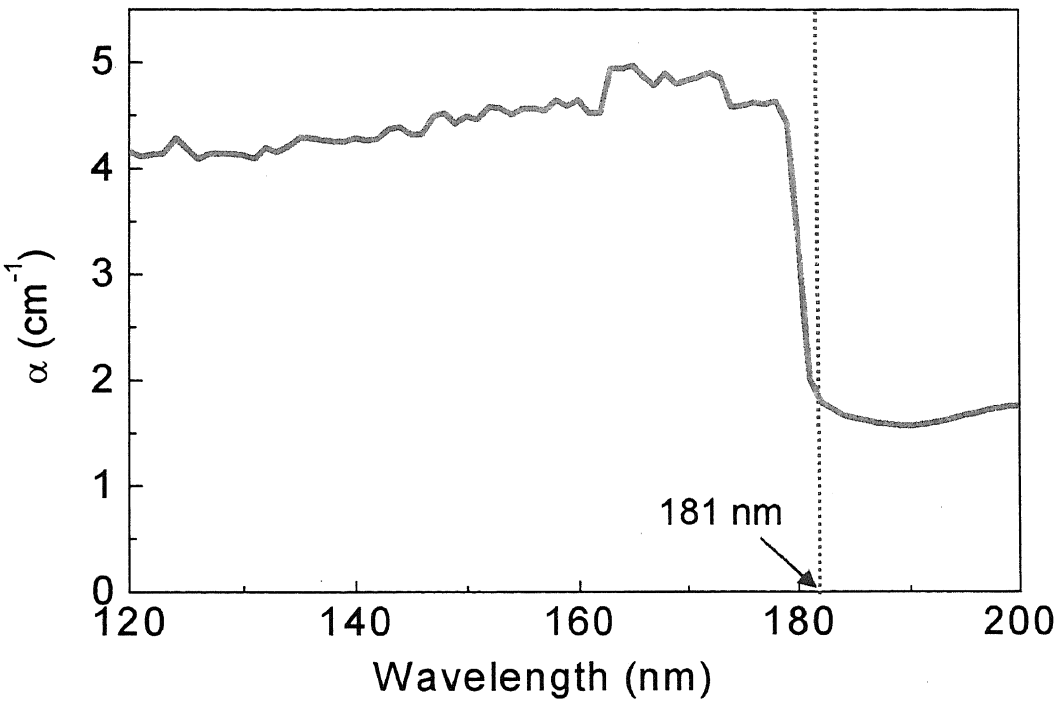

Fig. 6.5. Absorption spectra of a 13 mm thick, CZ method-grown Nd^{3+}:$YLiF_4$.

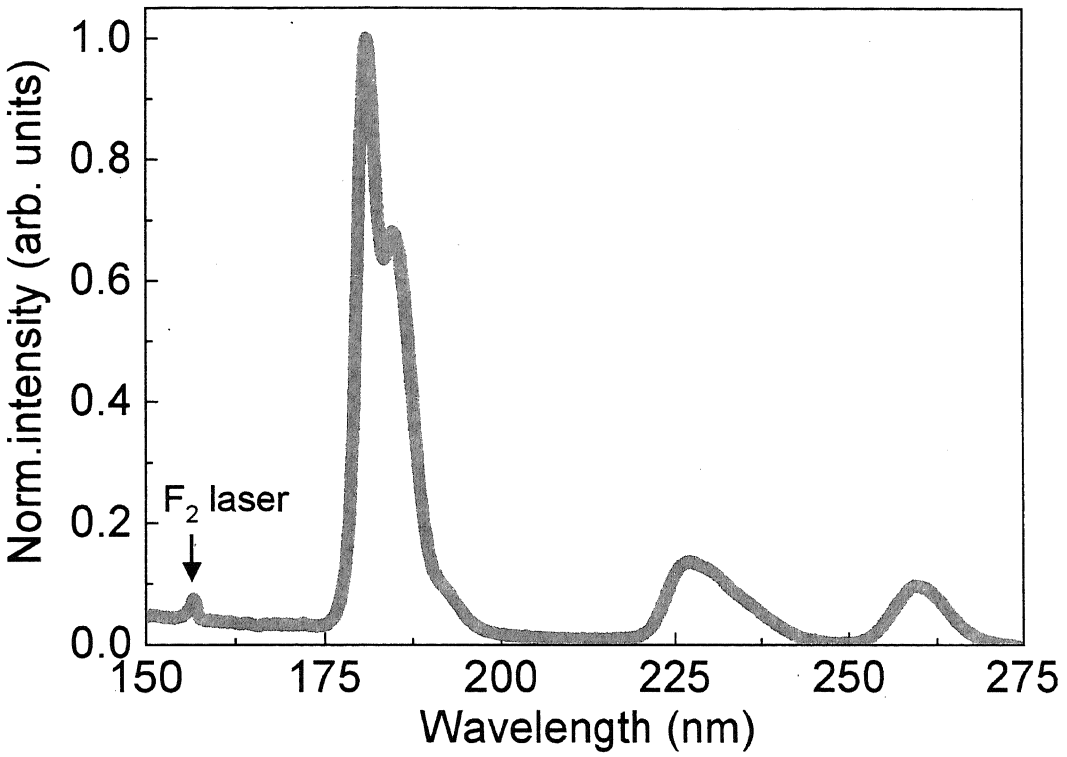

Fig. 6.6. Fluorescence spectra of Nd^{3+}: $YLiF_4$. Strongest fluorescence peak is located at 181 nm.

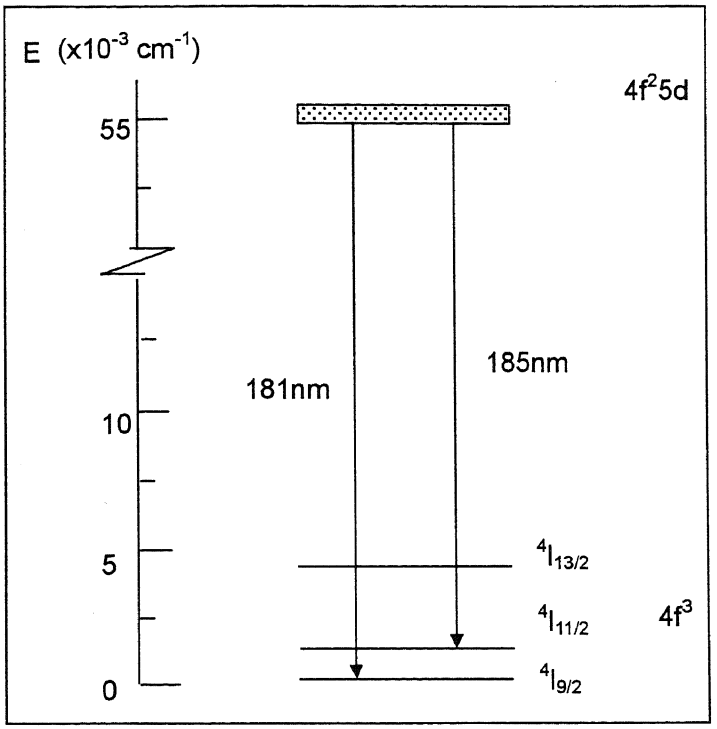

Fig. 6.7. Energy level diagram of Nd^{3+}: $YLiF_4$ showing allowed transition giving rise to fluorescence at 181 nm and 185 nm.

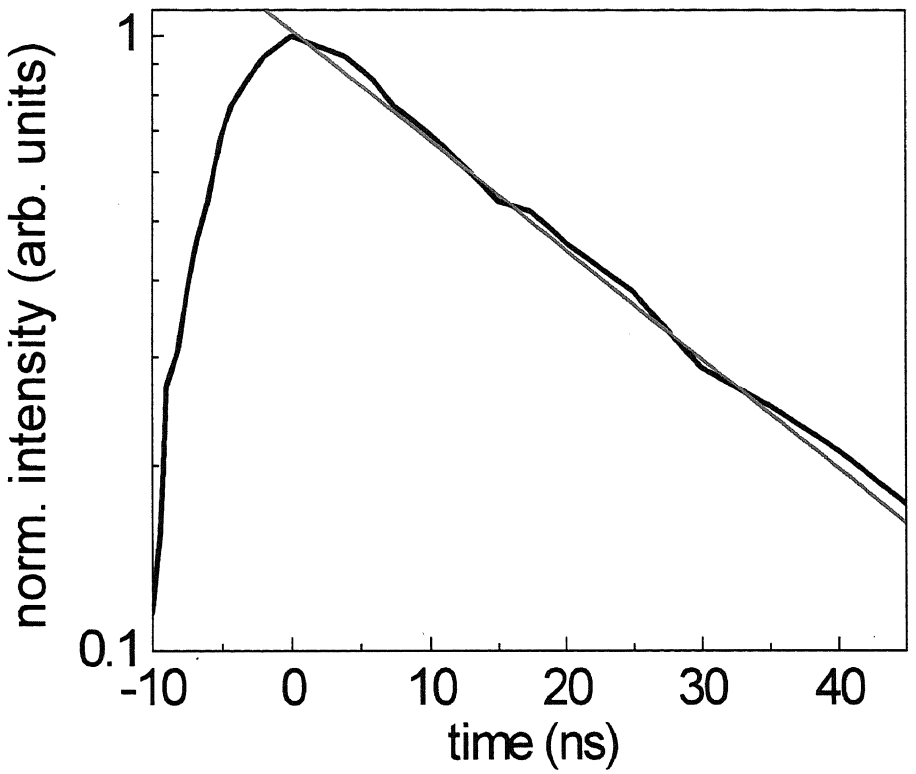

Fig. 6.8. Temporal profile for the decay of Nd^{3+}: $YLiF_4$ fluorescence. It has a lifetime of 21.79 ns.

Table 6.1. Summary of the optical characteristics of CZ method-grown Nd^{3+}:LaF and Nd^{3+}:$YLiF_4$.

	Nd^{3+}:LaF_3	**Nd^{3+}:$YLiF_4$**
Absorption edge [nm]	168	181
Absorption cross section at 157 nm [cm^{-2}]	3.24×10^{-19}	1.67×10^{-20}
Emission wavelength [nm]	172	181
Absorption cross section at emission wavelength [cm^{-2}]	2.71×10^{-20}	7.40×10^{-21}
Lifetime [ns]	9.85	21.79

edge, a lower absorption cross section at the proposed pump wavelength (157 nm), and a longer emission wavelength at 181 nm. In this regard, Nd^{3+}:LaF_3 has better prospects as a VUV laser material.

The feasible strategy is to consider LaF_3 host with the addition of BaF_2 to shift the transmission edge to a shorter wavelength. Since barium has a smaller atomic number compared to lanthanum, it follows from the discussion in Section 2.1 that BaF_2 would have a wider band gap compared with LaF_3 and hence, a shorter wavelength transmission edge.

In order to facilitate the growth and characterization of this new material, the μ-PD method is used because of its merits as discussed in Section 4.2.

6.3. Optical properties of μ-PD method-grown Nd^{3+}:$(La_{0.9},Ba_{0.1})F_{2.9}$ and Nd^{3+}:LaF_3

The samples used in our experiments are shown in Fig. 6.9. They are both 1 mol.% Nd^{3+}-doped. They are 20 mm in length and 2 mm in diameter. They were grown as described in Section 5.4. None of the samples have visible cracks or inclusions.

Figure 6.10 shows the absorption coefficient, α, of a 1-mm thick $(La_{0.9},Ba_{0.1})F_{2.9}$, LaF_3, and BaF_2 in the VUV region. Their absorption edges are estimated to be about 180 nm, 210 nm, and 138 nm for $(La_{0.9},Ba_{0.1})F_{2.9}$, LaF_3, and BaF_2, respectively. Clearly, $(La_{0.9},Ba_{0.1})F_{2.9}$ has a shorter wavelength absorption edge compared to LaF_3. This indicates that it will have better VUV transmission characteristics, given the same doping ion. Moreover, its short wavelength absorption edge makes it more suitable as a short wavelength solid-state optical material.

For 1 mol.% Nd doping concentration, the number density of Nd^{3+} ions in

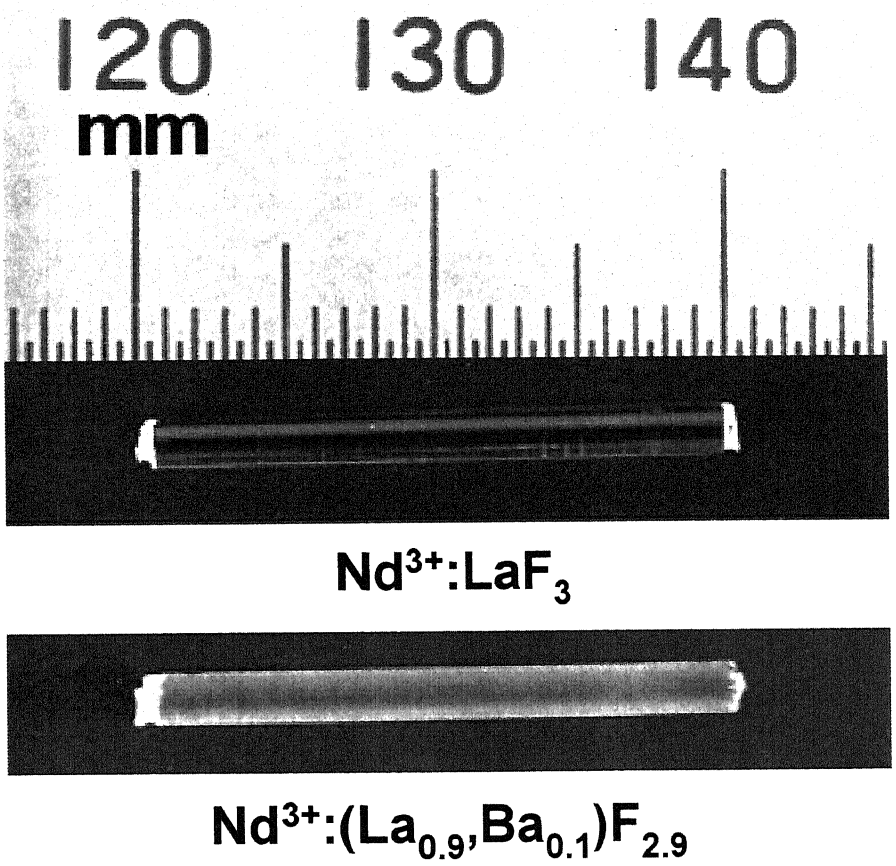

Fig. 6.9. Photographs of (a) Nd^{3+}:$(La_{0.9},Ba_{0.1})F_{2.9}$ and (b) Nd^{3+}:LaF_3 crystals. Both samples are 20 mm in length and 2 mm in diameter. Neither has visible cracks nor inclusions.

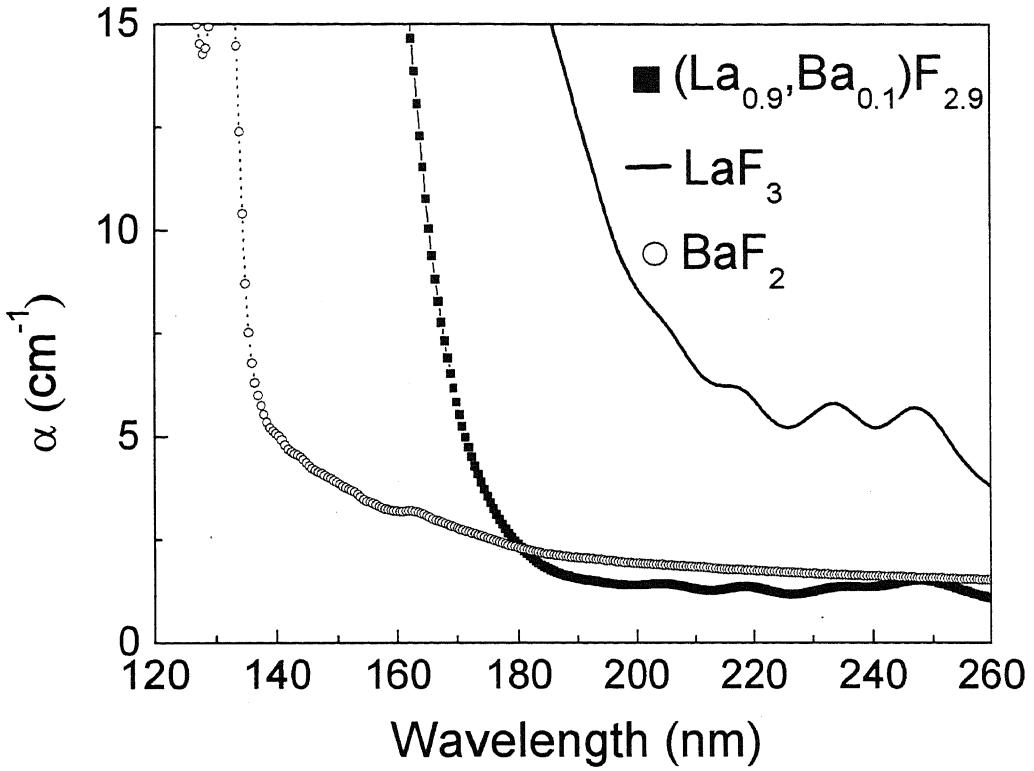

Fig. 6.10. Absorption spectra of 1-mm thick $(La_{0.9},Ba_{0.1})F_3$, LaF_3, and BaF_2 hosts with absorption edges at 180 nm, 210nm, and 138 nm, respectively.

$(La_{0.9},Ba_{0.1})F_{2.9}$ and LaF_3 host is $1.65x10^{20}$ cm^{-3} and $1.81x10^{20}$ cm^{-3}, respectively and their absorption cross sections at the proposed excitation wavelength, 157 nm, is $7.4x10^{-20}$ cm^2 and $6.86x10^{-20}$ cm^2, respectively. This means that Nd^{3+}:$(La_{0.9},Ba_{0.1})F_{2.9}$ would have better absorption at the excitation wavelength.

Figure 6.11 shows the VUV fluorescence from the Nd^{3+}:$(La_{0.9},Ba_{0.1})F_{2.9}$ sample. The plot also shows the scattered excitation for reference. This is the 157 nm excitation that reached the detector after being scattered from the surface of the sample. By considering the energy levels of Nd^{3+} activator ions as well as the selection rules for angular momentum and spin, the broad peaks can be attributed to interconfigurational transitions from the $4f^25d$ excited state configuration to the different manifolds of the $4f^3$ ground state configuration while the sharp peaks are characteristic of intraconfigurational transitions within the manifolds of the $4f^3$ configuration. The most intense peak located at 178 nm may be attributed to the allowed dipole transition from the $4f^25d$ configuration to the $^4I_{15/2}$ manifold of the $4f^3$ configuration [4].

Using the same set up, the fluorescence spectrum from Nd^{3+}:LaF_3 shown in Fig. 6.12 is obtained. Its VUV fluorescence peak is located at around 175 nm, which is close to that from previous reports [1-3] and also with the CZ-grown crystal discussed earlier. A slight shift in the peak position could be due to the difference in doping concentration. The effect of doping concentration will be discussed in detail in Section 6.5. The figure also shows the spectrum form Nd^{3+}:$(La_{0.9},Ba_{0.1})F_{2.9}$, for comparison. The red shift in the Nd^{3+}:$(La_{0.9},Ba_{0.1})F_{2.9}$ fluorescence peak may be due to the effect of BaF_2. The transmission of a BaF_2 host is shown in Fig. 6.10 for reference. Nd^{3+}:$(La_{0.9},Ba_{0.1})F_{2.9}$ is observed to have a more intense and broader fluorescence compared with Nd^{3+}:LaF_3. It has a fluorescence bandwidth (full width at half maximum) of 12 nm while Nd^{3+}:LaF_3

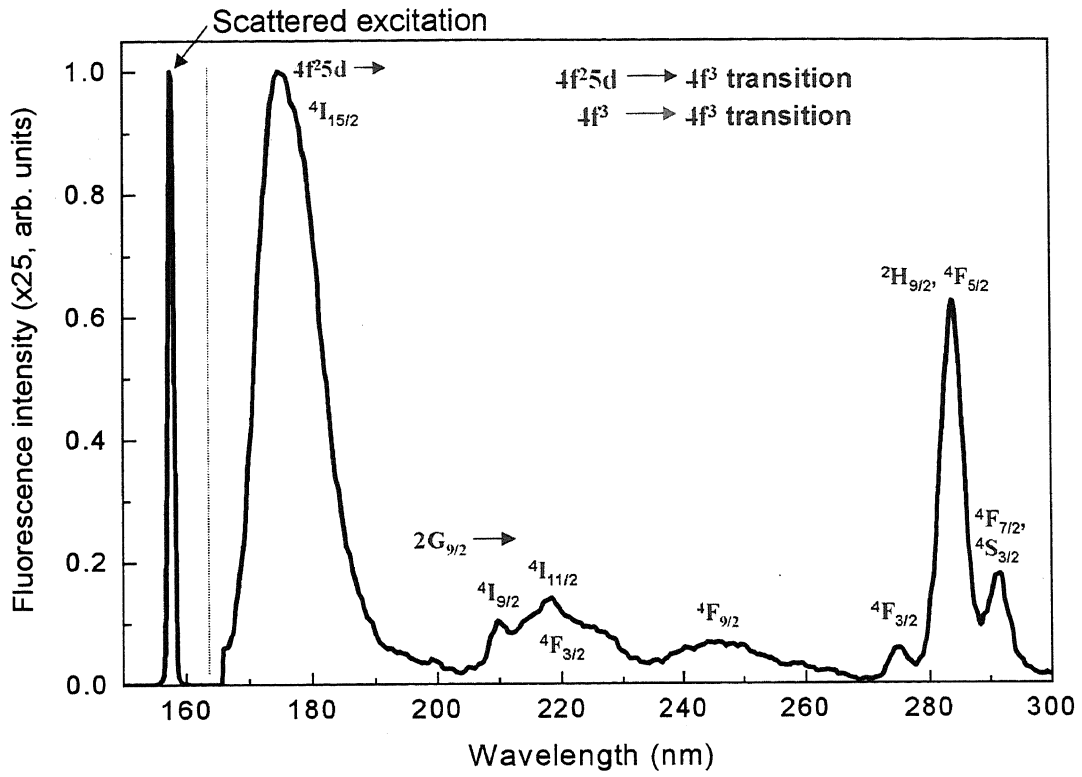

Fig. 6.11. F_2 laser-induced fluorescence spectra of Nd^{3+}:$(La_{0.9},Ba_{0.1})F_{2.9}$. It has a dominant peak located at 178 nm. The broad peaks can be attributed to interconfigurational transitions from the $4f^25d$ excited state configuration to the the different manifolds of the $4f^3$ ground state configuration while the sharp peaks are characteristic of intraconfigurational transitions within the manifolds of the $4f^3$ configuration.

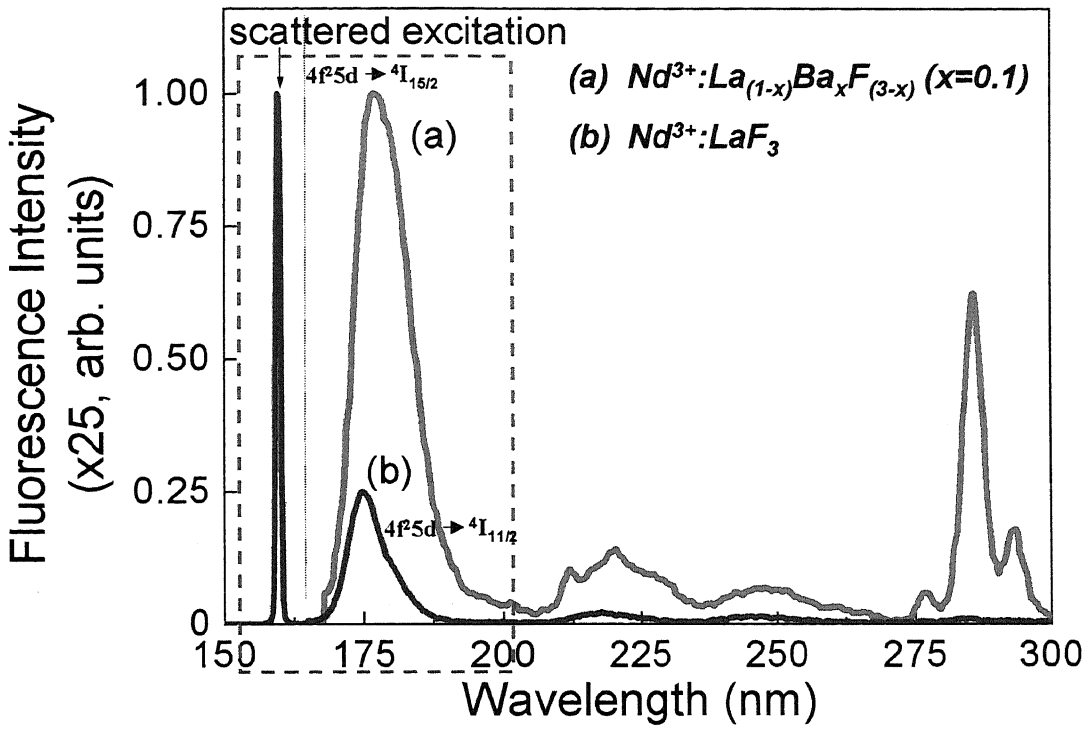

Fig. 6.12. F_2 laser-induced fluorescence spectra of Nd^{3+}:$(La_{0.9},Ba_{0.1})F_{2.9}$ and Nd^{3+}:LaF_3. Nd^{3+}:$(La_{0.9},Ba_{0.1})F_{2.9}$ has the most intense peak located at 178 nm. Nd^{3+}:LaF_3 has a dominant peak located at 175 nm. The obtained spectra are corrected for the spectrograph and CCD detector spectral responses.

has a bandwidth of 8 nm. This is emphasized in Fig. 6.13. The energy spread of the Stark splitting characteristic of the $^4I_{15/2}$ (5770 cm^{-1} to 6340 cm^{-1}) manifold translates to a theoretical span of at least 2 nm in the fluorescence spectrum compared to 0.7 nm for the $^4I_{11/2}$ manifold [5]. Considering other broadening mechanisms such as the vibronic interconfigurational d→f transition and the finite spectral response of the spectrograph system, the larger Stark splitting characteristic of the $^4I_{15/2}$ manifold is speculated to account for the 4 nm difference in the full width at half maximum that was observed in the experiment. In this regard, Nd^{3+}:$(La_{0.9},Ba_{0.1})F_{2.9}$ will have better laser characteristics in terms of better tunability and the capability for amplification of shorter pulses. In particular, the shortest pulse that a material can amplify can be estimated from

$$t_p \text{ [ps]} = 0.3/\Delta\nu \text{ ,} \qquad (6.2)$$

$$\Delta\nu \text{ [THz]} = [(c/\lambda_1)-(c/\lambda_2)] \text{ ,}$$

where $\Delta\nu$ is the bandwidth; c = 300 μm/ps is the speed of light in vacuum; and λ_1, λ_2 are the boundaries of the tunable wavelength region. Carrying out the calculations, Nd^{3+}:$(La_{0.9},Ba_{0.1})F_{2.9}$ and Nd^{3+}:LaF_3 are capable of amplifying 2.6 fs and 3.8 fs pulses, respectively. Moreover, laser emission from Nd^{3+}:$(La_{0.9},Ba_{0.1})F_{2.9}$ has better prospects since this material is more transparent at the 178-nm emission. The absorption cross sections of these two materials at their corresponding peak emission wavelengths are 9.75×10^{-22} cm^2 and 6.01×10^{-21} cm^2 for Nd^{3+}:$(La_{0.9},Ba_{0.1})F_{2.9}$ and Nd^{3+}:LaF_3, respectively.

The streak camera image of the F_2 laser (157 nm emission)-induced Nd^{3+}:LaF_3 fluorescence is shown in Fig. 6.14. Also shown in the same figure is the 157-nm excitation pulse for reference. The location of the fluorescence peak is in good agreement with the spectrum that was measured by a VUV spectrograph and CCD array detector shown in Fig. 6.12. This is the first streak camera image in the VUV region.

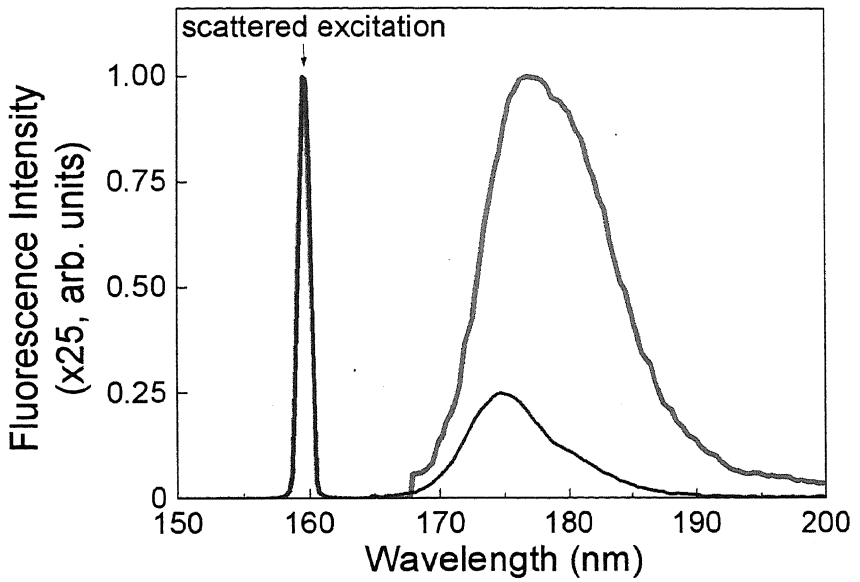

Fig. 6.13. VUV fluorescence spectra of the two samples emphasizing the broader fluorescence bandwidth from Nd^{3+}:$(La_{0.9},Ba_{0.1})F_{2.9}$ with full width at half maximum (FWHM) of 12 nm compared with 8 nm for Nd^{3+}:LaF_3.

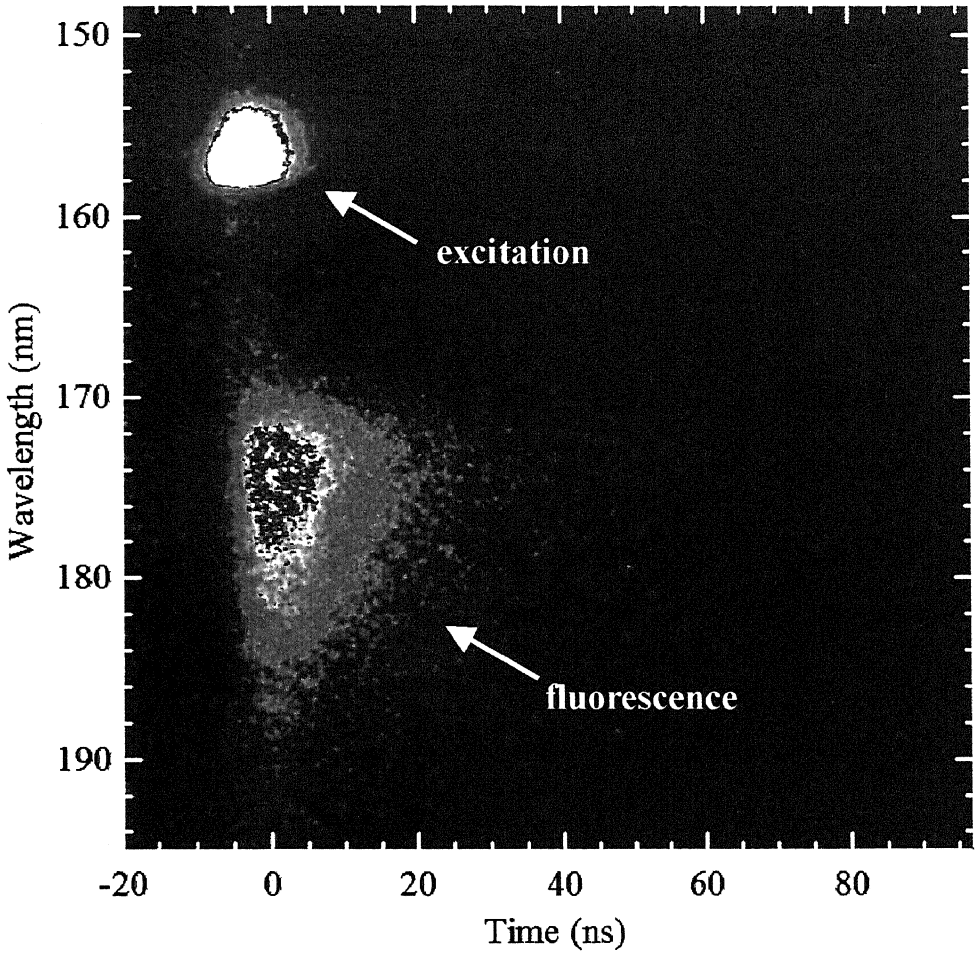

Fig. 6.14. Vacuum ultraviolet streak camera image of the fluorescence from a Nd^{3+}:LaF_3 crystal when excited by a F_2 laser. Also shown is the streak camera image of the 157-nm excitation pulse. The image is temporally and spectrally calibrated.

The temporal profiles of the VUV fluorescence from Nd^{3+}:$(La_{0.9},Ba_{0.1})F_{2.9}$ and Nd^{3+}:LaF_3 are shown in Fig. 6.15. The fluorescence from Nd^{3+}:$(La_{0.9},Ba_{0.1})F_{2.9}$ has a lifetime of 6.1 ns. On the other hand, the fluorescence from Nd^{3+}:LaF_3 has a lifetime of 8.9 ns. Also shown in the same figure is the temporal profile of the 157-nm F_2 laser excitation pulse. It has a pulse width of 5 ns.

A comparison of the optical characteristics of these two materials is summarized in Table 6.2. As a VUV laser material, Nd^{3+}:$(La_{0.9},Ba_{0.1})F_{2.9}$ has the advantage of having a shorter wavelength transmission edge, higher absorption cross section at the proposed excitation wavelength (157 nm), higher fluorescence cross section leading to more intense fluorescence, and broader fluorescence bandwidth. However, it has a fast decay time and a longer emission wavelength. The fast fluorescence decay time would be disadvantageous for a laser material because this would lead to a higher lasing threshold in order to satisfy population inversion, which is necessary for lasing to occur. In this case, Nd^{3+}:LaF_3 would have better prospects as the shortest wavelength VUV laser. On the other hand, Nd^{3+}:$(La_{0.9},Ba_{0.1})F_{2.9}$ would be more suitable as a VUV scintillator because of its high light yield and fast decay time.

6.4. Femtosecond Laser-induced fluorescence from Nd^{3+}:LaF_3

Up conversion pumping of laser materials is an attractive route to convert low frequencies to higher frequencies. Using a solid-state laser as pump, an all-solid-state VUV laser would then be possible.

Fluorescence spectra was obtained in the femtosecond regime by using the third harmonics of a (290 nm) Ti:sapphire regenerative amplifier. Due to the geometry of the experimental set-up described in Section 5.2, a CZ method-grown crystal cut into

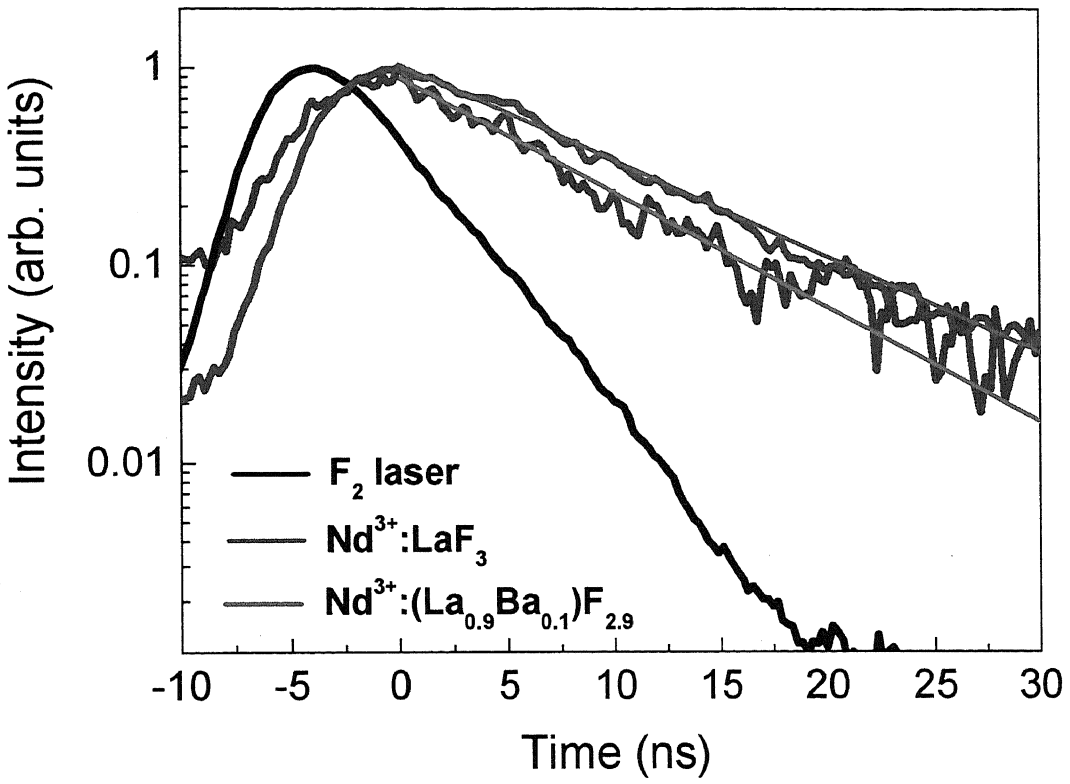

Fig. 6.15. The fluorescence from Nd^{3+}:LaF_3 has a lifetime, τ, of 8.9 ns while the fluorescence from Nd^{3+}:$(La_{0.9},Ba_{0.1})F_{2.9}$ decays faster with a lifetime of 6.1 ns. Also shown is the temporal profile of the excitation pulse with a pulsewidth of 5 ns.

Table 6.2. Comparison of the optical characteristics of micro-PD method grown Nd^{3+}:$(La_{0.9},Ba_{0.1})F_{2.9}$ and Nd^{3+}:LaF_3.

	Nd^{3+}:$(La_{0.9},Ba_{0.1})F_{2.9}$	**Nd^{3+}:LaF_3**
Absorption edge [nm]	180	210
Absorption cross section at 157 nm [cm^{-2}]	7.4×10^{-20}	6.86×10^{-20}
Emission wavelength [nm]	178	175
Emission bandwidth [nm]	12	8
Absorption cross section at emission wavelength [cm^{-2}]	~ 9.75×10^{-22}	~ 6.01×10^{-21}
Fluorescence cross section [cm^{-2}]	~ 1.73×10^{-21}	~ 1.62×10^{-21}
Shortest pulse that can be amplified [$sech^2$, fs]	2.6	3.8
Lifetime [ns]	6.16	8.91
Laser threshold		

a cuboid with its top, bottom, and 2 sides polished, was used. The streak camera image of fluorescence from Nd^{3+}:LaF_3 and the pump pulse are shown in Fig. 6.16a and Fig 6.16b, respectively. The spectral profile of fluorescence is shown in Fig. 6.17 while the temporal profile is shown in Fig. 6.18. Since the sample is practically transparent in this wavelength region, the observed fluorescence was speculated to be due to two-photon absorption. However, evaluation of the relative intensity of fluorescence with pump intensities from 4mW to 38 mW revealed a linear plot with a unity slope as shown in Fig. 6.19. To understand this phenomenon, the sample's absorption spectrum in the UV region was obtained. The absorption spectrum of the sample from 200 to 400 nm, shown in Fig. 6.20, reveals the presence of multiple absorption bands, particularly at 290 nm. Hence, single photon fluorescence is more probable than the non-linear two-photon case. In this respect, an electron absorbs one photon from an incoming pulse, thereby promoting it to an excited metastable state. Specifically, an electron in the ground state absorbs a 290-nm photon causing it to be promoted to $^2H_{11/2}$ manifold (34119 cm^{-1}) of the $4f^3$ configuration. Since fluorides have low phonon energies, the lifetimes of intermediate levels are long enough for electrons to accumulate. Subsequent energy transfer would promote an electron to the $4f^25d$ configuration. Relaxation to the $4f^3$ configuration results to fluorescence at 175 nm. A schematic diagram of the energy level transitions is shown in Fig. 6.21. The results obtained with a femtosecond pump were compared with those obtained using a nanosecond F_2 laser (157 nm) as pump. The streak camera image, spectral, and temporal profiles are shown in Fig. 6.22, Fig. 6.23, and Fig. 6.24, respectively. The fluorescence characteristics are similar for the femtosecond and nanosecond pumping schemes. In this respect, Nd^{3+}:LaF_3 has good prospects as an all-solid-state VUV laser material pumped by 290-nm solid-state lasers.

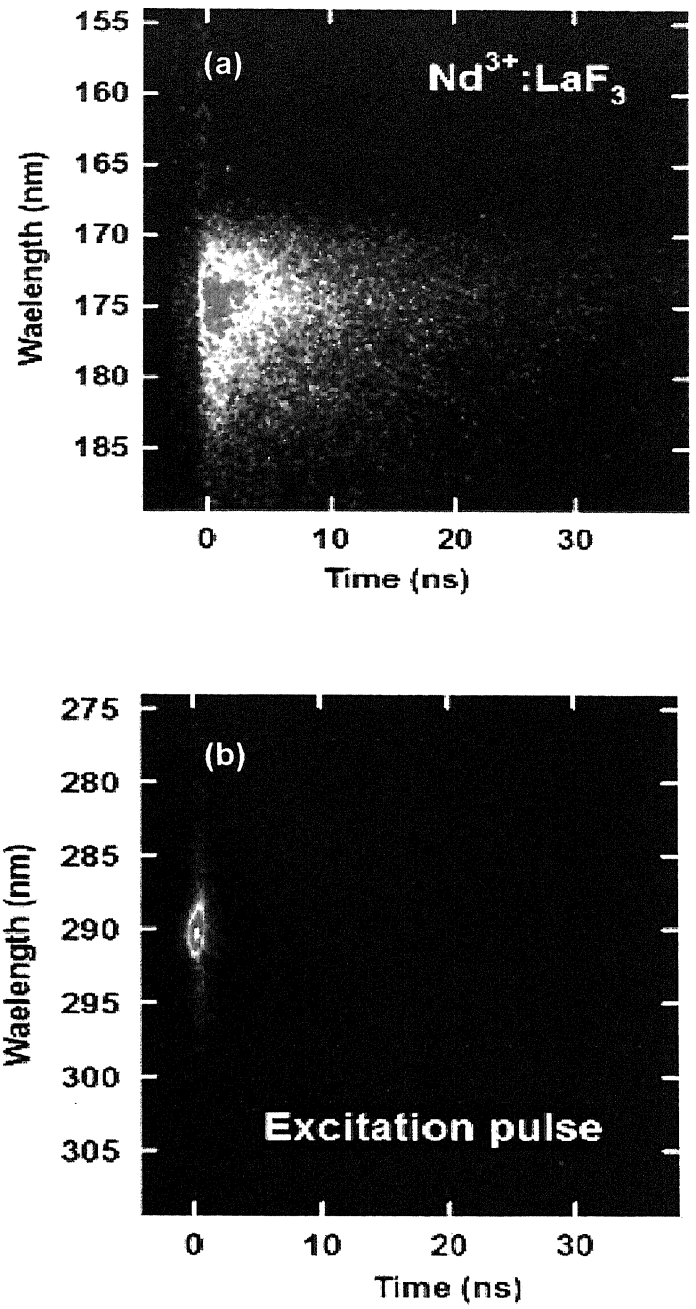

Fig. 6.16. (a) Streak camera image of fluorescence from a cuboid $Nd^{3+}:LaF_3$ excited by 290-nm femtosecond pulses shown in (b).

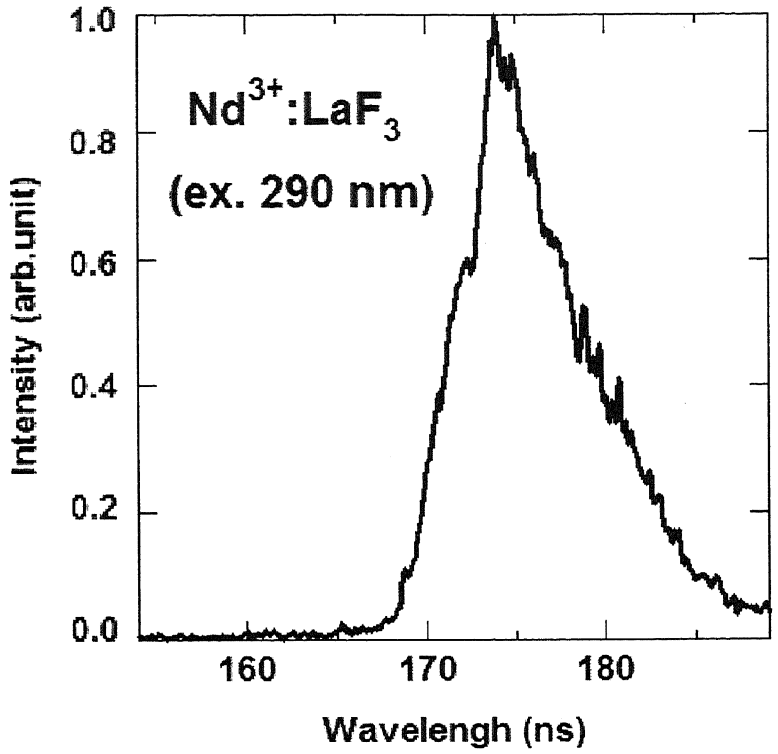

Fig. 6.17. Spectral profile of the fluorescence from a cuboid $Nd^{3+}:LaF_3$ excited by 290-nm femtosecond pulses.

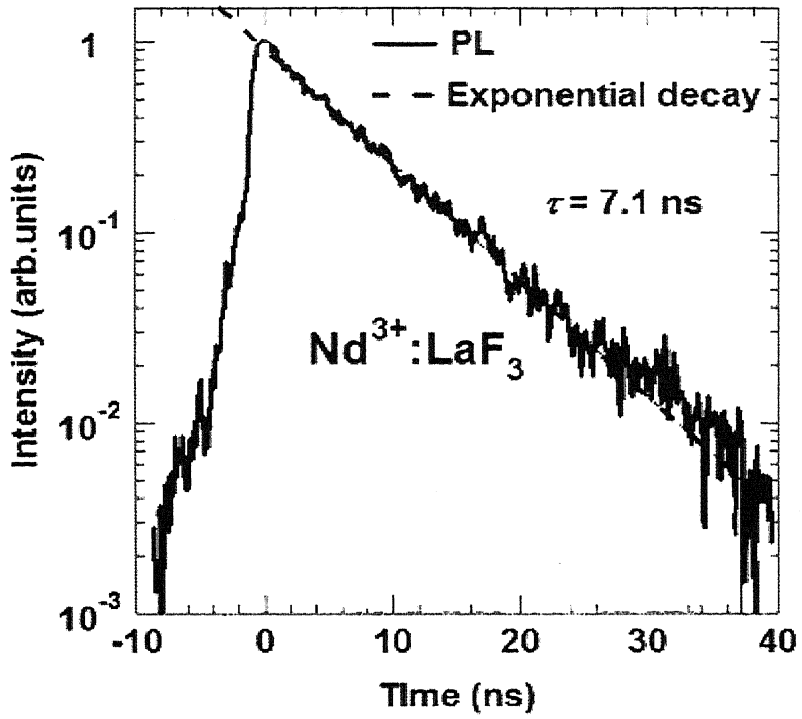

Fig. 6.18. Temporal profile of the fluorescence from a cuboid Nd^{3+}:LaF_3 excited by 290-nm femtosecond pulses.

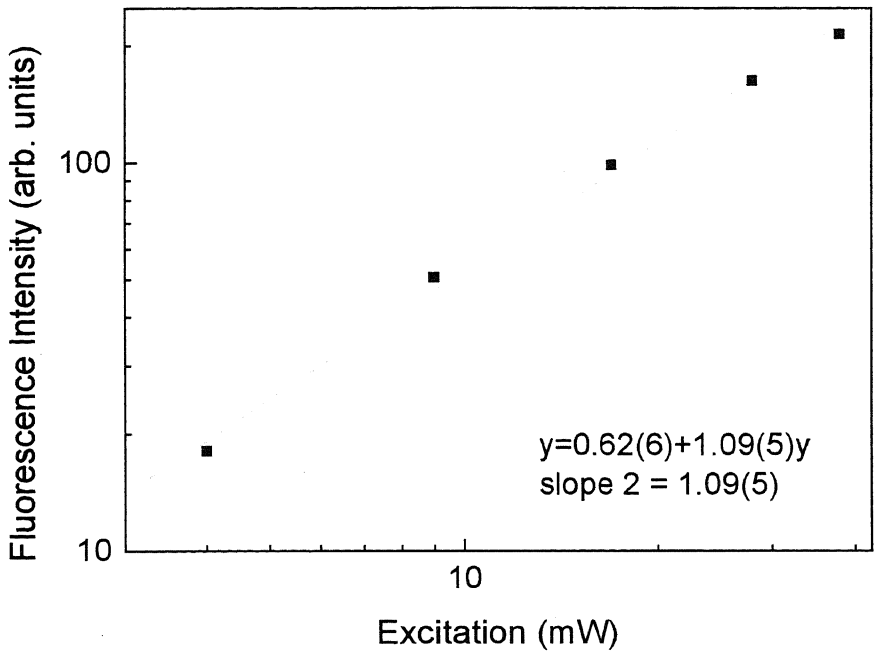

Fig. 6.19. Fluorescence intensity as a function of pump power. The linear dependence with a unity slope implies that fluorescence mechanism may be due to a single photon phenomenon.

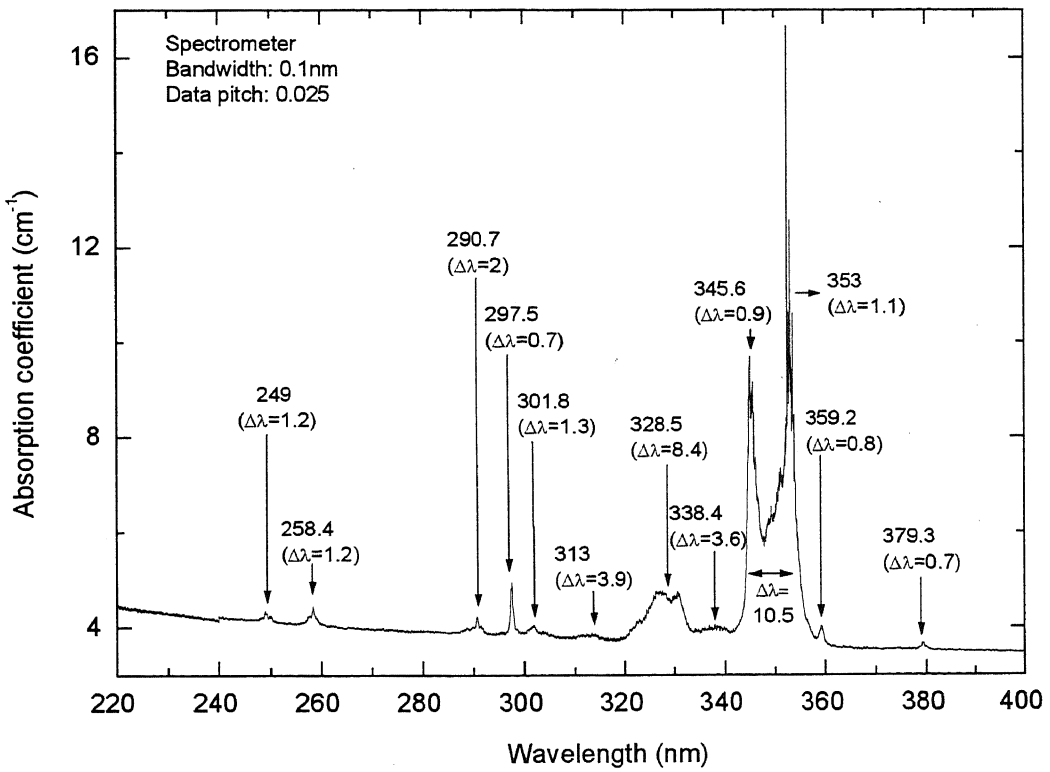

Fig. 6.20. Absorption spectra of a cuboid Nd^{3+}:LaF_3 showing multiple absorption bands from 200-400 nm. The sample has an absorption peak at the 290-nm excitatin wavelength.

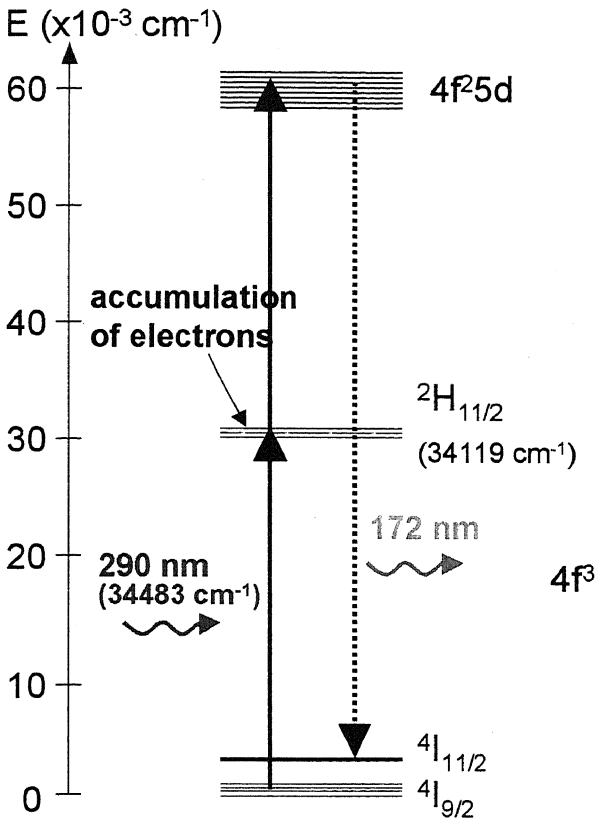

Fig. 6.21. Schematic diagram of the energy level transitions arising to 175-nm fluorescence when pumped with 290-nm femtosecond pulses.

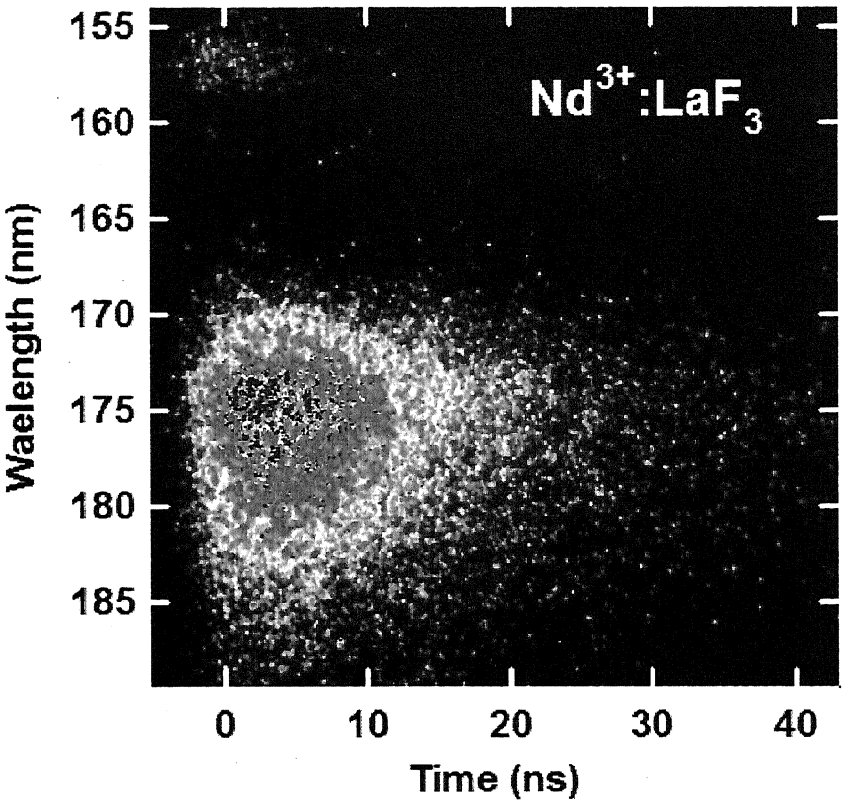

Fig. 6.20. Streak camera image of fluorescence from a cuboid Nd^{3+}:LaF_3 excited by 157-nm pulses from an F_2 laser.

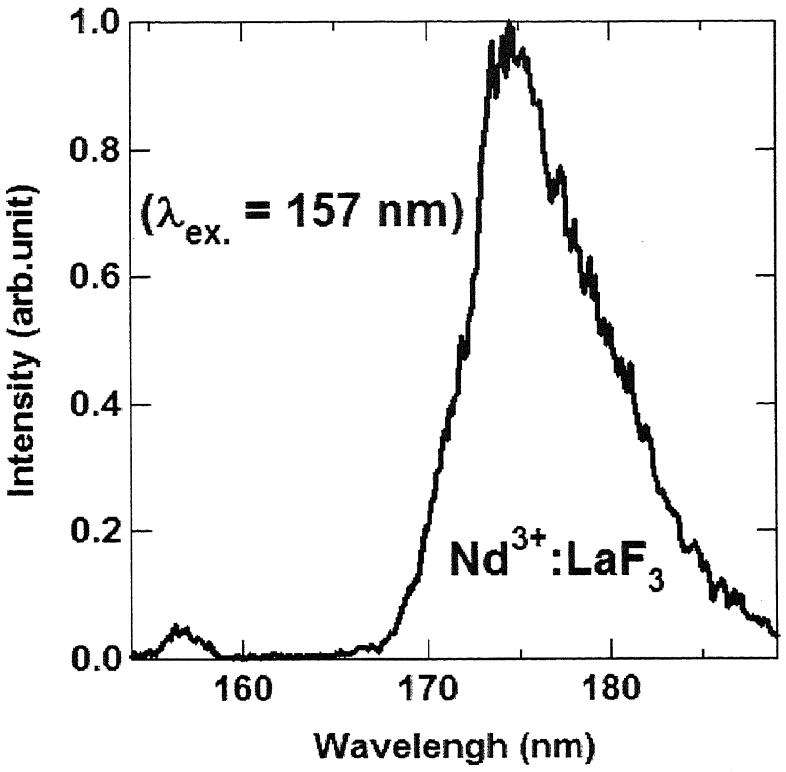

Fig. 6.23. Spectral profile of fluorescence from a cuboid Nd^{3+}:LaF_3 excited by 157-nm pulses from an F_2 laser.

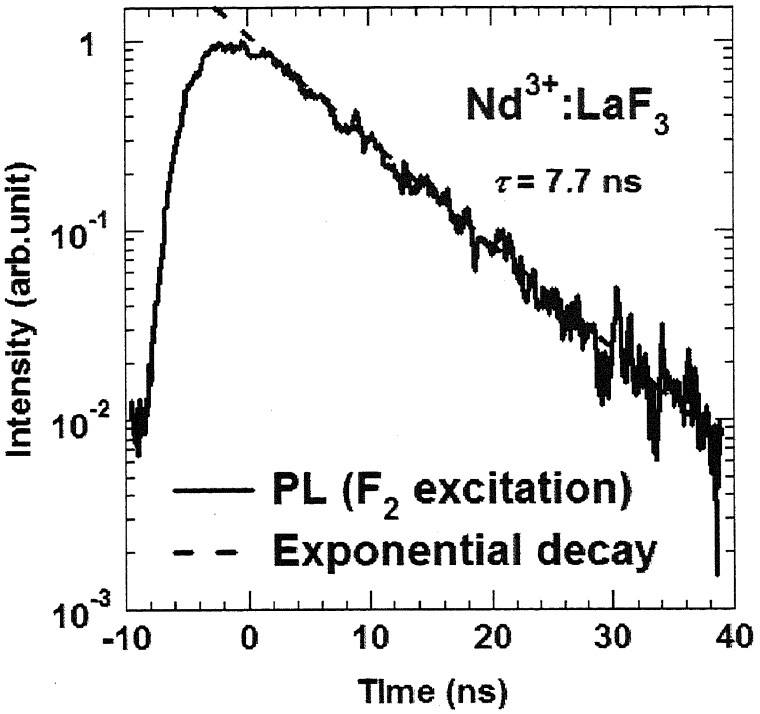

Fig. 6.24. Temporal profile of fluorescence from a cuboid Nd^{3+}:LaF_3 excited by 157-nm pulses from an F_2 laser.

6.5. Effect of Nd doping concentration

As the active ions greatly influence laser performance, the effect of Nd concentration to the material's optical properties is investigated.

Figure 6.25 shows the fluorescence spectra of Nd^{3+}:LaF_3 for different Nd concentrations from to 5% to 15%. As doping concentration is increased, pump absorption is expected to increase. As a consequence, it is intuitive that fluorescence would intensify due to the increase of charge carriers. However, as Fig. 6.25 shows, fluorescence intensity is lowest for the highest doping level (15%). A previous report by Waynant and Klein [3] observed similar decrease in fluorescence intensity when doping is increased but the fluorescence lifetime remained unchanged even at high doping concentrations. They therefore attributed the decrease in fluorescence intensity to increase in the reabsorption of the emitted light brought about by an increase in the absorption coefficient as doping increases. The difference in intensity of the scattered excitation may be due to surface effects. On the other hand, as doping concentration increases, the interaction between the wavefunctions of the dopant and the host matrix would increase. This would lead to the narrowing of the band gap as doping is increased. Consequentially, a slight shift in the fluorescence peak could arise.

For comparison, concentration dependence studies are carried out in the near-infrared (IR) region. Absorption spectra of Nd^{3+}:LaF_3 for 2.5% to 15% Nd concentration is shown in Fig. 6.26. Spectra are evaluated from 700 – 1000 nm. At the excitation wavelength, 798 nm, absorption is observed to increase with increasing concentration.

Near-IR fluorescence is evaluated using the 798 nm line of a Xe light source. Figure 6.27 shows the fluorescence spectrum for Nd concentrations from 0.25 % to 15%.

Several peaks are observed from 850 nm to 1200 nm. As concentration increases from 0.25% to 2.5%, fluorescence is observed to intensify. However, increasing the doping concentration further results to decrease in fluorescence intensity as can be observed from 5% to 15% doping concentration. This decrease in intensity despite the increase in absorption indicates the presence of concentration quenching for doping levels greater than 2.5%.

To confirm that concentration quenching brings about the decrease in intensity, the fluorescence lifetime is obtained. Fig. 6.28 shows a log plot of the fluorescence lifetime for Nd doping concentrations from 2.5% to 15%. Fluorescence lifetime is longest for 2.5% Nd concentration. As Nd concentration is increased to 15%, fluorescence lifetime decreases. As concentration increases, the number of defects and trapping centers that prevent the recombination of charge carriers also increases. Moreover, interaction between Nd ions increase as the Nd concentration increases. Therefore, less of the charge carriers are able to recombine and contribute to the fluorescence. This explains the decrease in fluorescence intensity and the increase in the decay time as emission is inhibited.

The effect of Nd^{3+} concentration in the VUV region needs further study in order to identify whether concentration quenching would play an important role in improving light yield. By carrying out further work in this direction, the optimum concentration level would be determined. With the improvement of the quality and size of Nd^{3+}-doped fluorides, an efficient and reliable vacuum ultraviolet laser will be realizable in the near future.

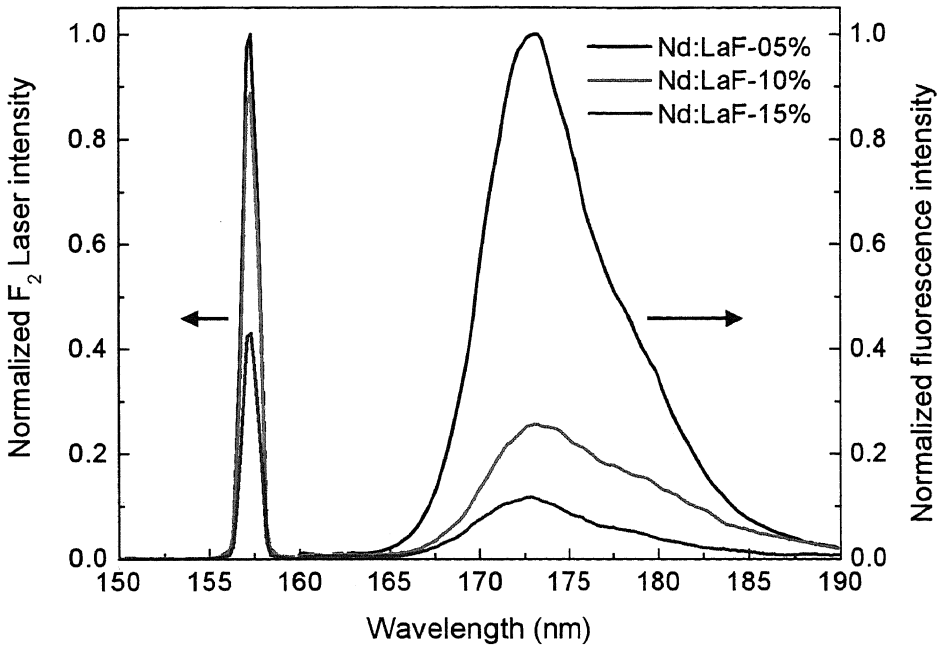

Fig. 6.25. Nd concentration dependence of fluorescence intensity.

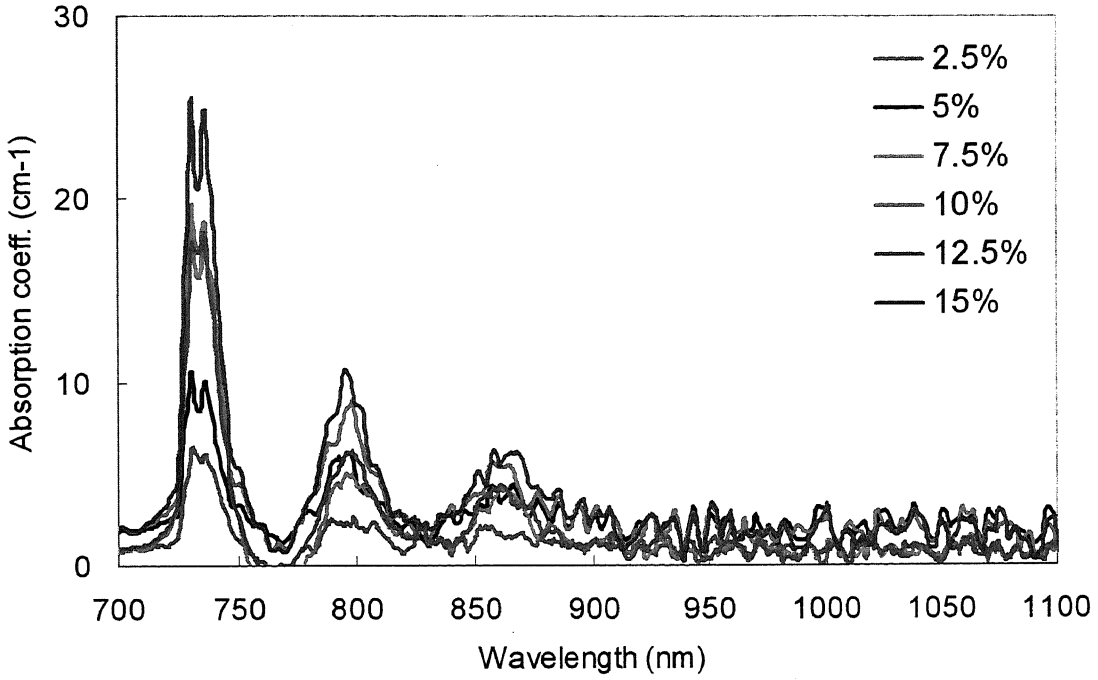

Fig. 6.26. Absorption coefficient in the near-IR region for different Nd concentrations.

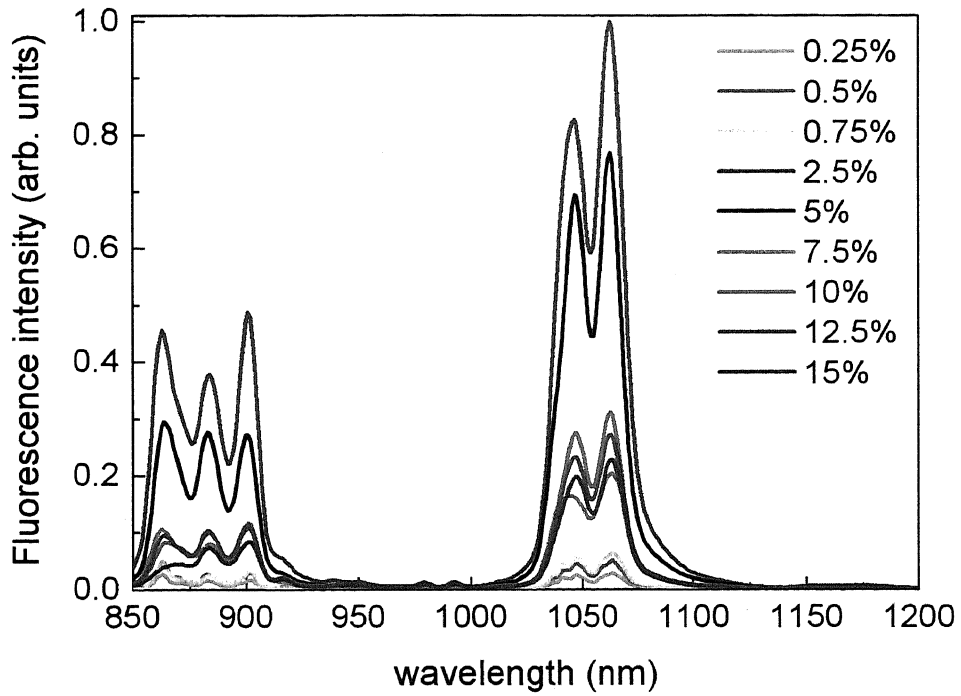

Fig. 6.27. Fluorescence spectra in the near-IR region for different Nd concentrations. Fluorescence intensity decreases for highly doped LaF_3 hosts despite the fact that absorption increases with doping.

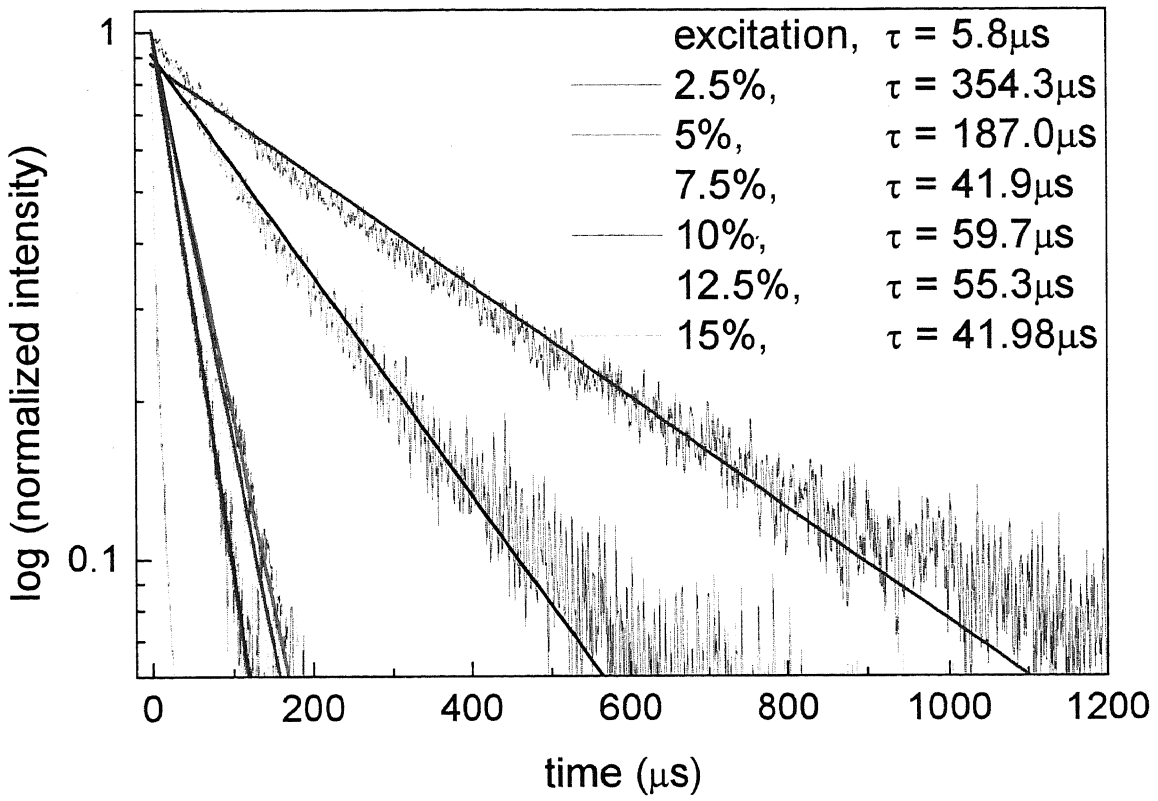

Fig. 6.28. Fluorescence lifetime decreases as doping level increases. This is indicative of fluorescence quenching for highly doped LaF_3 hosts.

References

[1] M.A. Dubinskii, A.C. Cefalas, E. Sarantopoulou, S.M. Spyrou, C.A. Nicolaides, R.Y. Abdulsabirov, S.L. Korableva, and V.V. Semashko, "Efficient LaF_3:Nd^{3+}-based vacuum-ultraviolet laser at 172 nm", J. Opt. Soc. Am. B, **9** (1992) 1148-1150.

[2] T. Srinivasan, H. Egger, K. Boyer, H. Pummer, C. K. Rhodes, T. S. Luk, D. F. Muller, M. Rothschild, J. Bokor, R. R. Freeman, W. E. Cooke, H. Schomburg, H. F. Döbele, B. Rückle, L. A. Bloomfield, B. Couillaud, Ph. Dabkiewicz, H. Gerhardt, T. W. Hansch, R. Hilblg, R. Wallenstein, R. M. Jopson, C. B. Collins, F. W. Lee, D. M. Shemwell, B. D. DePaola, S. Olariu, I. Iovitzu Popescu, R. W. Waynant, M. D. Levenson, K. Jain, C. G. Willson and B. J. Lin, "Vacuum Ultraviolet Laser Emission from Nd^{3+}:LaF_3", Appl. Phys. B, 12th International Quantum Electronics Conference, **28** (1982) 198-207.

[3] R.W. Waynant and P.H. Klein, "Vacuum ultraviolet laser emission from Nd^{+3}:LaF_3", Appl. Phys. Lett., **46** (1985) 14.

[4] G. H. Dieke and H. M. Crosswhite, "The spectra of the doubly and triply ionized rare earths", Appl. Opt. **2** (1963) 675.

[5] A. Kaminskii, *Laser Crystals: Their Physics and Properties* (Springer-Verlag, Germany, 1990) 2nd ed., p. 123.

Chapter 7. Summary, Conclusions, and Recommendations

Two CZ method-grown fluoride crystals namely, LaF_3 and $YLiF_4$ and two μ-PD method-grown fluorides namely $(La_{1-x},Ba_x)F_{3-x}$ and LaF_3, all doped with Neodymium (Nd^{3+}) ions were investigated and characterized in terms of absorption, fluorescence, and fluorescence lifetime, with the goal of investigating Nd^{3+}-doped fluorides as VUV laser media.

First, the optical properties of CZ method-grown $Nd^{3+}:LaF_3$ and $Nd^{3+}:YLiF_4$ were investigated. Although $Nd^{3+}:YLiF_4$ had a lower absorption cross section at its emission wavelength (181 nm) and a longer lifetime compared with $Nd^{3+}:LaF_3$, it had a longer wavelength absorption edge (179 nm compared to 165 nm), a lower absorption cross section at the proposed pump wavelength (157 nm), and a longer emission wavelength. In this regard, $Nd^{3+}:LaF_3$ had better prospects as a short wavelength VUV laser material.

Next, BaF_2 was added to shift the transmission edge to a shorter wavelength. $Nd^{3+}:(La_{1-x},Ba_x)F_{3-x}$ (x=0.1) or $Nd^{3+}:(La_{0.9},Ba_{0.1})F_{2.9}$ crystal was successfully grown for the first time using the μ-PD method modified for fluoride crystal growth, for fast and economical materials screening. For comparison, $Nd^{3+}:LaF_3$ was also grown using the same growth parameters. Both of these crystals were 20 mm in length and 2 mm in diameter.

As a VUV laser material, $Nd^{3+}:(La_{0.9},Ba_{0.1})F_{2.9}$ had the advantage of having a shorter wavelength transmission edge, higher absorption cross section at the proposed excitation wavelength (157 nm), higher fluorescence cross section leading to more intense fluorescence, and broader fluorescence bandwidth. However, it had a fast decay time and a longer emission wavelength. In this case, $Nd^{3+}:LaF_3$ would have better

prospects as the shortest wavelength VUV laser. On the other hand, Nd^{3+}:$(La_{0.9},Ba_{0.1})F_{2.9}$ would be more suitable as a VUV scintillator because of its high light yield and fast decay time.

Up conversion pumping of laser materials was an attractive route to convert low frequencies to higher frequencies. Using a solid-state laser as pump, an all-solid-state VUV laser would then be possible. To investigate this aspect, a CZ method-grown Nd^{3+}:LaF_3 cut into a cuboid was excited by the third harmonics of a (290 nm) Ti:sapphire regenerative amplifier. Fluorescence characteristics were similar for the femtosecond and nanosecond pumping schemes.

The effect of doping concentration was also investigated. Fluorescence spectrum for different concentration levels revealed the presence of concentration quenching in the infrared region. Fluorescence intensity was observed to increase up to 2.5% Nd^{3+} concentration. Beyond 2.5%, fluorescence intensity decreased accompanied by fast fluorescence decay times. In the VUV, fluorescence intensity seemed to decrease at high concentrations. At the moment, it is not yet clear whether this was brought about by quenching or by increased absorption of the fluorescence.

The effect of Nd^{3+} concentration in the VUV region needs further study in order to identify whether concentration quenching would play an important role in improving light yield. By carrying out further work in this direction, the optimum concentration level would be determined. With the improvement of the quality and size of Nd^{3+}-doped fluorides, an efficient and reliable vacuum ultraviolet laser will be realizable in the near future.

ACKNOWLEDGEMENTS

Now that I am at the last phase, I dare not forget where I have been nor the people I have met along the way...

My deepest gratitude goes to Professor Nobuhiko Sarukura for providing me this opportunity to acquire my degree at the Graduate University for Advanced Studies. Under his supervision, I have learned valuable knowledge and have improved my skills in laser systems and their applications. I thank him for believing that I am capable of doing research; and for providing opportunities for me to be involved in the exchange of scientific information through symposia and conferences.

I am also indebted to Prof. Shingo Ono for mentoring me and teaching everything that I need to know in vacuum ultraviolet research.

This work would not have been as successful without my co-authors and collaborators. My sincerest thanks to Professor Akira Yoshikawa and Dr. Kentaro Fukuda for growing and providing the fluoride crystals used in my experiments and for their useful comments and suggestions. I also thank Dr. Seo Young Seok for laboring with me and for encouraging me during the difficult stages of research. I thank Dr. Yusuke Furukawa for assisting me with my experiments with the streak camera and for his suggestions and ideas for improving the experiments. I thank Dr. Elmer Estacio for the knowledge he has imparted as well as his valuable ideas and discussions for improving my work. I thank Dr. Hidetoshi Murakami, Dr. Yasushi Fujimoto, Professor Masahiro Nakatsuka, Mr. Toshihisa Suyama, Dr. Rayko Simura, and Professor Tsuguo Fukuda for their support and useful discussions.

My life in Japan wouldn't have been as enjoyable had not it been for my colleagues. For this, I thank Carlito Ponseca, Minh Honh Pham, Toshihiro Tatsumi, Ayumi Saiki, Dr. Shigeki Saito, and Dr. Tomoharu Nakazato.

I thank Ms. Satomi Suzuki and Ms. Seto for taking care of necessary documents especially those in Japanese as well as for their encouragements.

I thank Dr. Romeric Pobre for believing that I am capable of making it in Japan, therefore recommending me to Professor Sarukura. I also thank him for his encouragements and prayers.

I thank my Vineyard family and my J-House family for their prayers, love, and support.

I dedicate this work to my family Dr. Macario Cadatal, Dr. Lourdes Cadatal, MacAnthony Cadatal, May-Ann Cadatal, Mabel Nunal-Cadatal, and Hannah Patricia Cadatal for their support in prayers, words, laughter, and tears. I thank them for trusting and believing in me without pressuring me to meeting their expectations. I also dedicate this work to Edward Raduban for his love, acceptance, prayers, and encouragements. I thank him for allowing me to pursue my dreams and for teaching me the right way. Without them, I wouldn't have had the proper emotional support needed to get past the hurdles. For that, I am truly grateful.

Most importantly, I thank my Father for His faithfulness. I thank Him for keeping His promise of seeing me through. I thank Him for giving me the wisdom and the intelligence that I need especially at times when I do not know. He is my alpha and omega, the source of all things. He indeed is great. To God is the glory.

Marilou Macasieb Cadatal

Appendix 1 Publications and Conferences

A1.1. Publication list

[1] M. Cadatal, Y. Furukawa, Y. Seo, S. Ono, E. Estacio, H. Murakami, Y. Fujimoto, N. Sarukura, M. Nakatsuka, K. Fukuda, R. Simura, T. Suyama, and A. Yoshikawa, Vacuum Ultraviolet Optical Properties of a Micro-Pulling Down Method Grown Nd^{3+}:$(La_{0.9},Ba_{0.1})F_{2.9}$, J. Opt. Soc. Am. B **25** (2008) B27-B31.

[2] M. Cadatal, Y. Seo, S. Ono, Y. Furukawa, E. Estacio, H. Murakami, Y. Fujimoto, N. Sarukura, M. Nakatsuka, T. Suyama, K. Fukuda, R. Simura, and A. Yoshikawa, Nd^{3+}:$(La_{1-x},Ba_x)F_{3-x}$ Grown by Micro-Pulling Down Method as Vacuum Ultraviolet Scintillator and Potential Laser Material, Jpn. J. Appl. Phys., **46** (2007) L985 - L987.

[3] M. H. Pham, M. Cadatal, T. Tatsumi, A. Saiki, Y. Furukawa, T. Nakazato, E. Estacio, N. Sarukura, T. Suyama, K. Fukuda, K. Jin Kim, A. Yoshikawa, and F. Saito, Laser Quality Ce^{3+}:$LiCaAlF_6$ Grown by the Micro-Pulling Down Method, Jpn. J. Appl. Phys., **47** (2008).

[4] E. Estacio, S. Saito, T. Nakazato, Y. Furukawa,N. Sarukura, M. Cadatal, M. Pham, C. Ponseca,Jr., H. Mizuseki, and Y. Kawazoe, Birefringence of β-BaB_2O_4 crystalin the terahertz region for parametric device design, Appl. Phys. Lett., **92** (2008) 091116-1 - 091116-3.

[5] N. Sarukura, H. Murakami, E. Estacio, S. Ono, R. El Ouenzerfi, M. Cadatal, T. Nishimatsu, N. Terakubo, H. Mizuseki, Y. Kawazoe, A. Yoshikawa and T. Fukuda, Proposed design principle of fluoride-based materials for deep ultravioletlight emitting devices, Opt. Materials, **30** (2007) 15-17.

A1.2. Local Publication List

[1] M. Cadatal, M. Pham, S. Ono, E. Estacio, H. Murakami, Y. Fujimoto, Y. Seo, T. Tatsumi, N. Sarukura, M. Nakatsuka, K. Fukuda, A. Yoshikawa, and T. Fukuda, "Comparison of vacuum ultraviolet (VUV) fluorescence from Nd^{3+} - doped LaF_3 and $YLiF_4$", Oyo Butsuri Gakkai Gakujutsu Koenkai Koen Yokoshu, **67** (2006) 985.

A1.3. International Conference

O-1. M. Cadatal, Y. Furukawa, Y.S. Seo, S. Ono, E. Estacio, H. Murakami, Y. Fujimoto,

N. Sarukura, M. Nakatsuka, K. Fukuda, R. Simura, T. Suyama, A. Yoshikawa, "Micro-Pulling Down Method Growth and Characterization of Nd3+:(La0.9, Ba0.1F2.9 as Potential Vacuum Ultraviolet Laser Material and Scintillator", The 4th Asian Conference on Crystal Growth and Crystal Technolog, Sendai, Japan May 21-24, 2008, paper S-24PM-I-3-5.

O-2. E. Estacio, S. Saito, T. Nakazato, Y. Furukawa, T. Tatsumi, M. Pham, M. Cadatal, C. Ponseca, H. Mizuseki, Y. Kawazoe, N. Sarukura, Observation of Birefringence in BBO Crystal in the Terahertz Region", The 4th Asian Conference on Crystal Growth and Crystal Technolog, Sendai, Japan May 21-24, 2008, paper R-24AM1-II-4B-6.

O-1. M. Cadatal, Y.Seo, S. Ono, E. Estacio, Y. Furukawa, H. Murakami, Y. Fujimoto, N. Sarukura, M. Nakatsuka, K. Fukuda, R. Simura, T. Suyama, and A. Yoshikawa, "Optical Properties of Micro-Pulling Down Method Grown Nd^{3+}:$(La_{1-x},Ba_x)F_{3-x}$ as Potential Vacuum Ultraviolet Laser Material and Scintillator",The 6th Asia Pacific Laser Symposium, Nagoya Japan, January 30-February 1, 2008, paper 30Fa11.

P-1. M. Cadatal, M. H. Pham, T. Tatsumi, A. Saiki, Y. Furukawa, E. Estacio, N. Sarukura, T. Suyama, K. Fukuda, K. Jin Kim, A.Yoshikawa, and F. Saito, "Ce:LiCAF Crystal Grown by the Micro-Pulling Down Method and its Ultraviolet Lasing Properties", Advanced Solid-State Photonics (Optical Society of America), Nara, Japan January 27-30, 2008, paper WB18.

P-2. M.Takahashi, I. Sekine, M.Cadatal, N. Sarukura, P. F. Moulton, A. Dergachev, "Reduction of Non-Linear Absorption in $Li_2B_4O_7$ by Controlling Temperature and Repetition Rate", Advanced Solid-State Photonics (Optical Society of America), Nara, Japan January 27-30, 2008, paper MC32.

P-3. M. M. Cadatal, Y.Seo, T. Tatsumi, M. H. Pham, C. Ponseca Jr., S. Ono, E. Estacio, Y. Furukawa, H.Murakami, Y. Fujimoto, N. Sarukura, M. Nakatsuka, K. Fukuda, R. Simura, T. Suyama, A. Yoshikawa, and T. Fukuda, "Nd^{3+}: $(La_{1-x},Ba_x)F_{3-x}$ Grown by Micro-PD Method as New Vacuum Ultraviolet Scintillator and Potential Laser Material", Fifth International Conference in Inertial Fusion Sciences and Applications, Kobe, Japan, September 9-15, 2007, paper Fpo53.

P-4. M. Cadatal, Y.Seo, S. Ono, E.Estacio, Y. Furukawa, H. Murakami, Y. Fujimoto, N.

Sarukura, M. Nakatsuka, K. Fukuda, R. Simura, T. Suyama, A. Yoshikawa, and T. Fukuda, "Nd^{3+}:$(La_{1-x},Ba_x)F_{3-x}$ grown by micro-pulling down as vacuum ultraviolet scintillator and potential laser material, Ultrafast Optics(UFO) /High Field Short Wavelength (HFSW), September 2-7, 2007 Sta. Fe. New Mexico, USA, paper

O-2. M. M. Cadatal, Y. Seo, T. Tatsumi, M. H.Pham, C. Ponseca Jr., S. Ono, E. Estacio, Y. Furukawa, H. Murakami, Y. Fujimoto, N. Sarukura, M.. Nakatsuka, K. Fukuda, R. Simura, T. Suyama, A.Yoshikawa, and T. Fukuda, "Nd^{3+}: $(La_{1-x},Ba_x)F_{3-x}$ grown via Micro-PD as New Vacuum Ultraviolet Scintillator and Potential Laser Material, Conference on Lasers and Electro-Optics Pacific Rim, Seoul, South Korea, August 27-September 2, 2007, paper ThE3-2.

O-3.C. Ponseca, E. Estacio, M. Cadatal, R. Pobre, R. Quiroga, H. Murakami, S. Ono, N. Sarukura, J. Nishizawa, K. Suto, T. Sasaki, T. Tanno, and K. Tominaga, "Numerical Calculations of the Frequency Spectra of Naphthalene and 1,4-dihydroxynaphthalene in the 0.5- to 6 Terahertz Region", Conference on Lasers and Electro-Optics Pacific Rim, Seoul, South Korea, August 27-September 2, 2007, ThH2-4.

P-5. M. M. Cadatal, Y. Seo, T. Tatsumi, M. H. Pham, C. Ponseca Jr., S.o Ono, E. Estacio, Y. Furukawa, H. Murakami, Y. Fujimoto, N. Sarukura, M. Nakatsuka, K. Fukuda, R. Simura, T. Suyama, A. Yoshikawa, and T. Fukuda, "Investigation of Nd^{3+}:$(La_{1-x},Ba_x)F_{3-x}$ as New Vacuum Ultraviolet Scintillator and Potential Laser Material", (Optical Society of America) Nonlinear Optics Materials, Fundamentals and Applications, July 30-August 3, 2007 Kona Hawaii, USA, paper WE29.

P-6. M. M. Cadatal, Y. Seo, T. Tatsumi, M. H.Pham, C. Ponseca Jr., S.Ono, E. Estacio, Y. Furukawa, H.Murakami, Y.Fujimoto, N. Sarukura, M. Nakatsuka, K. Fukuda, R. Simura, T. Suyama, A. Yoshikawa, and T. Fukuda, "Nd^{3+}: $(La_{1-x},Ba_x)F_{3-x}$ as Vacuum Ultraviolet Scintillator and New Laser Material", Conference on Lasers and Electro-Optics/Quantum Electronics and Laser Science Conference, May 6-11, 2007, Baltimore Convention Center, Maryland, USA, paper JTuA104.

O-4. C. Ponseca, M. Cadatal, R. Pobre, R. Quiroga, H. Murakami, S. Ono, N. Sarukura, J. Nishizawa, K. Suto, T. Sasaki, T. Tanno, K. Tominaga, "accurate Modeling of Inter- and Intra- molecular Interactions in 1,4-Dihydroxynaphthalene in the 0.5-6 Terahertz Region", Conference on Lasers and Electro-Optics/Quantum Electronics and Laser

Science Conference, May 6-11, 2007, Baltimore Convention Center, Maryland, USA, paper CFS2.

O-5. N. Sarukura, M. Cadatal, Y. Seo, E. Estacio, S. Ono, R. El Ouenzerfi, A. Quema, H. Murakami, T. Nishimatsu, N. Terakubo, H.Mizuseki, Y. Kawazoe, A. Yoshikawa, and T. Fukuda, "Band-structure design of wide-gap fluoride hetero-structures for deep-ultraviolet light-emitting diodes", The 5th Asia Pacific Laser Symposium, Guangxi, China, November 23-27, 2006.

O-6. C. Ponseca Jr., A. Quema, M. Cadatal, E. Estacio, R. Pobre, R. Quiroga, H. Murakami, S. Ono, N. Sarukura, T. Tanno, T. Sasaki, K. Suto, J. Nishizawa, K. Tominaga, "Terahertz (THz) transmission spectroscopic analysis of mono- and di-substituted hydroxynaphthalenes in the 0.5- to 6-THz region using GaP THz wave generator", 31st International Conference on Infrared and Millimeter Waves (IRMMW) and 14th International Conference on Terahertz Electronics, Shanghai, China September 2006.

O-7. C. Ponseca Jr., M. Cadatal, A. Quema, E. Estacio, H. Murakami, S. Ono, and N. Sarukura, A. Argyros, M. Large and M. van Eijkelenborg, "Terahertz - time domain spectroscopy (THz-TDS) of microstructured poly(methylmetacrylate) (PMMA) polymer fiber", 31st IRMMW and 14th International Conference on Terahertz Electronics, Shanghai, China September 2006.

A1. 4. Local Conference

O-1. G. De Los Reyes, C. Ponseca Jr., M. Cadatal, A. Quema, E. Estacio, R. Pobre, R. Quiroga, H. Murakami, S. Ono, N. Sarukura, T. Tanno, T. Sasaki, K. Tominaga, "Terahertz (THz) transmission spectroscopic analysis of mono- and di-substituted hydroxynaphthalenes in the 0.5- to 6-THz region using GaP THz wave generator", 53rd Spring Meeting of the Japanese Society of Applied Physics, Tokyo, Japan 2006, paper 25P-M-10.

O-2. M. Cadatal, M. Pham, S. Ono, E. Estacio, H. Murakami, Y. Fujimoto, Y. Seo, T. Tatsumi, N. Sarukura, M. Nakatsuka, K. Fukuda, A. Yoshikawa, and T. Fukuda, "Comparison of vacuum ultraviolet (VUV) fluorescence from Nd^{3+} - doped LaF_3 and $YLiF_4$", 67th Autumn Meeting of the Japanese Society of Applied Physics, Shiga, Japan, 2006, paper 30A-ZE-6.

O-3. K. Fukuda, M. Cadatal, A. Yoshikawa, N. Sarukura, T. Fukuda, "Growth and VUV Fluorescence of Nd^{3+} doped Fluoride Single Crystals", 67th Autumn Meeting of the Japanese Society of Applied Physics, Shiga, Japan 2006, paper 29p-ZF-4.

O-4. K. Fukuda, S. Ishizu, T. Yanagida, A. Yoshikawa, M. Cadatal, N. Sarukura, H. Takahashi, T. Suyama, and M. Nikl, "Growth of Nd:LaF_3 Single Crystal using Czhocralski Method", 67th Autumn Meeting of the Japanese Society of Applied Physics, Shiga, Japan 2006, paper 7a-ZA-3.

O-5. M. M. Cadatal, Y.Seo, T. Tatsumi, M. H. Pham, C. Ponseca Jr., S. Ono, E. Estacio, Y. Furukawa, H. Murakami, Y. Fujimoto, N. Sarukura, M. Nakatsuka, K. Fukuda, R. Simura, T. Suyama, A. Yoshikawa, and T. Fukuda, "Micro – Pulling Down – Grown Nd^{3+}:$(La_{1-x},Ba_x)F_{3-x}$ as New Vacuum Ultraviolet Scintillator and Potential Laser Material", 54th Spring Meeting of the Japanese Society of Applied Physics, Tokyo, Japan 2007, paper.

O-5. M.M. Cadatal, M. Hong Pham, S. Ono, C. Ponseca Jr. , E. Estacio, H. Murakami, Y. Fujimoto, Y. Seo, T. Tatsumi, N. Sarukura, M. Nakatsuka, K. Fukuda, A. Yoshikawa, and T. Fukuda, "Investigation of the Optical Properties of Nd^{3+}-doped LaF_3 and $YLiF_4$ in the Deep Ultraviolet (DUV) and Vacuum Ultraviolet (VUV) Region", The 24th Samahang Pisika ng Pilipinas (SPP) Physics Congress, Davao City, Philippines 2006, paper spp-2006-008, ISSN 1656-2666, Vol. 3.

O-6. M. Cadatal, M. H. Pham, T. Tatsumi, Y. Furukawa, E. Estacio, N. Sarukura, T.Suyama, K. Fukuda, K. Jin Kim, and A. Yoshikawa, "All-solid-state ultraviolet laser from micro-pulling down method grown Ce:LiCAF with direct pumping by the fourth harmonic of a Nd:YAG laser", The 25th Samahang Pisika ng Pilipinas (SPP) Physics Congress, Laguna, Philippines 2007, paper spp-2007-042, ISSN 1656-2666 Vol. 4.

O-7. M. Cadatal, Y. Seo, S. Ono, N. Sarukura, T. Suyama, K. Fukuda, R. Simura, and A. Yoshikawa, "Nd^{3+}:$(La_{1-x},Ba_x)F_{3-x}$ Grown by Micro-Pulling Down Method as Potential Vacuum Ultraviolet Laser Material and Scintillator", The 25th Samahang Pisika ng Pilipinas (SPP) Physics Congress, Laguna, Philippines 2007, paper spp-2007-053, ISSN 1656-2666 Vol. 4.